The sea has many voices,
Many gods and many voices.

– T.S. Eliot, *The Dry Salvages* (1941)

PERFORMANCE OF A GLIDER-MOUNTED MULTI-FREQUENCY ECHOSOUNDER FOR DETECTING DENSE MESOZOOPLANKTON LAYERS IN SITU

by

Delphine Mossman

BSc Applied Math & Statistics and Marine Vertebrate Biology, Stony Brook University, 2020

A Thesis Submitted in Partial Fulfillment
of the Requirements for the Degree of

Master of Science

in the Graduate Academic Unit of Biology

Supervisor:	Kimberley Davies, PhD, Biological Sciences
Examining Board:	Jeff Houlahan, PhD, Biological Sciences, Chair Cassidy D'Aloia, PhD, Ecology & Evolutionary Biology Kimberley Davies, PhD, Biological Sciences Grace Saba, PhD, Marine and Coastal Sciences, Rutgers University

This thesis is accepted by the Dean of Graduate Studies

THE UNIVERSITY OF NEW BRUNSWICK

August, 2022

Abstract

The goal of this thesis is to test the performance of a glider-mounted multifrequency echosounder for measuring the biomass distribution of zooplanktonic prey, *Calanus finmarchicus*, of large whales in the Bay of Fundy. Biomass data from biological samples obtained using plankton net tows was compared to acoustic data from the echosounder collected concurrently over a nine-day period in the Bay of Fundy. The correlation between expected and observed backscatter was found to depend primarily on the frequency band and not other factors such as community composition or site. *C. finmarchicus* biomass was best predicted by observed backscatter in the 200 to 455 kHz frequency band, though there was considerable uncertainty in the relationship. The linear model developed in this thesis may be built upon to estimate *C. finmarchicus* biomass from acoustic backscatter in other areas of the North Atlantic without the need for validation with biological samples.

Acknowledgements

No man (or woman) is an island, and I would not have been able to complete this thesis without an ocean of support surrounding me.

An immense thank you to my supervisor, Kim Davies, for her unfailing support and guidance these past couple of incredibly challenging years. Through the difficulties of moving to a new country, undertaking a Master's degree, and conducting field research during a pandemic, you have been a constant source of support and stability for me, and I am incredibly grateful. Thank you as well to the Davies' lab members, who have also supported me directly and indirectly. And, of course, thank you to my committee members, Cassidy D'Aloia and Jeff Houlahan, for your time and effort in helping me make this thesis the best it can be. Many thanks as well to Joe Warren and Scott Loranger for your acoustic modelling help and explanations, and to Nick Hawkins for the glider photo (Figure 6).

Special thank you to the glider team at CEOTR—especially Jude van der Meer, who accompanied us on our field work in 2020—to the kind folks at the Canadian Whale Institute, and to Capt. Danny Barker and his crew for enabling this thesis work to happen at all. Thank you as well to my funders, including the Canadian Foundation for Innovation, the National Science and Engineering Council of Canada, the Marine Environmental Observation, Prediction and Response Network, the Ocean Tracking Network, and Fisheries and Oceans Canada.

Finally, thank you to my support network of friends and family for always encouraging my dreams and my work, and for listening to me discuss zooplankton modelling. I could not have done it without you.

Table of Contents

List of Tables

List of Figures

Introduction

1.1 Zooplankton patchiness in the ocean

Zooplankton are critical members of global ocean and freshwater ecosystems. They are a key driver of biogeochemical cycles, such as the carbon pump, and are sensitive to climate change, which can affect a zooplankton community's rate of element cycling and sequestration (Steinberg and Landry, 2017). Herbivorous zooplankton regulate phytoplankton populations through predation, with zooplankton grazing often explaining more variability in phytoplankton concentration over short time scales than bottom-up processes, such as sinking (Landry et al., 2009). Over decadal time scales, the diversity of zooplankton may help to mitigate and lessen the effects of top-down cascades in pelagic ecosystems, since interspecies competition can buffer the effects of a decrease in higher-order predator abundance (Pershing et al., 2015). Variable zooplankton density also drives the movement of their predators to and from marine "hotspots," areas where zooplankton density is high due to biophysical features, such as upwelling (Hazen et al., 2013; Ohman et al., 2019). Many studies show that top predators congregate in these hotspots, making them important foraging habitat for a wide variety of animals (Baumgartner et al., 2003b; Hazen et al., 2013; Bailey et al., 2012). Therefore, measuring the *in situ* concentration, biomass, and distribution of zooplankton in the water column can give biologists information about predator foraging habitat, food web structure, and pelagic productivity.

Planktonic concentration in the water column is not uniform: rather, plankton are typically found in swarms that are concentrated into thin (relative to the water column depth), patchy, variable-concentration layers. Large-scale plankton aggregation within particular ocean regions is driven in part by equally large-scale physical processes such as water mass advection, upwelling processes, latitudinal temperature gradients, the presence or absence of sea ice, etc. (Pinel-Alloul, 1995). Patchiness, on the other hand, is a mesoscale process, usually on scales between 10 to 1000 metres (Wiebe et al., 1976; Folt and Burns, 1999). Patches are a result of ecological interactions between plankton, their prey, and their predators. For example, most motile zooplankton species undergo diel vertical migration as a strategy to feed on near-surface layers of prey while also avoiding visual predators by moving towards the surface at night and back to deeper depths during the day (Folt and Burns, 1999). Diel-vertical migration represents the largest migration of biomass on earth, yet is simultaneously understudied in all oceans. In addition, some zooplankton also undergo ontogenetic vertical migration at certain life stages as a strategy to avoid predators and conserve energy during seasonal periods of food shortage (Miller and Clemons, 1988; Tsuda et al., 1999). These vertical migration behaviours lead to thin layer formation in the water column, and the high concentration within these thin layers makes them important target regions for those feeding zooplanktivorous predators that are adapted to be able to access them.

Measuring zooplankton concentration *in situ* is typically accomplished using a variety of sampling tools. Commonly used tools include net-sampling devices (ranging in configuration from one to ten nets per device), optical plankton counters (OPCs),

plankton imaging devices, and hydroacoustic echosounders (Baumgartner 2003; Herman, 1988; Gaardsted et al., 2010; Skjoldal et al. 2013; Wiebe et al. 1976). There are, however, limitations to all conventional zooplankton sampling methods, and commonly a combination of tools is used to obtain a complete description of planktonic distribution. Net-sampling methods have the advantage of providing biological samples with which to identify community members and life stages for population dynamics analyses, but are too coarse in resolution to resolve the distribution and concentration of thin layers (Whitmore et al., 2019; Ohman et al., 2019). Biological sampling is also biased due to avoidance by fast moving taxa such as euphausiids and larval fish, and by causing damage to fragile zooplankton structures, especially gelatinous structures (Whitmore et al., 2019). OPCs, imaging devices, and echosounders use sensors to detect zooplankton at high sampling frequencies, thus resolving thin layers, but at lower taxonomic resolution than nets. Typically, these instruments are deployed from a research vessel, the cost of which precludes long-term, consistent, and/or large-area sampling of zooplankton distribution (Benoit-Bird et al., 2018; Schofield et al., 2007). Due to the aforementioned challenges faced by sampling methods, zooplankton sampling is not widely performed, with the ultimate result that they are among the most under-sampled taxonomic groups in the ocean despite having widespread populations.

1.2 Measuring zooplankton from autonomous platforms

1.2.1 Gliders and their sensors

In recent decades many new autonomous oceanographic platforms have been developed to help address the under-sampling problem. Moorings, buoys, autonomous underwater vehicles (AUVs) and satellites have all been used (Benoit-Bird et al., 2018; Gaube et al., 2013). Platforms are typically powered by battery or solar power, and either archive data or transmit it to shore via satellite communications. Mobile AUVs and small, power-efficient sensors can be cost-effective tools to collect data over the extensive scales of time and space necessary to study zooplankton patchiness. One type of AUV called a profiling electric glider utilises variable buoyancy to move vertically and horizontally through the water column (Benoit-Bird et al., 2018; Rudnick et al., 2004). Electric gliders are programmed to navigate among waypoints by dead-reckoning (using a previous position and measurements of speed and heading to calculate current position). Glider buoyancy engines function by utilising a piston or pump to change the density of the nose of the glider, either by flooding and evacuating a compartment with sea water or by flooding and pumping oil from an internal reservoir to an external bladder (Jenkins et al., 2003; Rudnick et al., 2004). At the start of each dive cycle, the glider is made negatively buoyant; fixed wings on either side of the main glider body transform some of the downward motion into horizontal motion, resulting in an average over-ground speed of 0.5 m/s. When it reaches the bottom of its dive, the glider is made positively buoyant and begins to rise, with the wings on either side again transforming some of the vertical motion to horizontal. The resulting sawtooth dive pattern is energy efficient, leaving most of the on-board battery life for instrumentation and communication (Jenkins et al., 2003; Rudnick et al., 2004; Figure 1).

Communication with the glider by shore-based pilots while it is deployed can be achieved to change mission parameters, alter waypoints, and monitor vital signs, all in near real-time. For near real-time communication, iridium satellites are used. Whenever the glider's communication antenna emerges from the water, it transmits data to the pilot, including its current GPS location, before continuing its mission parameters or awaiting further instructions (Rudnick et al., 2004; Schofield et al., 2007; Figure 1).

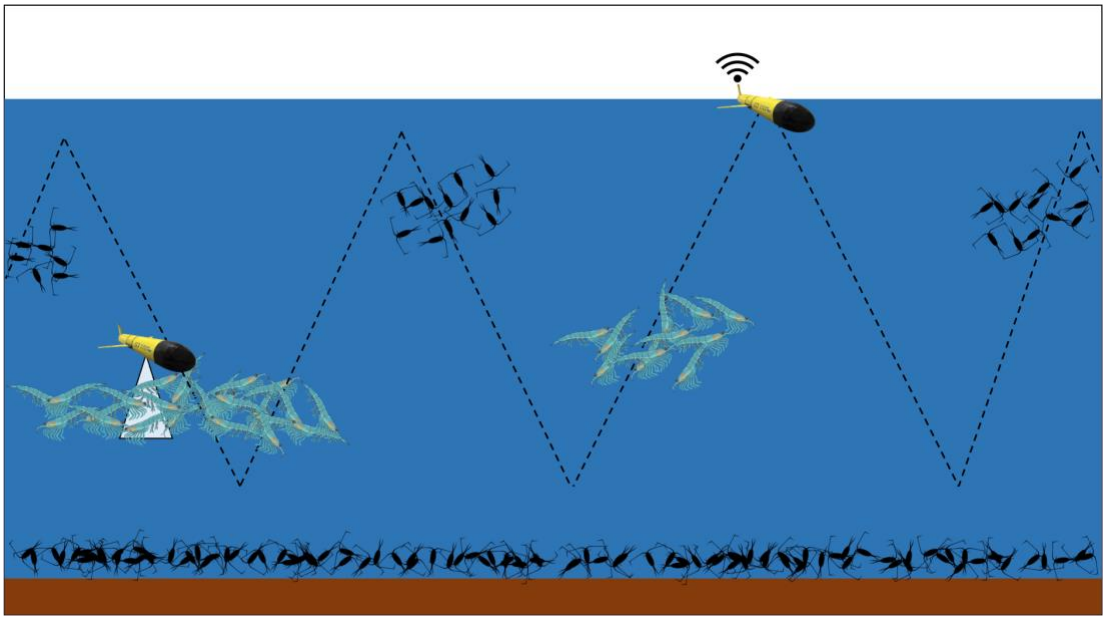

Figure 1. Diagram of a typical profiling electric glider path (dashed line) through the water column. Pale blue triangle represents the echosounder beam; green animals are krill, and black animals are copepods. The glider symbol is shown at two points along its path; while sampling underwater (left) and while communicating at the surface (right).

1.2.2. Basic principles of hydroacoustic echosounders

Hydroacoustic echosounders are a standard choice of sensor to study the abundance of many different size classes of ocean organisms, from zooplankton to large

schools of fish, but it is only in the last five years that they have been engineered to function onboard gliders (Benoit-Bird, 2015; Benoit-Bird, 2018; Chave et al., 2018; Reiss et al., 2021; Ruckdeschel 2017). Put in very simple terms, echosounders consist of one or more sound transducers and a sound receiver. The transducers produce acoustic energy in bursts (pings) at particular frequencies. Some of this sound energy scatters off of organisms in the water column. Some of the scattered energy returns back to the instrument (so-called 'backscatter' or 'echo') and is received by the sound receiver (Simmonds and MacLennan, 2005). After data processing and modelling is applied to these data, the acoustic backscatter can be interpreted as a measure of organismal concentration in the water column.

Echosounder transducers can be designed to produce single frequency, multifrequency or broadband sound waves (Simmonds and MacLennan, 2005). A single frequency echosounder is simple to use and has the lowest power requirements (which is important to minimise glider battery consumption), but provides no information about the size or identity of sampled organisms (Benoit-Bird et al., 2018). Broadband echosounders are power-hungry because they produce sound energy across a continuous spectrum of frequencies, but they are desirable because they provide the best possible size and taxonomic resolution that an echosounder can (Lavery et al., 2010). Multifrequency echosounders represent a compromise between single frequency and broadband echosounders. They produce narrowband pings at multiple frequencies (up to four in commercially available sensors), resulting in less power consumed per ping than a broadband echosounder while still allowing for some size class differentiation, from which coarse taxonomic information can usually be inferred (i.e., copepod vs.

euphausiid vs. fish) (Benoit-Bird et al., 2018; Simmonds and MacLennan, 2005). In the case of multifrequency echosounders, the size class of the target organisms is a critical consideration when choosing which frequencies the echosounder transducer will produce. This choice must be made when the echosounder is designed and cannot be changed afterward. Smaller organisms are better sampled by higher frequencies because low frequency sound waves have a longer wavelength and, as a result, these long waves bypass small organisms (Simmonds and MacLennan, 2005). Larger organisms are also sampled by higher frequencies, but by examining the differences in echoes between adjacent frequencies, one can create a filter to obtain the echoes from only smaller organisms (Figure 2). Common acoustic frequencies used to sample copepods range from ~ 200 to 769 kHz. Euphausiids are typically targeted using 120 kHz echosounders, while standard fish echosounders are typically 38 or 64 kHz (Simmonds and MacLennan, 2005). A standard multifrequency echosounder that could measure all of these taxonomic groups would need transducers that produced sound at each of 64, 120, 200 and 455 kHz.

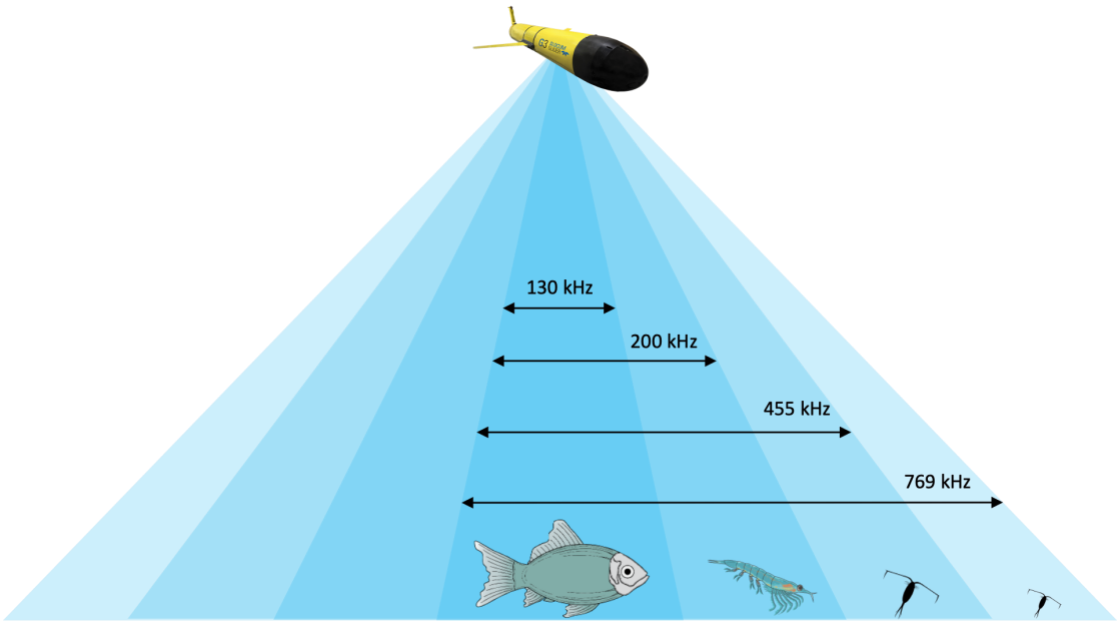

Figure 2. Conceptual diagram showing that as transducer frequency increases, the size range of organisms sampled by the echosounder also increases. Isolating acoustic backscatter from a particular size class is done by taking the difference in acoustic backscatter between two frequencies and retaining only echoes where the difference is in a predetermined frequency band. For example, to isolate the euphausiid size class shown in this diagram, one would take the difference in backscatter between 200 kHz and 130 kHz.

Until the development of glider-mounted units, echosounders were primarily mounted on the hull of a vessel or towed behind it. This has been a successful method of collecting acoustic backscatter data since the 1980s (Lavery et al., 2007). However, there is a significant problem with this approach for measuring zooplankton patches deep in the water column: data collection at high frequencies (300 kHz or more) is range-limited due to attenuation of the echo in the water. As with any physical process, as a sound signal travels through the water, it loses energy to its surroundings; the higher frequency the sound, the more rapidly energy is lost. This decreases the ratio of signal power to noise (unwanted sounds) power, or signal-to-noise ratio (SNR); if the

SNR is too low, then the returning echo from a target may not have enough energy to return to the sound receiver and register a detection (Simmonds and MacLennan, 2005). Attenuation becomes worse, i.e., the SNR approaches 1 at closer distances to the echosounder, in the higher frequencies relative to the lower frequencies. For example, for pings at 130 kHz, SNR may not reach 1 until 75 m from the transducer; at 769 kHz, SNR approaches 1 at a range of only 20 m. As a result, transducers mounted to a vessel or tow body at the surface facing downward cannot sample the deepest layers of smaller zooplankton such as copepods, which occur up to hundreds of metres below the surface, because the sound attenuates at shallow depths.

A profiling glider-mounted echosounder eliminates this problem because the glider transports the acoustic transducer down into the water column and into the plankton layers, thus it is able to measure zooplankton communities at all depths in the water column (Guihen, 2018; Figure 3). As the glider moves through the water column, it samples a parallelogram-prism-shaped section of water (the area coverage, or swath), determined by the maximum range (R) of the echosounder beam before attenuation makes the signal too weak for detection, and the dive angle (θ) of the glider (Figure 3).

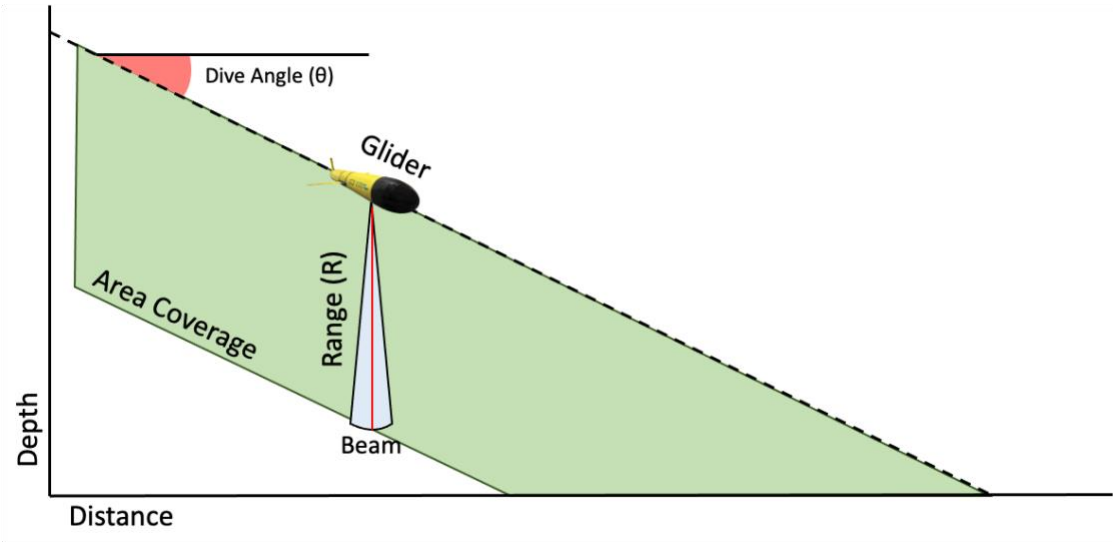

Figure 3. Diagram of a typical glider path with acoustic coverage highlighted in green. Recreated from Guihen 2018. Dashed line indicates the glider path. Blue cone under the glider indicates the acoustic beam emitted by the echosounder. Key dimensions discussed in the text are labelled.

1.2.3. Abundance of target taxa in hydroacoustic data

Typically, the goal of hydroacoustics is to measure the concentration of a target taxon or taxa in the water column. However, plankton communities are diverse and isolating the backscatter from single taxa in echosounder data is challenging. Mixed plankton communities can cause complex acoustic echoes where no one taxon dominates the scattering at all frequencies, or even one frequency (Lavery et al., 2007). In the Northwest Atlantic, most zooplankton communities are usually dominated in biomass by copepods (in a range of sizes), with euphausiids and gelatinous zooplankton also being commonly present. Copepod biomass can be underestimated by echosounders when compared with net-derived estimates because their small size and material properties make them weak scatterers of sound even at very high abundances and frequencies, and their backscatter is frequently masked by stronger scatterers in the

water column (Lavery et al., 2007). Siphonophores, a gelatinous zooplankton taxon, present an important challenge in acoustic studies due to the presence of pneumatophores which are filled with carbon monoxide gas (Warren et al., 2001). The density of the pneumatophore gas is much lighter than the water. As a result of the high density contrast of the gas-filled chamber, the pneumatophore scatters sound very strongly. Siphonophores therefore can overwhelm the backscattering signal from a zooplankton community in which they are present at certain frequencies, even if they are present in very small concentrations (Lavery et al., 2007). It is thus important to know whether siphonophores are present in a zooplankton community, as their presence or absence can greatly affect the echosounder measurements across a wide range of frequencies, including those frequencies at which copepods scatter sound most strongly.

Validation of echosounder data with plankton abundance data collected with nets or imaging devices deployed in the same area as the echosounder is a standard step taken to convert acoustic backscatter into biological abundance and vice versa (Lavery et al., 2007; Simmonds and MacLennan, 2005). A net system with multiple opening and closing nets is considered the gold standard of biologically sampling planktonic communities because it allows for depth-stratified sampling of thin layers and it provides biological samples of the planktonic community in the area which can be examined and taxonomically identified (Wiebe et al., 1976). In some cases, a plankton imaging system may also be used to provide data on the abundance and community composition for the validation (Davis et al., 2005). The first step of this validation is known in the bioacoustics community as the "forward problem." The forward problem involves calculating *expected* acoustic backscatter from net-collected zooplankton

samples using standard scattering models and relating that to backscatter *observed* by the echosounder (see Methods). Once the forward problem is solved, it can be used to solve the "inverse problem" in which zooplankton concentration is inferred from echosounder measurements (Simmonds and MacLennan, 2005). **The goal of this thesis is to study the ability of a glider-mounted echosounder to measure a zooplankton community by solving the forward problem.**

1.3 The Bay of Fundy planktonic ecosystem and study area

Two basins in the outer Bay of Fundy off the coast of New Brunswick were chosen for the study: Grand Manan Basin and Owen Basin (Figure 4). The outer Bay of Fundy is a rich ecosystem and feeding habitat for many marine predators. Together, these basins represent the area where North Atlantic right whales, basking sharks, and red phalaropes have been historically concentrated during summer months to forage on lipid-rich copepods (Baumgartner et al., 2003a; Baumgartner et al., 2003b; Fisheries and Oceans Canada, 2014). High numbers of rorqual whales and abundant fish communities are supported by copepods and euphausiid aggregations in the Bay. Grand Manan Basin (depth ~280 m) is a designated North Atlantic right whale critical habitat located at the mouth of the Bay of Fundy, and is primarily influenced by offshore water masses. High concentrations of *C. finmarchicus* had been found in this basin in previous studies (Baumgartner et al., 2003a; Baumgartner et al. 2003b; Michaud and Taggart, 2011). In contrast, Owen Basin is northwest of Grand Manan, shallower (depth ~150 m) and is under greater influence of coastal water due to its closer proximity to land. These study sites were selected due to their oceanographic properties and status as historical

feeding grounds for North Atlantic right whales. Patches of *C. finmarchicus* are known to primarily occur in waters between 90 and 150 metres deep, and in both the flat basin bottom as well as the sloped basin edges (Michaud and Taggart, 2011; Woodley and Gaskin, 1996). Therefore, the survey domain was selected as the most likely area to find high densities of *C. finmarchicus* to conduct the validation study.

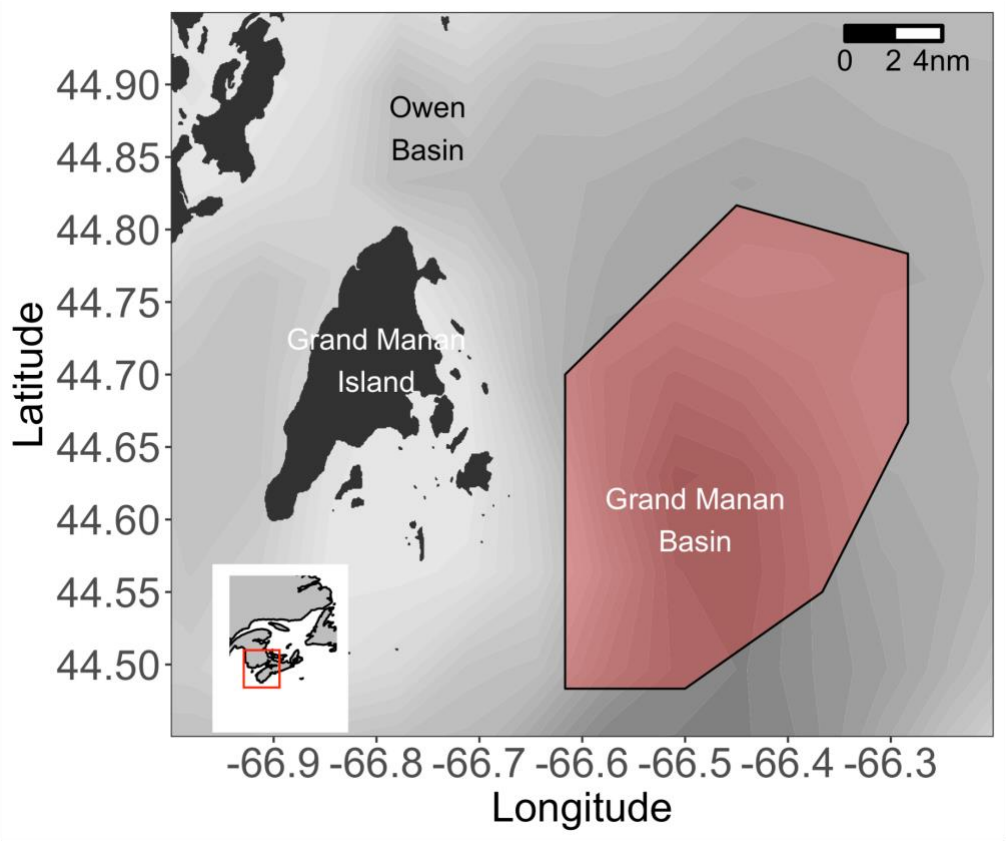

Figure 4. Map of study area for the September 2020 field season, with North Atlantic right whale critical habitat in Grand Manan Basin (as defined by the Species At Risk Act) in red. Inset displays part of Atlantic Canada, with the Bay of Fundy outlined in red.

The Bay of Fundy was an annual foraging stronghold for right whales from at least 1980 until 2010, and many studies were undertaken in that time period to characterise the planktonic ecosystem (Murison and Gaskin, 1989; Baumgartner and

Mate, 2003; Baumgartner et al. 2003a; Baumgartner et al., 2003b; Michaud and Taggart, 2011). Starting in 2010, North Atlantic right whales virtually abandoned this area, and few have been sighted there for the last 11 years (Davies et al., 2019). Right whales have also abandoned nearby foraging areas in the Gulf of Maine and western Scotian Shelf. The disappearance has been driven by a significant decline in *C. finmarchicus* biomass throughout Atlantic Canadian and US Gulf of Maine waters, which has been correlated with both warming sea surface temperatures and changes in the spatial distribution and calving rates of right whales (Sorochan et al., 2019; Meyer-Gutbrod et al. 2018; Record et al. 2019; Meyer-Gutbrod et al. 2021). The effect of this regime shift on the planktonic ecosystem in the Bay of Fundy has not been studied, and there is no contemporary data on *C. finmarchicus* distribution within the Grand Manan Basin right whale critical habitat. Such information is important to quantify and understand in order to continue the conservation of North Atlantic right whales. Glider-mounted echosounders and other plankton sampling devices need to be deployed to characterise the contemporary ecosystem and determine possible factors that led to its abandonment as a feeding ground. Future deployments of a glider-mounted echosounder in this same habitat may also be able to use the calibration data obtained from this study to obtain *Calanus* biomass estimates from acoustic data alone. Furthermore, the addition of a glider-mounted hydrophone to acoustically detect whales from the same glider would allow for complete habitat modelling in offshore areas where shipboard sampling of zooplankton communities is not physically possible or feasible.

1.4 Research objectives

I aim to assess the performance of a glider-mounted multifrequency echosounder for measuring the distribution and concentrations of zooplankton layers, and in particular late-stage *C. finmarchicus* copepod concentrations, in the Bay of Fundy.

In order to address this question, I have the following research objectives:

1. Characterise the zooplankton community and its vertical distribution in two basins in the outer Bay of Fundy. Grand Manan Basin represents a *C. finmarchicus* dominant habitat and Owen Basin may not.
2. Compare zooplankton biomass and community composition collected by a glider-mounted multifrequency echosounder and shipboard sampling devices in each basin, with a focus on discriminating among thin layers of meso- and macrozooplankton.
3. Statistically compare expected and observed acoustic backscatter, and explore processes that may explain any discrepancies between estimates.

Methods

2.1 Sampling equipment

A Hydro-Bios MultiNet Midi (hereafter MultiNet) was used to collect the biological plankton samples (Figure 5). It was equipped with five nets of 200 μm mesh, with a net opening of 0.25 m^2. 200 μm is an accepted mesh size for capturing large mesozooplankton (Makabe et al., 2012). Each net was opened and closed in sequence based on water pressure to collect vertically structured plankton samples during a single cast. Nets are held closed by spring tension until the MultiNet reaches the first sampling depth, at which point the first net (net 1) opens in less than 1 second. Once the next sampling depth is reached, net 1 closes and net 2 opens at the same time, and so on until the MultiNet reaches the surface with net 5 open. The nets were equipped with two digital flowmeters to estimate flow through the nets, filtering efficiency, and filtered volume. The MultiNet was flown obliquely through the water and sampled on the ascent (upcast), ascending at approximately 0.5 m/s. The flow of water through the net (a combination of the water current speed and boat speed) was capped at 4 knots, though occasionally it rose slightly above that speed. Samples were collected over many tens of metres in the cod end of the net, which was later rinsed into a sampling jar of a 10% by volume buffered formalin solution for preservation.

An open-style, galvanised steel cage was used to collect OPC and Conductivity-Temperature-Depth (CTD) data before and after each MultiNet tow (Figure 5). The cage was lowered vertically in the water at approximately 1 m/s, and the CTD sampled at 1 Hz on the downcast, providing a vertical profile with a vertical resolution of 1 m.

The OPC also sampled on the downcast at a rate of 2 Hz. As water and accompanying matter (including zooplankton, suspended organic nonliving particles, etc.) flows into the OPC from below, it occludes light shining from photodiodes through the sampling tunnel and onto a mirror. The degree of occlusion and attenuation of the light by particles passing through the tunnel is interpreted by the instrument's electronics as particle count and size, where size is measured as equivalent spherical diameter (ESD) (Gaarsted et al., 2010; Herman, 1992). As this particular instrument (meaning the same serial number) had already been used in published studies to examine *C. finmarchicus* abundance in the Grand Manan Basin (Baumgartner, 2003), it was an excellent validation tool for this habitat and this study.

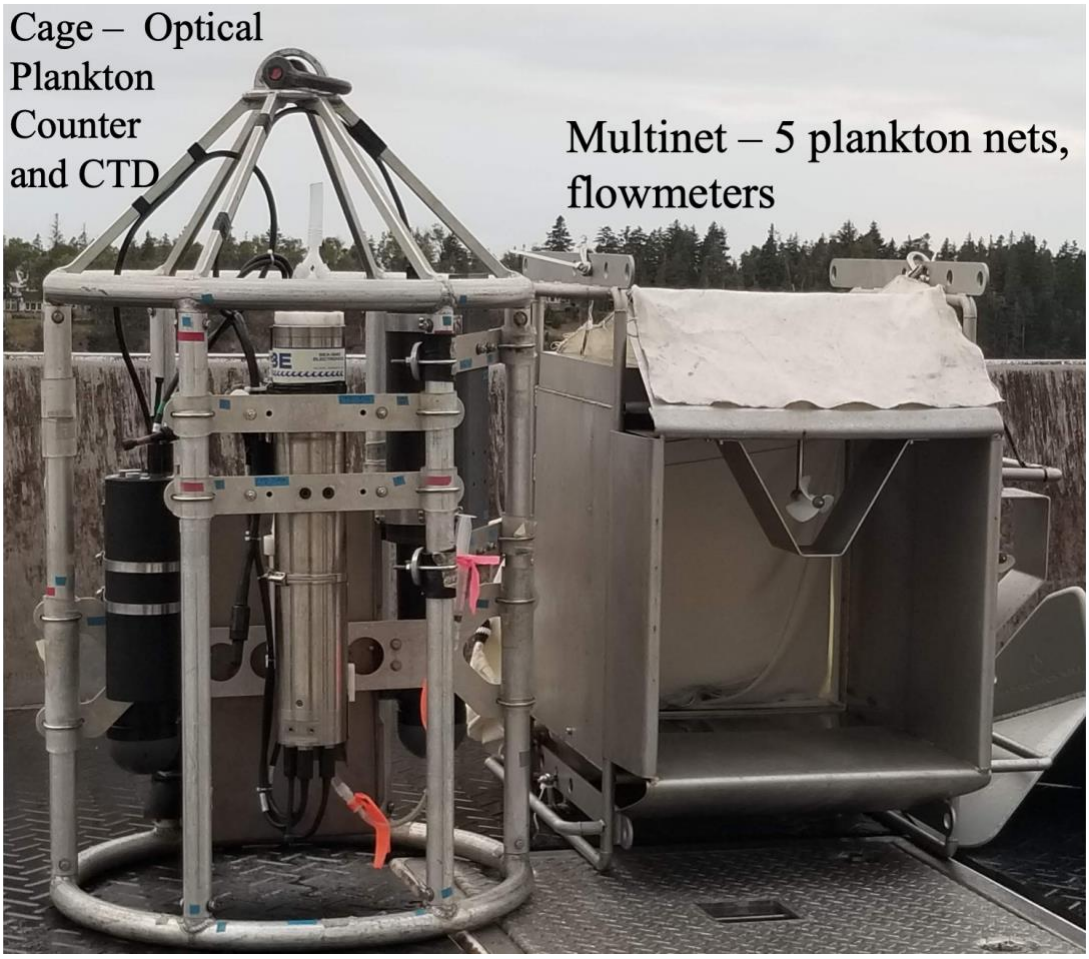

Figure 5. Labelled photograph of the cage (left) and MultiNet (right) used in this study. Photograph taken by author.

The glider used was a G3 Slocum electric profiling glider equipped with a 150 m buoyancy engine (meaning its maximum sampling depth is 150 m) (Figure 6). It travelled approximately 1 nautical mi./hr (about 0.5 m/s) over ground, and had an average descent/ascent rate of 15.3 cm/s. The glider sampled during its dives (downcasts) and climbs (upcasts) at an oblique angle of approximately 22.5 degrees. The glider carried a CTD, optode, fluorometer and optics sensors, and a four-frequency echosounder integrated into an extended half-science bay. The CTD measured

temperature and salinity at 0.5 Hz, the optode measured oxygen at 0.5 Hz, and the fluorometer and optics sensors measured chlorophyll concentration at 1 Hz.

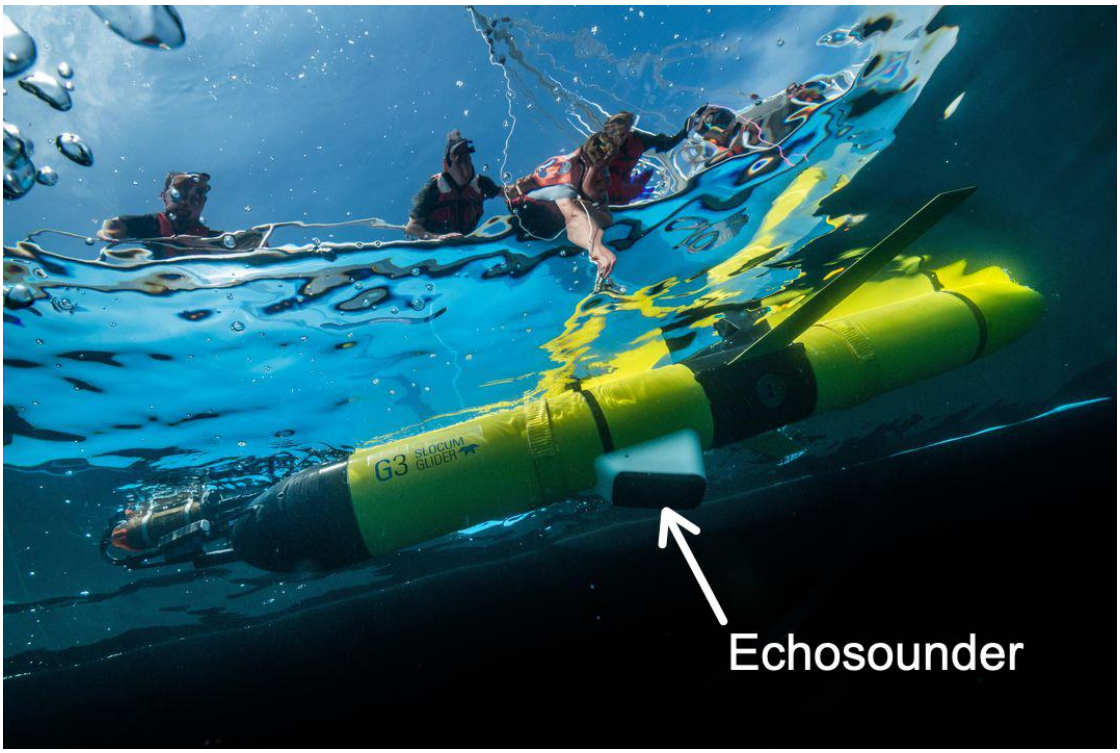

Figure 6. The G3 Slocum profiling glider used in this thesis. Echosounder is labelled. Photograph courtesy of Nick Hawkins.

The glider-mounted, single-beam echosounder, the Acoustic Zooplankton Fish Profiler or AZFP (ASL Environmental Sciences), emitted sound at 130, 200, 455 and 769 kHz, and was oriented so that the transducer faced vertically downward on the downcast. The angle of the transducer meant that the echosounder only sampled during downcasts, and was inactive during upcasts. Because the ping period and burst interval were the same length of time (1 second), the unit pinged continuously (Table 1).

Table 1. Echosounder settings used during the 2020 Bay of Fundy field season.

Frequencies	130 kHz, 200 kHz, 455 kHz, and 769 kHz
Ping Rate	1 second
Burst Interval	1 second
Pings Per Burst	1
Pulse Length	300 μs
Digitization Rate	20000 samples/s (0.0385 m/sample)
Range	3200 samples (approximately 120 m)
Noise Floor Parameters	12564 counts (130 kHz), 9660 counts (200 kHz), 13604 counts (455 kHz), and 10780 counts (769 kHz)
Sound Speed	1460 m/s
Lockout?	No lockout
Averaging?	No spatial or temporal averaging

2.2 Modelling acoustic backscatter from echosounder data

In brief, an echosounder functions by sending out acoustic signals ("pings") at known intervals and frequencies, and then listening for the echoes that return after the pings scatter off of an object with a boundary across which there is a change in acoustic properties ("target"). The echoes that return back to the echosounder make up only a portion of the total reflected sound, and are known as the "backscatter" from the target. Target strength (TS) is a logarithmic measurement of the proportion of sound energy from the initial ping backscattered by a particular target; in other words, it is a measure of how well the echosounder can "see" a particular target at a particular frequency. Target strength is related to another acoustic property, the backscattering cross-section (σ_{bs}), via the following equation:

$$TS = 10\log_{10}(\sigma_{bs}) \quad \textbf{(1)}$$

σ_{bs} is the linear equivalent to TS, and thus, it also measures the proportion of sound energy backscattered by a target, but linearly instead of logarithmically. It is strongly influenced by target size; smaller targets will generally have a smaller σ_{bs} (and a more negative TS as a result) at any given frequency.

For the echosounder used in this study, a single ping is made up of four pulses of sound, one from each frequency. One pulse is composed of many samples, each covering a predefined distance interval (also called the bin size) which is related to the digitization rate of the echosounder (Figure 7).

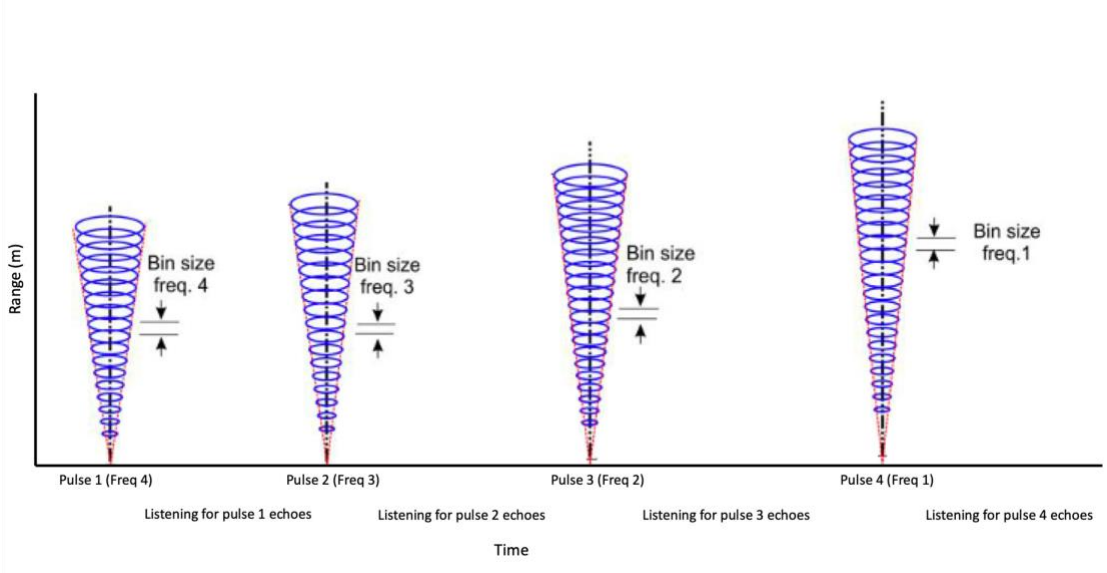

Figure 7. Generic structure of a single ping for a four-frequency echosounder. Recreated from ASL AZFP Operator's Manual.

For zooplankton in particular, it is not reasonable to measure target strengths from each individual plankton; instead, σ_{bs} is used along with the volume of water sampled by the echosounder (V_0) to obtain the volume backscattering coefficient ($S_{v(echo)}$):

$$S_{v(echo)} = \sum \sigma_{bs}/V_0 \quad \textbf{(2)}$$

The intensity of $S_{v(echo)}$ can be used to obtain information about plankton abundance and biomass, and the difference between $S_{v(echo)}$ measurements taken at different frequencies can inform the size distribution of the plankton community. This is due to the difference in target strengths of zooplankton at different frequencies; at higher frequencies, the TS of large zooplankton have plateaued, whereas the TS of small zooplankton are still increasing (Figure 8). Therefore, a larger difference in scattering strength between two frequencies is consistent with scattering by smaller copepods.

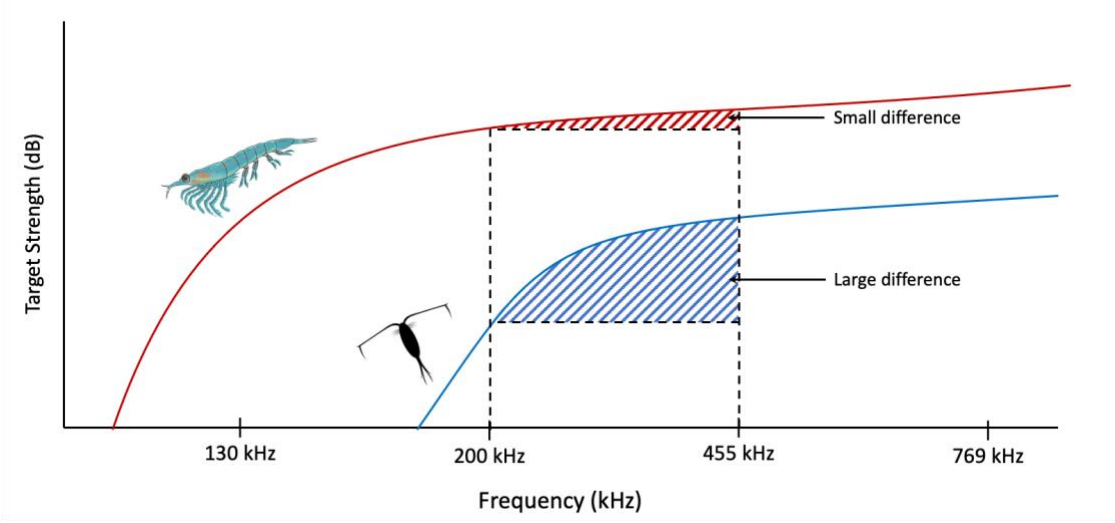

Figure 8. Conceptual frequency vs. target strength diagram illustrating the difference in scattering strength for krill (top, red line) and copepods (bottom, blue line) at different frequencies. The comparison between the difference in scattering strengths between 455 kHz and 200 kHz is highlighted.

2.3 Field sampling

Field sampling was undertaken from the 19th to the 26th of September, 2020. A total of six sampling days were completed—three in Owen Basin and three in Grand Manan Basin. All sampling took place during daylight hours. Each glider and vessel transect took place over the course of half of one tidal cycle (i.e., from low to high tide, or from high to low tide), and was oriented such that the glider and vessel would be moving with the water current, because the strong tidal currents in the Bay of Fundy make glider sampling against the tide impossible. This design granted the strongest probability that the glider-mounted AZFP and the vessel-based zooplankton samplers were sampling the same water mass—a section of water with distinct physical properties, such as salinity and temperature—and, presumably, the same zooplankton community associated with that water mass.

During each sampling day, the glider was deployed during slack tide in such a way that its transect went with the coming tide, leading to a highly predictable, straight-line flight pattern (Figure 9). The glider was also programmed to surface once every two hours to transmit its location to the vessel (allowing the vessel to follow it) and to get a GPS fix to stay on course before continuing its transect. Finally, because the tidal cycle in the Bay of Fundy is approximately six hours from slack tide to slack tide, the glider was pre-programmed to end its transect after that amount of time and await pickup by the vessel. On average, the glider could travel approximately 5 nautical miles during each transect.

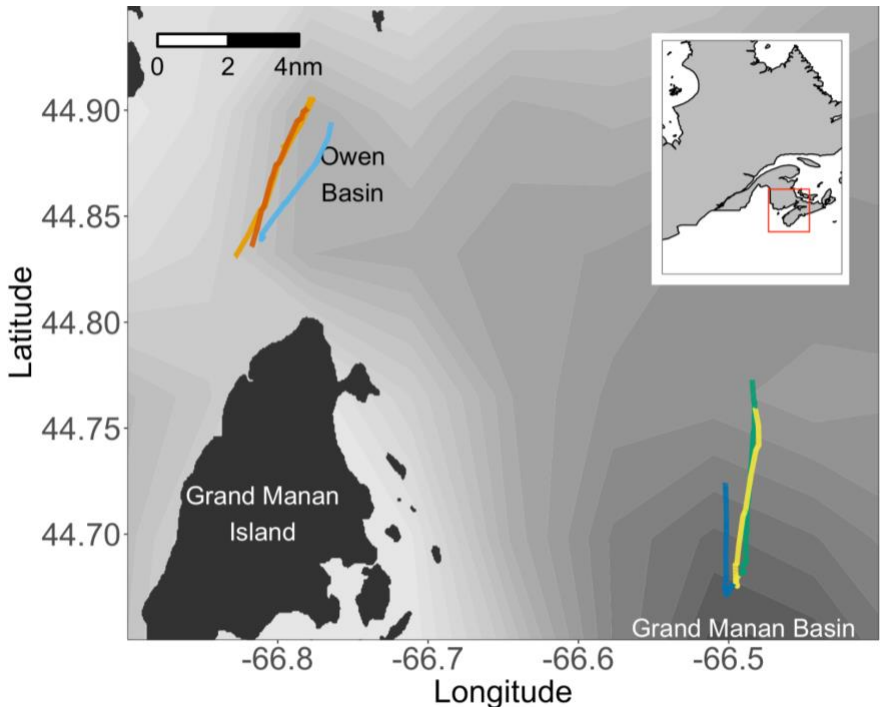

Figure 9. Map of glider transects (coloured lines) performed during the September 2020 field season in the Bay of Fundy. Inset displays part of Atlantic Canada, with the Bay of Fundy outlined in red.

While the glider was on its transect, the vessel collected ship-based measurements at each glider surfacing point (henceforth each station), starting with its deployment position (goal n=3 samples per glider trackline). At each station, a MultiNet deployment (n = 18 total, 9 per basin) was performed between two cage deployments (n = 36 total, 18 per basin) in the same direction as the glider was travelling. This process was repeated until the glider completed its transect (Figure 10). Vessel sampling was generally within 0.5 nautical miles of the glider transect.

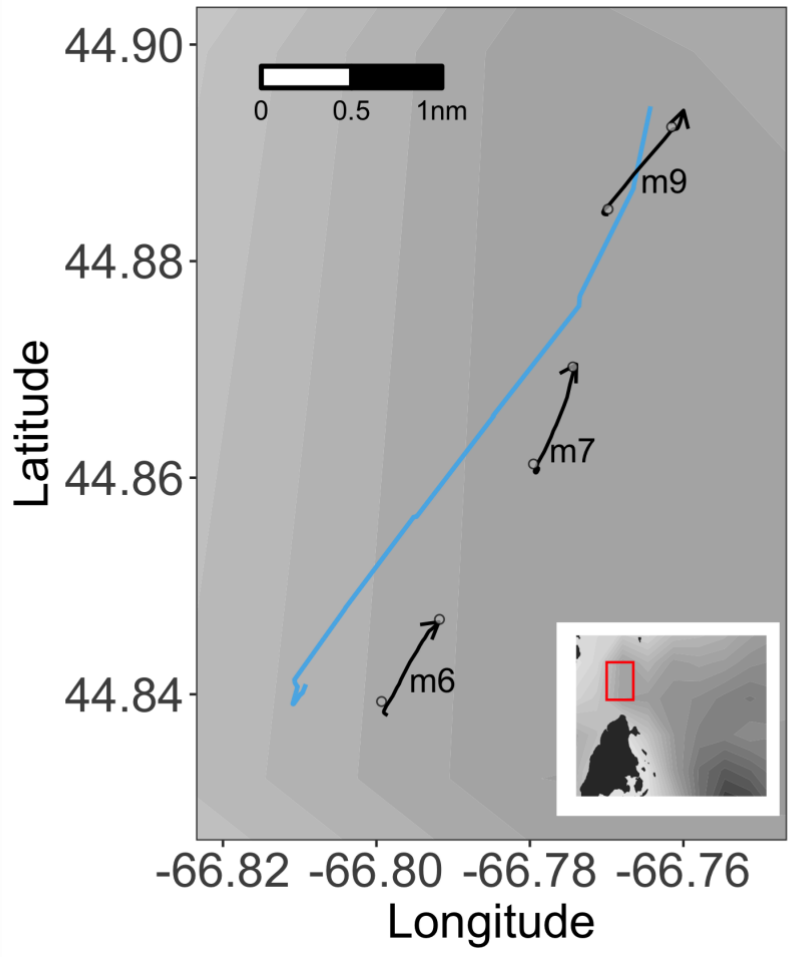

Figure 10. An example from September 20th of the co-location of the glider transect (blue line) and vessel-based measurements. Each labelled black line is a MultiNet tow, and each grey circle is a cage deployment. Inset map shows study area, with area where the tow was performed outlined in red.

2.4 Echosounder data processing

Acoustic data were processed using a custom Matlab script written for this thesis. When deployed, the AZFP automatically converts received voltage data (engineering units) to decibels (standard acoustic units), which reduces post-processing effort. However, the range (distance out from the echosounder) for each sample of each ping is recorded as distance from the instrument, and not absolute depth in the water column (Figure 11, panel A). In order to obtain the depth of each sample of a ping, the following equation was used:

$$\text{Depth of sample (m)} = \text{Depth of glider (m)} + \text{Range of sample (m)} \quad \textbf{(3)}$$

Once this transformation was performed, seafloor echoes were easily identified as a line of strong scattering (Figure 11, panel B). Data 0 to 3 m above the seafloor were removed; removal of data slightly above the seafloor also removes potential scattering from sediment. Data within 5 m of the echosounder were also removed. This was done to avoid near-field scattering effects, which is a standard procedure because the near-field sound wave propagation processes are complex and not necessarily linearly related to the amount of plankton scattering in the water column. Removing data within a certain distance from the transducer is the standard method of dealing with near-field scattering effects (Simmonds and MacLennan, 2005). Given a wavelength λ and a distance across the transducer face a, the transition from near-field to far-field scattering occurs at a range R_b equal to:

$$R_b = a^2/\lambda \quad \textbf{(4)}$$

It is considered best practice to remove data within $2R_b$ metres of the transducer, as the transition from near- to far-field scattering is a gradient (Simmonds and MacLennan, 2005). For the echosounder used in this study, the greatest R_b value was approximately 2.5 m for pings at 769 kHz.

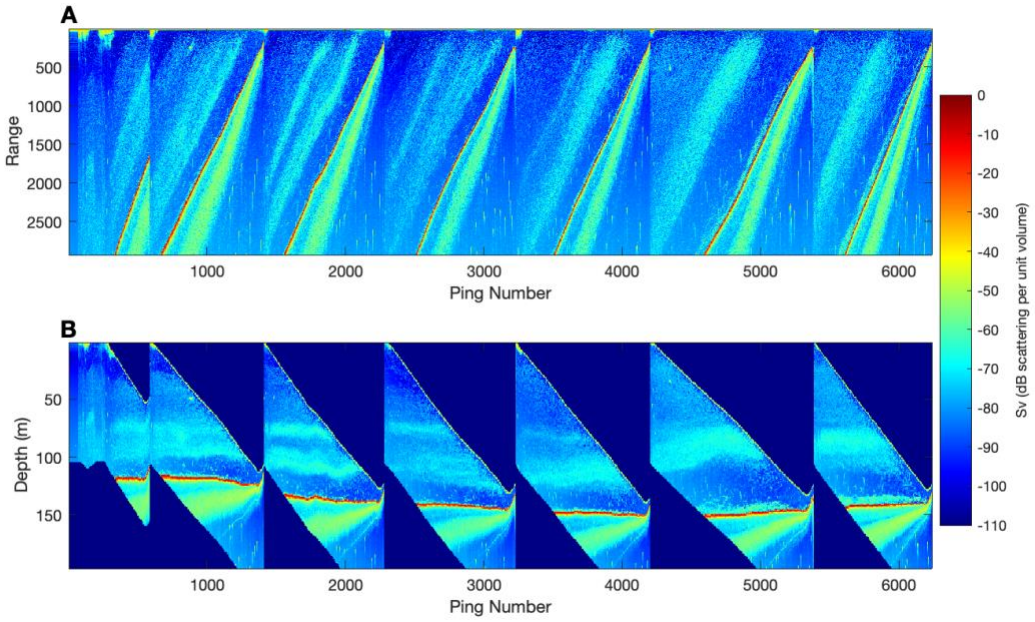

Figure 11. A—Raw acoustic data at 130 kHz from the echosounder collected on September 20th, 2020, in Owen Basin. This data has not been transformed into true depth space. B—The same acoustic data as in panel A but now averaged into depth bins and transformed to be a function of depth, as opposed to range. Very dark blue areas (< -110 dB) in panel B are unsampled portions of the water column. A swarm of zooplankton is apparent in the mid-water column as light blue scattering between ~ 60 and 70 dB below 60 m depth. The seafloor is clearly visible as a bright red line between 120 to 150 m depth; apparent echoes present below seafloor are an artefact of the instrument.

Once initial data cleanup was performed, the data were averaged into 1 m depth bins. The *in situ* noise floor in decibels was then estimated by taking a moving average

over 10 metres of the entire depth range of each dive of each day, then finding the minimum value of those averages. This approach assumes that the minimum average $S_{v(echo)}$ was located in empty water and contained only noise (including electronic self-noise). Once the noise floor was found, it was subtracted from the averaged echo data. This left only the echo data from zooplankton of interest, revealing scattering layers of zooplankton (Robertis and Higginbottom, 2007; Ruckdeschel, 2017; Ruckdeschel et al., 2020). This process is similar to manually removing the unwanted static from a talk radio signal to improve the clarity of the speaker's voice.

Frequency differencing between adjacent frequencies was then performed by subtracting the higher frequency ping values in decibel space from the lower frequency values (Figure 12). The differences were used to "mask" the observed data of the higher frequency in the difference to obtain only scattering consistent with copepods between 1.3 and 3 mm in size, the observed range of prosome lengths of *C. finmarchicus* (Table 2). This masking procedure is an attempt to filter out the echoes from scatterers other than the target species by utilising the differences in target strengths (Figure 8). If the decibel difference between two adjacent frequencies is too small or too large, then the echo cannot be due to copepods (Figure 12). After this masking step, the unmasked 0 to130 kHz band should be composed primarily of euphausiid echoes, while the other three frequency bands should contain mostly copepod echoes.

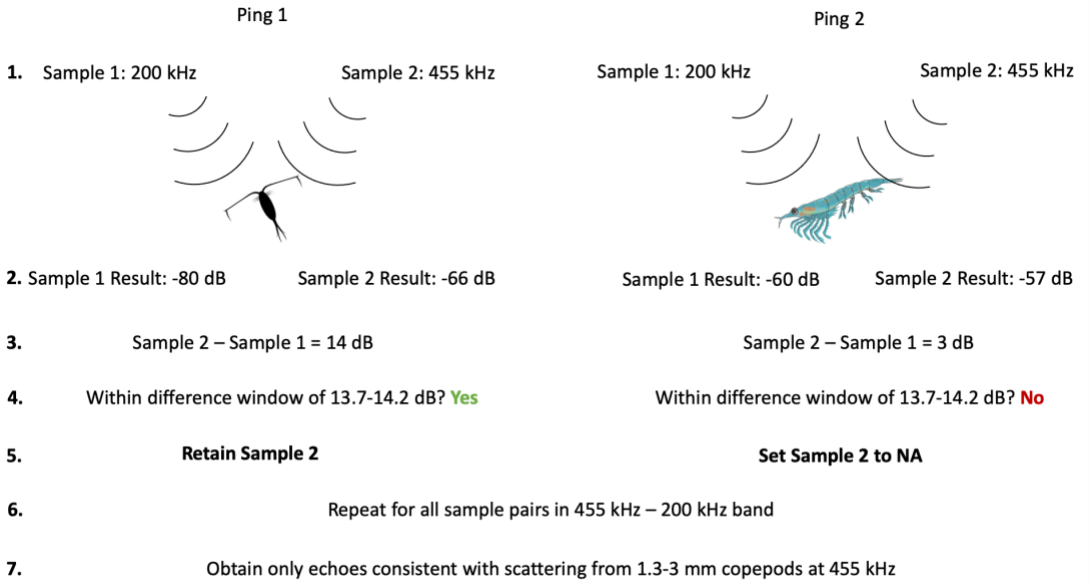

Figure 12. Conceptual diagram showing the masking procedure used to obtain echoes from copepods in a predefined size range (in this case, 1.3 to 3 mm in length).

Table 2. Decibel difference windows consistent with scattering from copepods between 1.3 and 3 mm in size. Lower and upper bound dB values were obtained from the difference in target strengths of a 3 mm copepod model and a 1.3 mm copepod model, respectively.

Frequency Difference	Lower Bound (dB)	Upper Bound (dB)
200 kHz to 130 kHz	7.8	8.8
455 kHz to 200 kHz	13.7	14.2
769 kHz to 455 kHz	7.4	7.5

2.5 The forward problem

For each biological net-sample, the conversion from biomass to expected acoustic backscatter ($S_{v(net)}$) was done using custom R code and the ZooScatR package (Gastauer et al., 2019). Only four taxonomic groups were taken into account in this exercise, because they comprised the majority of the samples: small copepods (≤ 1 mm

prosome length), large copepods (>1 mm prosome length), siphonophores, and euphausiids.

The calculation of $S_{v(net)}$ requires an estimate of target strength (TS) for each taxonomic group (Equation 5). Target strength depends on the shape, size, and material properties of the target the beam of sound strikes. Because target strength is also frequency dependent, four TS values are needed for each taxonomic group, one for each frequency of the echosounder used in this study. Siphonophore TS at each frequency was calculated using the solution to the perfect sphere model for pneumatophores (Warren, 2001). Euphausiid and copepod TS at each frequency were calculated using the distorted wave Born approximation, using a prolate spheroid for the copepod model and a bent cylinder for the euphausiid model, the standard conventions for those taxonomic groups (Becker and Warren, 2014; see Table 3). Once the target strengths were obtained, the following equation was used to determine the total $S_{v(net)}$ contribution in decibels from each relevant taxa in the net (using the concentration [Z] for each taxa Z) and for each frequency (i):

$$S_{v(i,Z)} = TS_i + 10log10([Z]) \quad (5)$$

In order to determine the total expected backscatter for each net of each tow at a single frequency, the backscatter from each taxon (for a total of *n* taxa) within each net was summed (after conversion from decibels to the linear space), to give an integrated backscatter for the entire net sample:

$$10^{S_v\,(net)/10} = \sum_{i=1}^{n} 10^{S_v\,(i)/10} \quad (\mathbf{6})$$

Equation 6 was then applied for each of the four frequencies used. Additionally, Equation 6 modelled expected backscatter three different ways: Model 1 - expected backscatter from all organisms in the net ($S_{v(net)}$), Model 2 - expected backscatter from copepods ($S_{v(copepod)}$), and Model 3 - expected backscatter from *C. finmarchicus* only ($S_{v(cfin)}$). These three models were chosen to examine decreasingly complex backscatter models and how their distribution compares to that of $S_{v(echo)}$. It is expected that $S_{v(cfin)}$ will be strongly correlated to $S_{v(echo)}$ in the 200 to 455 kHz frequency band, as it includes only one type of scatterer. On the other hand, $S_{v(copepod)}$ and $S_{v(net)}$ may not be well correlated with $S_{v(echo)}$ in any frequency band, due to combining expected backscatter across animals of many different size classes and with varying scattering strengths (Table 4).

Table 3. Target strengths of the major taxa at each of the four echosounder frequencies used. "Large copepods" refers to species with an average length ≥1 mm, while "small copepods" refers to species with an average length <1 mm.

	TS @ 130 kHz (dB)	**TS @ 200 kHz (dB)**	**TS @ 455 kHz (dB)**	**TS @ 769 kHz (dB)**	**Citation**
Siphonophore pneumatophores	-80	-70	-80	-80	Warren, 2001
Euphausiids	-69.93	-71.04	-73.46	-71.56	ZooScatR package (mean length 18.1 mm, length-to-girth ratio 10.5) (Gastauer et al., 2019)
Large copepods	-147.6	-140.2	-126.0	-117.1	Warren calculation using mean + 1 SD copepod size (0.75 + 0.34 mm)
Small copepods	-157.4	-149.9	-135.7	-126.6	Warren calculation using mean copepod size (0.75 mm)
C. finmarchicus	-129.7	-122.3	-108.3	-99.9	Warren calculation using mean *C. finmarchicus* size (2.17 mm)

Table 4. Modelling experiments for expected backscatter with model name, contents, and justification.

Expected Backscatter Model	**Model Contents**	**Hypothesis and Reasoning**
$Sv_{(net)}$	Copepods, euphausiids, and siphonophore pneumatophores	Poor correlation – echosounder is better than MultiNet at measuring full community

$Sv_{(copepod)}$	Copepods only	Good correlation – echosounder and MultiNet measure copepods equally well, many types of copepods in the water
$Sv_{(cfin)}$	Stage C5 C. finmarchicus only	Good correlation – echosounder and MultiNet measure copepods equally well, this is the target organism of the thesis

2.6 OPC sample processing

Each OPC cast was manually inspected to determine where the cage switched from descending to ascending, in order to determine the cutoff point for usable OPC data. Once these cutoff points were determined, the *opcr* package (Johnson, 2021) was used, first to visualise any issues with the data (such as high attenuance or a slow descent rate) and then convert particle counts into particle density (particles/m^3) at 1 m depth intervals following the procedures in Herman (1992) and Baumgartner (2003). The median and interquartile ranges of the abundance of particles in the 1.5 to 2 mm ESD size range were calculated as a function of depth and grouped by basin; this size range was chosen because it is the optimum detection range for *C. finmarchicus* (Baumgartner, 2003). The calibration formula in Baumgartner (2003) was then used to derive an estimate of C5 *C. finmarchicus* abundance from the OPC particle abundance.

2.7 Biological zooplankton sample processing

For each MultiNet sample (n = 80), species composition and abundance were measured by Natasha Hynes, the Davies Lab technician and trained zooplankton taxonomist, following the same protocol as the Atlantic Reference Lab at the Huntsman Marine Sciences Centre. First, all macrozooplankton in each sample were counted and identified. Then, the mesozooplankton fraction was split until it contained, estimated by sight alone, between 200 and 300 animals. All animals in this fraction were counted and identified to a reasonable degree of taxonomic resolution; in this case, a reasonable degree is based on taxonomist ability, familiarity with the species in the region, and time restraints. Copepodite *C. finmarchicus* and *C. hyperboreus* were staged in addition to being identified. If less than 75 *C. finmarchicus* were in the split, a second split was sorted with only *C. finmarchicus* being identified and counted. This second split and count was done to obtain as accurate an estimation of *C. finmarchicus* count in the sample as possible in the case of low abundances. The abundance in each sample was determined by multiplying the counts by the split fraction.

In addition, length and width data were obtained for macrozooplankton, dominant mesozooplankton, *C. finmarchicus* stages C3 to C6, and any zooplankton with a gas bladder until a normal distribution of data was obtained (Van Guelpen et al., 1982). Normality was assessed by examining the length distribution histogram. Obtaining a size distribution for zooplankton groups of interest was necessary for acoustic modeling, as size distribution is an important factor in determining modelled backscatter.

Depth-integrated densities (individuals/m^3) were calculated by dividing abundance by the total volume of water measured the MultiNet flowmeter (obtained using OceanLab 3). Depth-specific densities (individuals/m^2) could then be calculated by multiplying the depth-integrated density for each taxa by the depth interval sampled by each net. An approximation of biomass (g/m^3) for copepods and euphausiids was calculated by multiplying density by individual dry weights (IDWs), found in the literature, for each species (Table 3).

The zooplankton samples were grouped into four community composition categories for the purpose of comparing with the echosounder data. In order to do so, the biomasses in g/m^3 of small copepods, *C. finmarchicus*, and Euphausiidae. in each net were obtained and examined to see which was the largest. If the largest biomass value was less than 0.015 g/m^3 (value chosen after examining a histogram of log-transformed biomasses by net and determining what value ~90% of biomass values were above), the label "Low biomass" was assigned to that net. If the largest biomass value was greater than 0.015 g/m^3, a label was assigned based on the group that had the largest absolute biomass value: "Small copepod dominant," "*C. finmarchicus* dominant," or "Euphausiid dominant." This procedure was repeated for every net in each tow, and for each tow in the data, until all nets were assigned one of four community composition categories. It was important to categorize low biomass nets separately from other nets so that nets with a large proportion of one taxon but very little biomass in total did not skew any potential influence of community composition on observed backscatter.

Table 5. Recorded copepod species in all the samples, their individual dry weights (IDWs), and citation for the dry weight value. Siphonophore IDW was assumed to be negligible, due to their tiny size and gelatinous nature.

Taxonomic Name	**IDW (µg)**	**Citation**
Acartia sp.	4	McClatchie, 1985
Centropages sp.	40	McClatchie, 1985
Eurytemora herdmani	6.745	Escribano and McLaren, 1992***
Metridia longa	262	Bamstedt and Ervik, 1984
Metridia lucens	70.95	Smith and Lane, 1988***
Metridia sp.	166.475	Average of *M. longa* and *M. lucens* values
Microcalanus spp.	6.98	Kosobokova and Hopcroft, 2010*
Microsetella norvegica	3.05	Kosobokova and Hopcroft, 2010*
Oithona atlantica	2.87	Weydmann et al., 2014**
Oithona similis	3.00	Kosobokova and Hopcroft, 2010*
Paracalanus spp.	5.55	Uye, 1982
Paraeuchaeta norvegica	200	Weydmann et al., 2014**
Paraeuchaeta sp.	200	Weydmann et al., 2014** (assumed to all be *P. norvegica*)
Pleuromamma robusta	379	Atkinson, Ward, and Murphy, 1996
Pseudocalanus spp.	11	McClatchie, 1985
Temora longicornis	2.5	Weydmann et al., 2014**
C. finmarchicus (stage I)	4.1	Smith and Lane, 1988
C. finmarchicus (stage II)	7.6	Smith and Lane, 1988
C. finmarchicus (stage III)	18.6	Smith and Lane, 1988
C. finmarchicus (stage IV)	51.9	Smith and Lane, 1988
C. finmarchicus (stage V)	156.1	Smith and Lane, 1988
C. finmarchicus (stage VI female)	268.3	Smith and Lane, 1988
C. glacialis (stage IV)	227	Sorochan et al., 2019
C. glacialis (stage V)	514	Sorochan et al., 2019
C. hyperboreus (stage IV)	304	Sorochan et al., 2019
C. hyperboreus (stage V)	1145	Sorochan et al., 2019

Calanus sp.	269.66	Average of all *Calanus* sp. IDWs across species and stages
Euphausiids****	29750	McClatchie, 1985

* Calculated by dividing mean g/m^2 by mean abundance/m^2 to obtain IDW
** Calculated by dividing maximum g/m^2 by maximum abundance/m^2 to obtain IDW
*** Average of all given IDWs in paper for different sexes/stages
**** *Meganyctiphanes norvegica* was the most common euphausiid collected; its IDW was used for all collected euphausiids

2.8 Data and statistical analysis

Statistics describing the variation in zooplankton density and biomass among depth strata and Basin were derived using all MultiNet and OPC tows collected within each Basin. Descriptive statistics included the relative proportion of each taxon, and mean, median, standard deviation, standard error and/or interquartile range of density or biomass. An ANOVA test was performed to determine whether the concentrations of stage 5 *C. finmarchicus* differed significantly based on basin or net depth. Because absolute net depth varied across tows, nets were post-hoc grouped into "deep" (nets 1 to 3) and "shallow" (nets 4 and 5) categories. The effects of net depth and basin were tested individually and interactively.

Each tow was matched with the echosounder downcast that was collected closest to a MultiNet station in time and space. This was done so that the expected and observed acoustic backscatter from the same sampling area could be compared using linear regression. Echosounder backscatter (either unmasked or masked) was then integrated over the net interval depths from the corresponding MultiNet tow. Z-scores for scattering in each frequency band were computed so that a direct comparison could be made between scattering in the 0 to 130 kHz band (with values ranging from -90 to -15 dB) and scattering in the other three frequency bands (with values ranging from 0 to

20 dB). For this calculation, the depth-integrated mean scattering from all dives in each basin was used to obtain the z-scores of mean scattering from all dives in 10m depth bins from 5m to the seafloor.

Least-squares linear regression analysis was performed to compare the observed scattering from the echosounder ($S_{v(echo)}$) to three models of expected scattering derived from the MultiNet data: Model 1 - modeling backscatter of all possible taxa in the net ($S_{v(net)}$), Model 2 - only copepod backscatter ($S_{v(copepod)}$), and Model 3 – only stage C5 *C. finmarchicus* backscatter ($S_{v(cfin)}$). Frequency band, basin, and community composition were also tested for their effects on the correlation. This regression was used to investigate how well the expected and observed backscatter matched; in other words, how well the net and the echosounder agreed. If there was perfect agreement between the net and echosounder, then one would expect all points to fall on the line $y = x$ and have an R^2 value of 1 in every group. The best performing model will be chosen based on correlation significance, as well as how closely it approaches the line $y = x$.

Results

3.1 Zooplankton community structure and distribution

Zooplankton species assemblages differed between Owen Basin and Grand Manan Basin, as well as among depth strata within each basin. This section describes these differences, focusing on those that are relevant to the detection of zooplankton by the echosounder.

Within Owen Basin, eight taxa accounted for approximately 90% of the total concentration (individuals/m^3) of net samples: *Centropages typicus*, *Oithona similis*, *Paracalanus* spp. *Temora longicornis*, *Calanus finmarchicus*, *Pseudocalanus* spp., Bryozoan larvae, and *Evadne nordmanni*. Of these, six are copepod species, whereas Bryozoan larvae and *E. nordmanni* (a type of cladoceran) are the only non-copepod species present in significant concentrations. By biomass, four taxa were responsible for 90% of the total biomass (g/m^3) of the Owen Basin samples: *C. typicus*, *C. finmarchicus*, *Meganyctiphanes norvegica*, and *Paracalanus* spp. *M. norvegica* is a euphausiid (krill) species; the other three are copepod taxa. *C. typicus* and *Paracalanus* spp. are small copepod taxa, whereas *C. finmarchicus* is a large, lipid-rich copepod.

Within Grand Manan Basin, seven taxa accounted for approximately 90% of the total concentration (individuals/m^3) of net samples: *C. typicus*, *Paracalanus* spp., *C. finmarchicus*, *O. similis*, *Pseudocalanus* spp., Siphonophora (nectophores only), and *Metridia lucens*. All of these taxa are copepods except the Siphonophora, which are gelatinous zooplankton. In terms of biomass, five taxa were responsible for 90% of the

total biomass (g/m^3) of the Grand Manan Basin samples: *C. finmarchicus*, *C. typicus*, *M. norvegica*, *M. lucens*, and *Calanus glacialis*. The only non-copepod species present in this high-biomass group was the euphausiid *M. norvegica*. *M. lucens* is a small copepod and *C. glacialis* is a large copepod.

Two dominant copepod species were chosen to be compared in more detail: one that is normally present in high abundance in both coastal and offshore waters (*C. typicus*) and one that is usually more abundant in offshore waters than coastal waters (*C. finmarchicus*). *C. typicus* was the most commonly sampled species by concentration in both basins, comprising a mean of 36% (± 3.8% S.E.) of the total Owen Basin concentrations and a mean of 28% (± 2.7% S.E.) of the total Grand Manan Basin concentrations of all taxa (Figure 13). *C. typicus* accounted for a mean of 52% (± 7.8% S.E.) of the biomass from Owen Basin and a mean of 22% (± 4.1% S.E.) of the biomass from Grand Manan (Figure 14). On average, *C. finmarchicus* accounted for only 5% (± 1.2% S.E.) of the total Owen Basin concentration and 21% (± 3.5% S.E.) of the total Grand Manan Basin concentration (Figure 13). *C. finmarchicus* was about twice as abundant in terms of mean relative biomass in Grand Manan Basin (47 % ± 4.0% S.E.) than in Owen Basin (23 % ± 5.3% S.E.).

Other copepod species that were more abundant in Owen Basin than in Grand Manan Basin included *T. longicornis* and *O. similis* (Figure 13). While *C. finmarchicus* was the only copepod species that was more abundant in Grand Manan Basin than in Owen Basin, the two euphausiid taxa, *Meganyctyphanes* and *Thyssanoessa*, and Siphonophora were all more abundant in Grand Manan Basin than in Owen Basin (Figures 13 and 14).

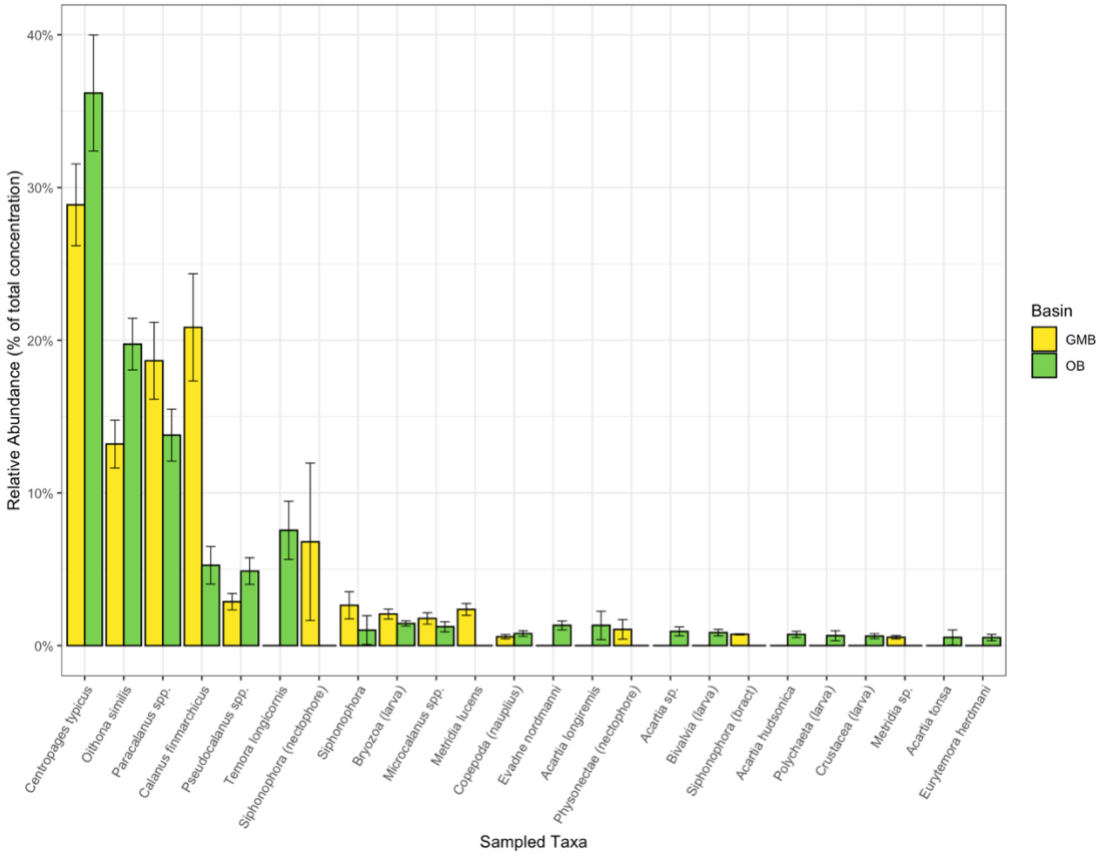

Figure 13. Bar plot depicting the mean ± 1 standard error of the depth-integrated proportional concentration of selected sampled zooplankton taxa sampled in either Owen Basin (OB, green bars) or Grand Manan Basin (GMB, yellow bars) in the Bay of Fundy (n = 16 total tows, 8 per basin). Only taxa which comprised an average of ≥ 0.5% of the total zooplankton concentration are plotted.

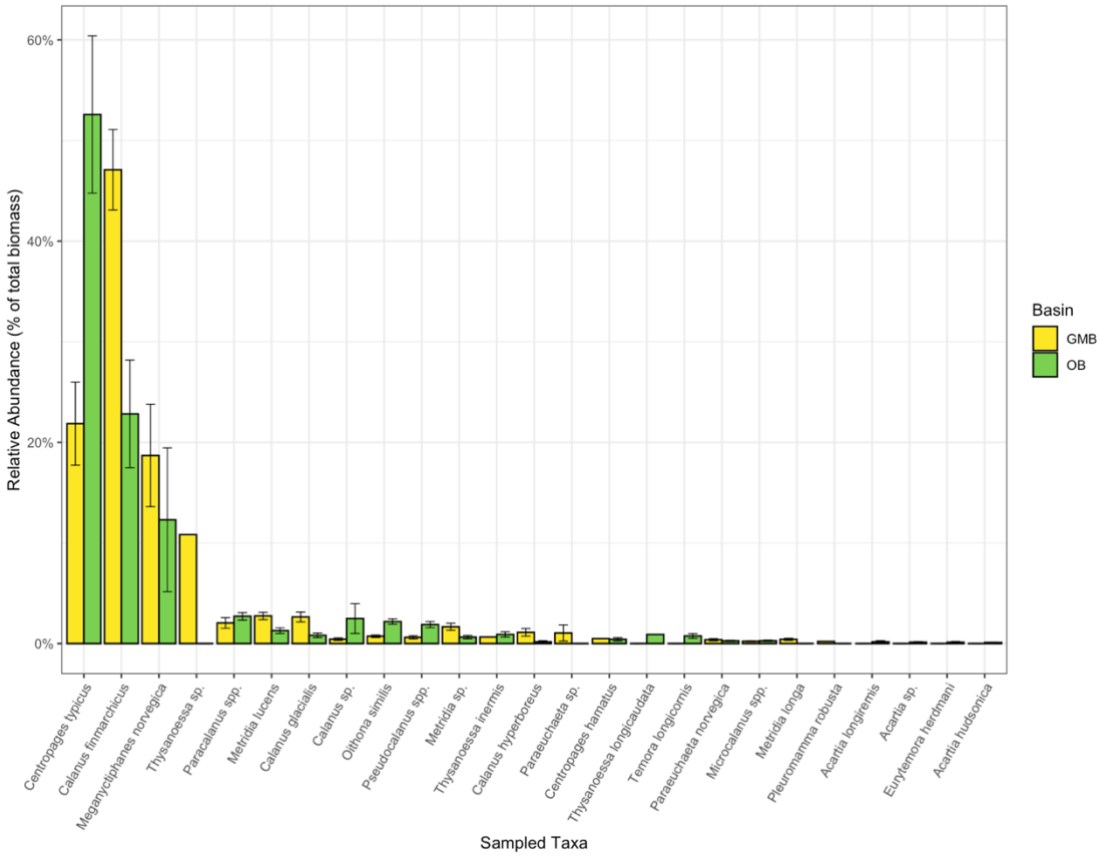

Figure 14. Bar plot depicting the mean ± 1 standard error of the depth-integrated proportional biomass of selected sampled zooplankton taxa sampled in either Owen Basin or Grand Manan Basin in the Bay of Fundy (n = 16 total tows, 8 per basin). Only taxa which comprised an average of ≥ 0.1% of the biomass, and for which literature values of individual biomass exist, are plotted.

Zooplankton taxa were generally distributed in depth-stratified layers, and different taxa dominated in different depth strata (Figure 15). Small copepods were present in every net and at every depth sampled but were generally most abundant at shallower net depths (net 5; 525 mean ± 88.1 S.E. individuals/m^3 OB; 590 ± 110 individuals/m^3 GMB). Siphonophore body parts were also most common in the shallowest nets (nets 4 and 5; 22.6 ± 11.5 individuals/m^3 OB; 36.5 ± 19.3 individuals/m^3 GMB), with gas-bearing pneumatophores found more rarely and in

different nets than the gelatinous bracts, nectophores, or colonies. Euphausiids, when present, were concentrated in the midwater nets (nets 3 and 4; 3.19 ± 3.13 individuals/m^3 OB; 2.11 ± 0.74 individuals/m^3 GMB), and were more common in Grand Manan Basin than Owen Basin. Finally, late-stage *C. finmarchicus* and other large copepods were present most often in the deepest nets (nets 1, 2 and sometimes 3, >100 m depth), becoming rarer as net depth decreased.

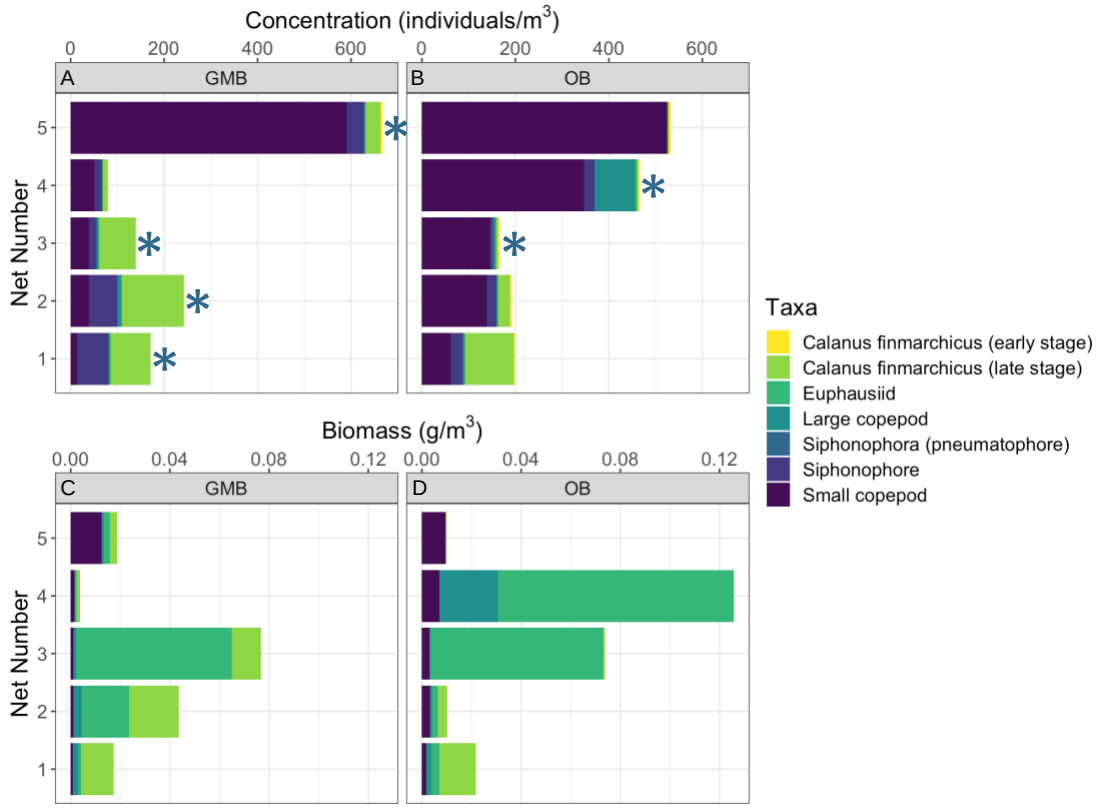

Figure 15. Mean net- and basin-specific abundance of dominant zooplankton taxa, expressed in either concentration (A, B), or biomass (C, D) units. A blue star next to the bar signals that siphonophore pneumatophores were found in the net. This figure shows how taxonomic dominance changes among both depth (net) strata and basins. In Grand Manan Basin, each net's depth interval is larger than in Owen Basin due to Grand Manan Basin's deeper depth. See Appendix B for data from each MultiNet individually, which includes depth ranges for each net.

It is important for later analyses to quantify which taxon was most dominant in a given plankton layer, as I tested whether they affect the correlation between the net and the echosounder at a particular frequency in that layer. For example, larger organisms exhibit more net avoidance, but are detected by the echosounder across a broad range of frequencies. By biomass, the most common dominant taxa in the nets was small copepods (total n = 36 nets), followed by *C. finmarchicus* (total n = 23 nets). *C. finmarchicus*-dominant nets were more common in Grand Manan Basin, while small copepod-dominant nets were more common in Owen Basin (Figure 15, Table 6). Euphausiid dominance was most common in Grand Manan Basin, and always occurred in nets 2 to 4 (i.e., mid-water to deep nets). Nets with low total biomass (i.e., collected samples outside of plankton layers) also most commonly occurred in Grand Manan Basin and always occurred in nets 1, 3, or 4 (Table 6).

Table 6. The number of nets over all tows in plankton layers dominated by certain taxa, or with biomass less than 0.015 g/m^3 in the case of the "low biomass" category.

Dominant Taxa	**n (GMB)**	**n (OB)**
C. finmarchicus	15	8
Euphausiid	6	2
Low biomass	8	5
Small copepods	11	25

3.2 *C. finmarchicus* distribution

C. finmarchicus was the primary species of interest for this thesis, therefore more refined information about their distribution and the distribution of their various life stages was examined. The highest late-stage *C. finmarchicus* concentrations were

found in the deepest nets (Table 7). Median late-stage *C. finmarchicus* concentrations were always less than 300 individuals/m^3 (Table 7). Most *C. finmarchicus* caught in the nets were at the diapausing C5 stage and were aggregated deep in the water column. This pattern was more apparent in Grand Manan Basin than in Owen Basin, but the high standard deviations of the abundance indicate a patchy distribution of *C. finmarchicus* at shallow and deep depths. When a two-way ANOVA was performed to test the effect of study basin and depth (shallow vs deep nets) on the log10 of concentrations of stage C5 *C. finmarchicus*, it was found that only net depth had a significant effect ($p < 0.05$).

Table 7. Median (± 1 SD) *C. finmarchicus* concentrations (individuals/m^3) for stages IV, V, and VI (female) in shallow water strata (nets 4 and 5; from ~70 m depth to the surface) and deep water strata (nets 1 to 3; from below ~70 m to 10 m above seafloor) in each of the two sampled basins.

Basin	**Stage**	**Surface Strata Concentration (individuals/m^3)**	**n**	**Deep Strata Concentration (individuals/m^3)**	**n**
GMB	All stages	70.1 ± 47.1	16	300.0 ± 272.0	24
GMB	IV	24.1 ± 31.5	16	17.0 ± 17.9	24
GMB	V	21.5 ± 18.5	16	280.0 ± 252.0	24
GMB	VI (female)	0.691 ± 0.780	16	3.88 ± 7.73	24
OB	All stages	20.0 ± 7.82	16	51.0 ± 251.0	24
OB	IV	0 ± 4.77	16	8.56 ± 57.4	24
OB	V	0 ± 3.15	16	27.2 ± 201.0	24
OB	VI (female)	0 ± 0.0808	16	1.04 ± 5.06	24

OPC data were used to describe the fine-scale vertical distribution of *C. finmarchicus* in the water column. Due to sporadically malfunctioning equipment, only

approximately half of the OPC casts returned usable data (see Appendix C for full list of OPC casts). Concentrations peaked at around 1750 C5 individuals/m^3 at ~130 m depth in Owen Basin, and around 2500 C5 individuals/m^3 in Grand Manan Basin at ~180 m depth. In both basins, mean C5 concentrations were low (close to 0) until around 80 m, and gradually increased from that point to the bottom of the sampled depth, remaining relatively constant near 25 to 50 individuals/m^3 from 80 m until the bottom of the sampling depth, where they jumped up considerably by orders of magnitude. Layers were relatively thin compared to the depth of the water column, with the deepest layer of *C. finmarchicus* C5 individuals in Grand Manan Basin being only about 5 m in thickness; however, the OPC does not sample the last ~ 10 m of the water column, so this is a minimum estimate of thickness. Estimated abundance of C5 in Owen Basin ranged from a minimum median of 0 to a maximum median of 50 individuals/m^3; in Grand Manan Basin, the range of the median particle abundance was 0 to 1393 individuals/m^3.

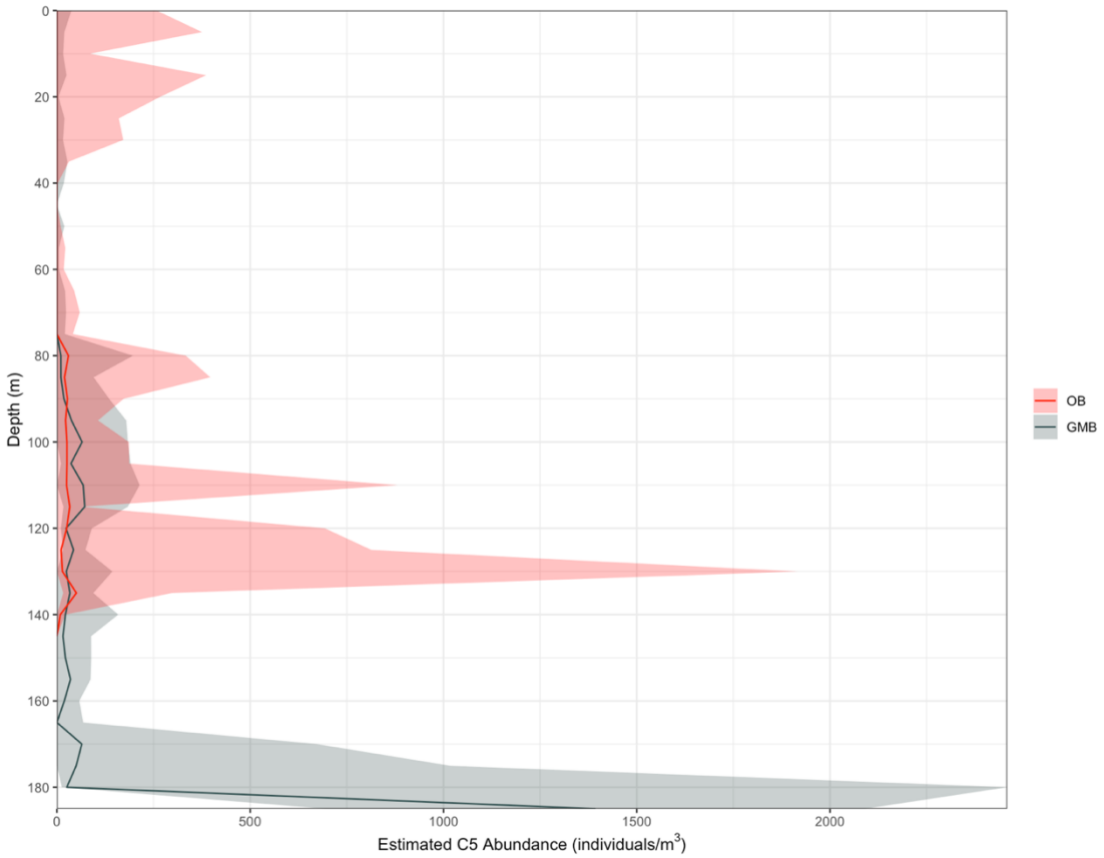

Figure 16. Vertical distribution of median (line) and interquartile ranges (shaded area) of estimated C5 *C. finmarchicus* abundance in Owen Basin and Grand Manan Basin. Conversion equation for C5 abundance from OPC particle abundance taken from Baumgartner (2003).

The OPC data findings are somewhat consistent with the MultiNet findings. In both basins, late-stage *C. finmarchicus* are found primarily in deep nets (Figure 15), which is consistent with OPC-derived abundance estimates increasing with depth (Figure 16). Grand Manan Basin also had greater abundances of late-stage *C. finmarchicus* than Owen Basin (Figure 15, panels A and B). Maximum abundances, and variance in abundance, derived from the OPC were higher than estimates from the MultiNet samples due to the higher sampling resolution (Figure 16; Figure 15, panels A and B). Much of the estimated C5 *C. finmarchicus* abundance is concentrated below the maximum sampling depth of the MultiNet in each basin. In Owen Basin, the maximum

sampling depth reached by the MultiNet was 132 m, whereas in Grand Manan Basin it was 167 m; both are close to or above the depth regions of maximum estimated C5 *C. finmarchicus* abundance derived from the OPC.

3.3 Echosounder data

The glider performed well during each transect, collecting CTD data and echosounder data as expected and staying on a straight-line course as it sailed with the tidal currents. The average length for glider transects was 5 nautical miles (Table 8). Zooplankton layers were observed in the echosounder data at all four frequencies (Figures 17 and 18), though layers were most evident in the 0 to 130 kHz and 200 to 455 Hz bands. Scattering layer distribution differed among frequency bands, indicating that multiple zooplankton size classes were present in the water column. For example, the distribution of layers in Figure 17, panel A, is generally contained within the midwater column, whereas in Figure 17, panel C, the strongest scattering layers are close to the seafloor.

Table 8. Summary of glider deployments in September 2020 in the Bay of Fundy.

Glider Deployment #	Date	Basin	Start Location (lat, lon)	End Location (lat, lon)	Transect Length (nautical mi)
1	19 Sept 2020	Owen Basin	44.88213°N 66.79711°W	44.83086°N 66.82842°W	6.84
2	20 Sept 2020	Owen Basin	44.84092°N 66.80919°W	44.89429°N 66.76427°W	4.09
3	21 Sept 2020	Grand Manan Basin	44.68147°N 66.49182°W	44.77272°N 66.48444°W	5.62
4	24 Sept 2020	Grand Manan Basin	44.68054°N 66.49347°W	44.75926°N 66.48219°W	5.49
5	25 Sept 2020	Grand Manan Basin	44.67662°N 66.49668°W	44.72413°N 66.50217°W	3.60
6	26 Sept 2020	Owen Basin	44.90078°N 66.78047°W	44.83562°N 66.81733°W	4.30

The echosounder data returned results that were broadly consistent with the MultiNet and OPC data, showing shallow, midwater, and deep scattering layers in most profiles in both Owen Basin and Grand Manan Basin. Some interesting features were particularly evident in the spectrogram data. Overall, the depth distribution of scattering in the 130 to 200 and 200 to 455 kHz bands were more similar to each other (Figures 17 and 18, panels F and G) and differed markedly from the other two frequency bands. Scattering was typically stronger over all frequencies in Grand Manan Basin than in Owen Basin, with the exception of the 200 to 455 kHz band, and there was a strong scattering layer in shallow waters present in Owen Basin that was absent in Grand Manan Basin (Figures 17 and 18 panels A to D). A deep layer of small scatterers near the ocean floor was particularly evident in the 200 to 455 kHz data (Figure 18, panel C). This is consistent with the deep *C. finmarchicus* layer seen in the MultiNet data (Figure 15) and OPC data (Figure 16). However, where the OPC measured a minimum layer

thickness of 5 m, the echosounder indicated a thickness of 30 to 40 m. This discrepancy is because the OPC does not sample close to the bottom, where most of the biomass was located.

In Owen Basin, scattering layers were visible in the average backscatter of the 130 to 200 kHz and 200 to 455 kHz frequency bands in shallow (<25 m) and deep (>115 m) depths (Figure 17, panels F and G). In contrast, in the 455 kHz to 769 kHz frequency band, frequency differences were lower overall than in the other frequency bands, and the largest decibel differences were found in the midwater column (75 m to 125 m) (Figure 17, panel H). This is consistent with the MultiNet data, where small copepods were found throughout the water column and non-*C. finmarchicus* large copepods were found in shallower nets (Figure 15, panels B and D). Finally, a layer of euphausiids was visible in the midwater column in the 0 to 130 kHz frequency band (Figure 17, panels A and E; note that in panel E, a less negative value means a stronger returning echo), which is also consistent with the MultiNet samples (Figure 15, panel D).

By contrast, in Grand Manan Basin, there was only one scattering layer in the 130 to 200 kHz and 200 to 455 kHz frequency bands, at deep depths (>145 m). In the highest frequency band (455 kHz to 769 kHz), greater decibel differences were found in shallow water (< 45 m) (Figure 18, panels F to H). This is also generally consistent with the patterns in MultiNet and OPC data, wherein small copepods were found in shallow water and large copepods (including late-stage *C. finmarchicus*) were found in deeper water (Figure 15, panels A and C). As in Owen Basin, there is evidence of midwater scattering by euphausiids in the 0 to 130 kHz band (Figure 18, panel E). It is important

to note that in the 200 to 455 kHz band, the greatest average decibel differences are found below the deepest depths sampled on average by the nets (Figure 18, panel G).

Figure 19 depicts the z-scores of the data in Figures 17 and 18, panels E to H to simultaneously and more easily visualise the depth patterns among frequencies. The layering of backscattering z-scores is also broadly consistent with the MultiNet data (Figure 19). In Owen Basin, more positive z-scores in the 455 to 769 kHz frequency band were found in very shallow and midwater to deep water depth bins, whereas positive z-scores in the 130 to 200 kHz and 200 to 455 kHz frequency bands were mostly confined to depths below 115 m (Figure 19, panel A); this pattern mirrors the distribution of small copepods and *C. finmarchicus*/other large copepods, respectively (Figure 15, panels B and D). In Grand Manan Basin, layers of positive z-scores in the 455 to 769 kHz frequency bands were located in shallow (< 65 m) water, versus layers of positive z-scores in the 130 to 200 kHz and 200 to 455 kHz frequency bands in deep (> 165 m) water (Figure 19, panel B). This again is similar to where small copepods and *C. finmarchicus* were found in the MultiNet tows (Figure 15, panels A and C). Finally, scattering in the 0 to 130 kHz frequency band, which most likely comes from euphausiids, was seen in both basins in the middle of the water column (75 to 165 m) (Figure 19). Euphausiids were primarily collected by the MultiNet at these midwater depths. There is a layer of shallow water scattering evident in Grand Manan Basin in the 0 to 130 kHz frequency band that is absent in the MultiNet data (Figure 19, panel B); this was likely from euphausiids that were too large to be captured by the nets.

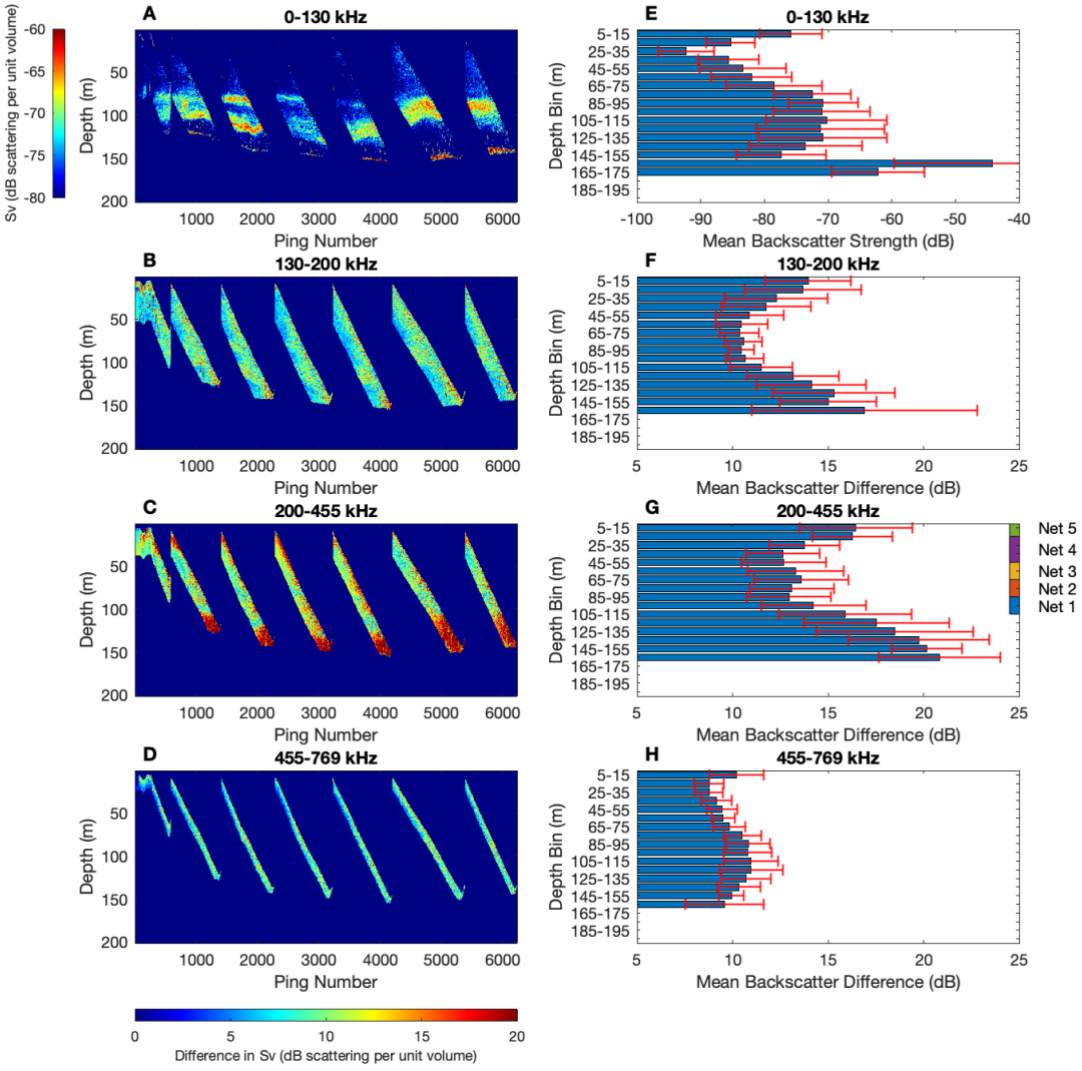

Figure 17. A to D: Fully processed and differenced echosounder data collected in Owen Basin on September 20th, 2020. Each panel represents acoustic scattering from zooplankton in the (A) 0 to 130 kHz, (B) 130 to 200 kHz, (C) 200 to 455 kHz and (D) 455 to 769 kHz bands, respectively. Ping number refers to the 1 Hz echosounder acoustic pulse as the glider moves across the basin. The direction of the transect pictured is from the southwestern edge of Owen Basin towards the centre in the northeast (see map in Figure 4). Hotter colours indicate higher zooplankton biomass in the water column. Panel A's colour scale is different from panels B through D as panel A is a single frequency's worth of acoustic data, while panels B through D are the decibel difference between two frequencies. E to H: Averaged decibel/decibel differences in the four frequency bands across all dives in Owen Basin. Red error bars are the standard error of the mean. Nets 1 through 5 in panel G are the average MultiNet net depths for tows in Owen Basin.

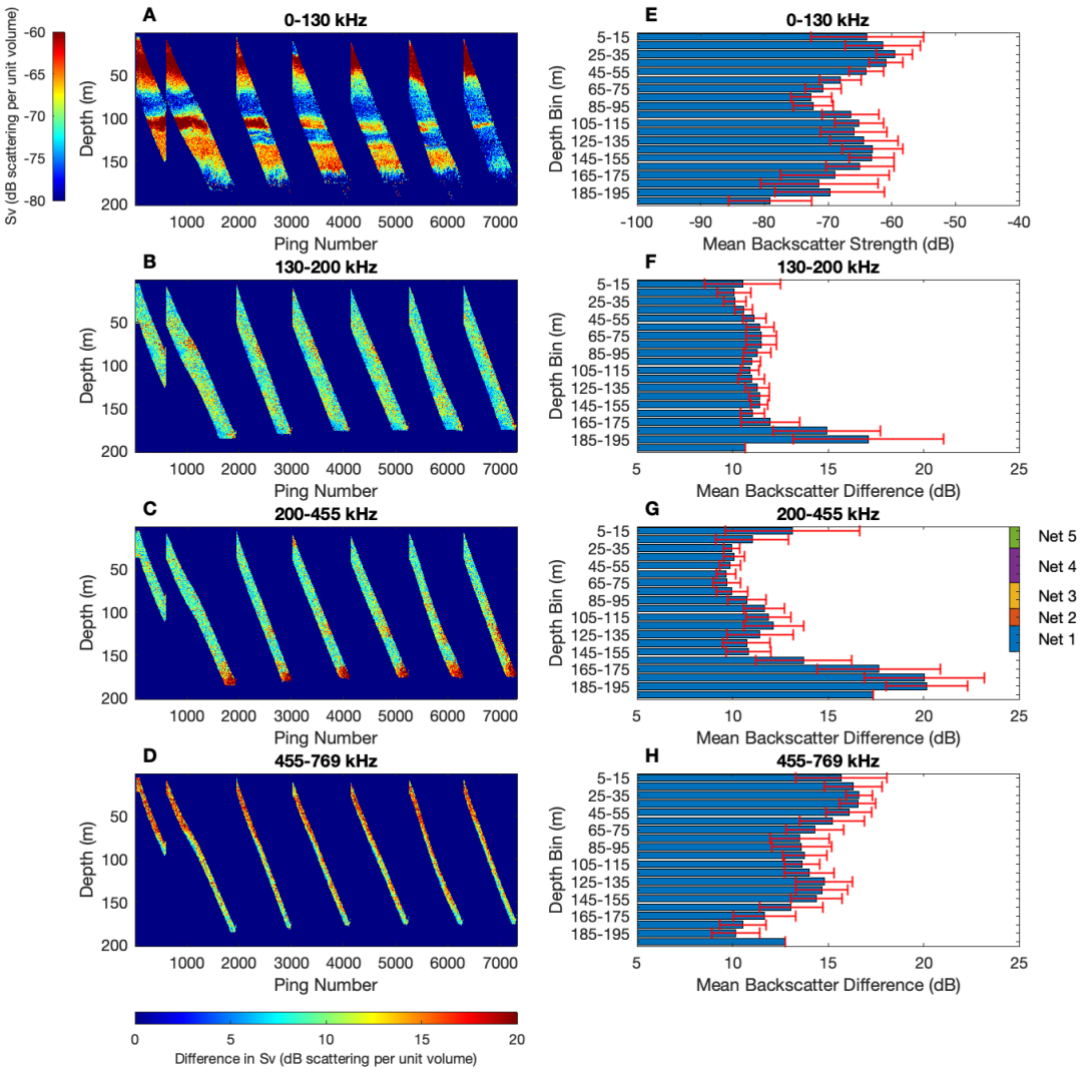

Figure 18. A to D: Fully processed and differenced echosounder data collected in Grand Manan Basin on September 21st, 2020. Each panel represents acoustic scattering from zooplankton in the (A) 0 to 130 kHz, (B) 130 to 200 kHz, (C) 200 to 455 kHz and (D) 455 to 769 kHz bands, respectively. The direction of the transect pictured is from near the middle of the basin to the northern edge (see map in Figure 4). Panel A's colour scale is different from panels B through D as panel A is a single frequency's worth of acoustic data, while panels B-D are the decibel difference between two frequencies. E to H: Averaged decibel/decibel differences in the four frequency bands across all dives in Grand Manan Basin. Red error bars are the standard error of the mean. Nets 1 through 5 in panel G are the average MultiNet net depths for tows in Grand Manan Basin.

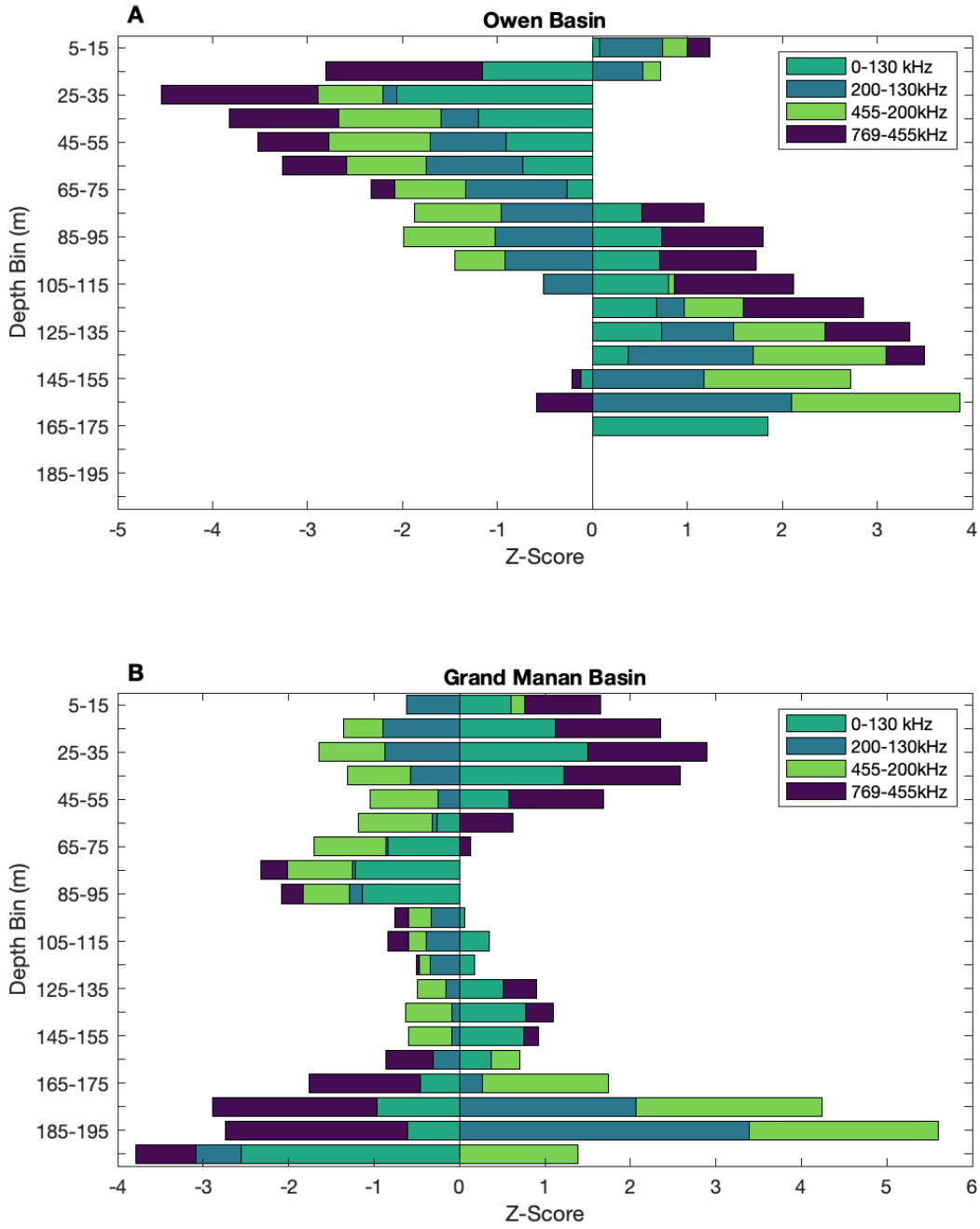

Figure 19. Standardised z-scores of averaged backscatter from Owen Basin (A) and Grand Manan Basin (B). One outlier in Owen Basin was removed. Bars are colour-coded by which taxa from Figure 15 was most likely to have produced the echoes in the corresponding frequency band; scattering in the 130 to 200 kHz and 200 to 455 kHz bands was likely produced by a mixture of *C. finmarchicus* and other large copepods, but the bars have been made distinct colours for legibility.

3.4 Correlation between backscatter derived from MultiNet and glider-echosounder

Correlations between masked $S_{v(echo)}$ and all $S_{v(net)}$ models were significant ($p < 0.05$) in every frequency band, and slopes were always less than one (Table 9). $S_{v(net)}$ also underestimated $S_{v(echo)}$ in all frequencies; this is normal and expected behaviour and is explained in the discussion section.

The correlation between expected and observed backscatter behaved normally for the expected backscatter from the entire net and the expected backscatter from *C. finmarchicus* only. The linear models using masked $S_{v(echo)}$ and $S_{v(net)}$ (Model 1), and masked $S_{v(echo)}$ and $S_{v(cfin)}$ (Model 3), had slopes greater than 0 in all frequency bands and approached the line $y = x$ as frequency increased (Figure 20, panels A and C; Table 9). Model 3 slopes were generally less than Model 1 slopes, but Model 1 R^2 values were generally less than Model 3 R^2 values (Table 9). Overall, Models 1 and 3 exhibited similar trends and explained a similar amount of variation in the dataset (Figure 20, panels A and C). In the 200 to 455 kHz and 455 to 769 kHz frequency bands, the linear model parameters were nearly identical between the two expected backscatter models, and R^2 values ranged from 0.15 to 0.20 (Table 9)

For the correlation between expected backscatter from copepods only and observed backscatter, I found an unusual result. The linear models using masked $S_{v(echo)}$ and $S_{v(copepod)}$ (Model 2) had slopes less than 0 in all frequency bands (Figure 20, panel B; Table 9). This result is not typical behaviour from the model, and potential reasons for it are explained in the discussion section.

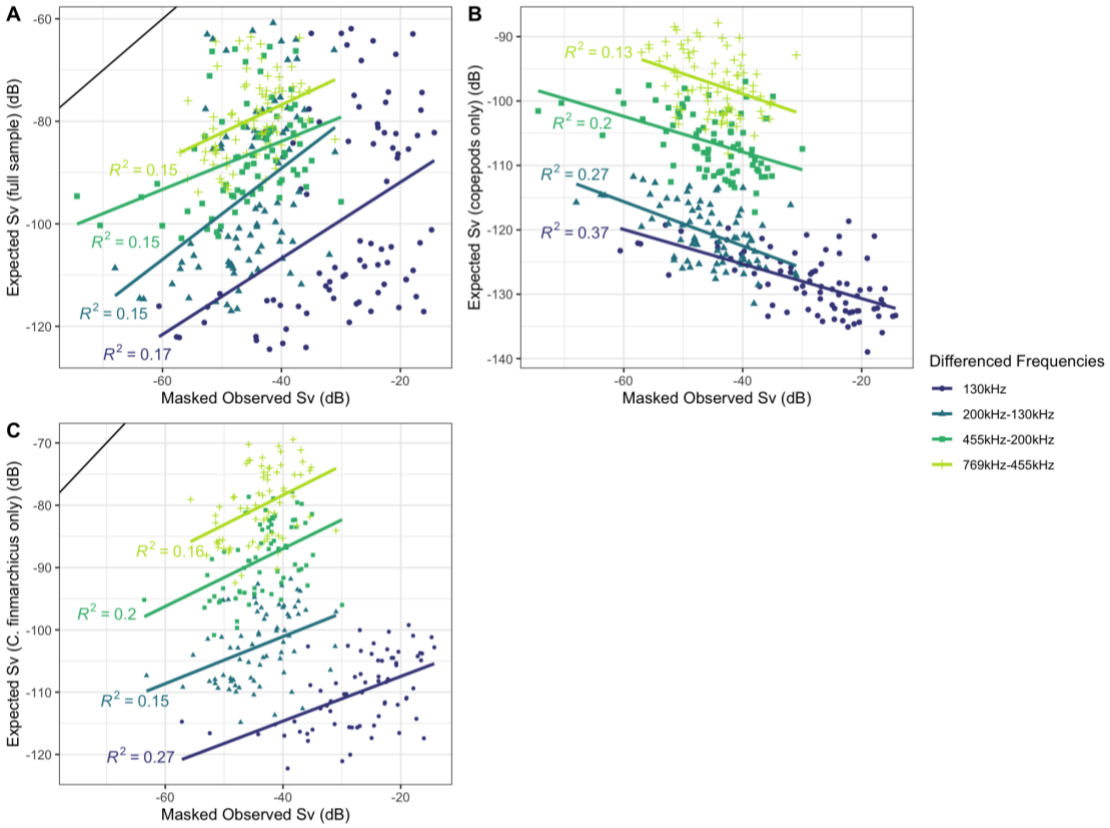

Figure 20. Scatter plots with linear models of masked $S_{v(echo)}$ correlated with $S_{v(net)}$ (A), $S_{v(copepod)}$ (B), and $S_{v(cfin)}$ (C). Black line in the upper left-hand corner of panels A and C is the line $y = x$, which would be a perfect 1:1 agreement between the observed and expected S_v values.

Table 9. Linear model regression coefficients for all nets (n = 80 nets) for the correlation between $S_{v(echo)}$ and various $S_{v(net)}$ models. Regression included only the frequency band as a grouping variable.

$S_{v(net)}$ Model	**Frequency Band (kHz)**	**Slope**	**Intercept**	**R^2**	**p-value**	**RMSE**
Model 1 - $S_{v(net)}$	0 to 130	0.74 ± 0.18	-76.9 ± 5.81	0.17	0.0001	24.85
Model 1 - $S_{v(net)}$	130 to 200	0.94 ± 0.24	-51.4 ± 11.01	0.16	0.0002	18.08
Model 1 - $S_{v(net)}$	200 to 455	0.47 ± 0.13	-65.0 ± 5.89	0.15	0.0004	17.05
Model 1 - $S_{v(net)}$	455 to 769	0.55 ± 0.15	-54.9 ± 6.70	0.15	0.0004	20.48
Model 2 - $S_{v(copepod)}$	0 to 130	-0.27 ± 0.04	-136.1 ± 1.25	0.37	<0.0001	16.52
Model 2 - $S_{v(copepod)}$	130 to 200	-0.36 ± 0.06	-137.1 ± 2.95	0.29	<0.0001	14.38
Model 2 - $S_{v(copepod)}$	200 to 455	-0.28 ± 0.06	-119.0 ± 2.86	0.20	<0.0001	12.80
Model 2 - $S_{v(copepod)}$	455 to 769	-0.31 ± 0.09	-111.5 ± 4.15	0.13	0.0001	18.56
Model 3 - $S_{v(cfin)}$	0 to 130	0.36 ± 0.07	-100.09 ± 2.01	0.28	<0.0001	24.13
Model 3 - $S_{v(cfin)}$	130 to 200	0.40 ± 0.11	-84.73 ± 4.91	0.17	0.0005	15.79
Model 3 - $S_{v(cfin)}$	200 to 455	0.47 ± 0.11	-68.3± 4.96	0.20	0.0001	17.41
Model 3 - $S_{v(cfin)}$	455 to 769	0.48 ± 0.13	-59.3 ± 5.79	0.16	0.0005	22.92

I tested whether correlations between $S_{v(echo)}$ and $S_{v(net)}$ were affected by the differing plankton communities sampled by the echosounder in the two study basins. First, I performed an MANOVA to test the effects of study basin and community composition on $S_{v(echo)}$ and the three $S_{v(net)}$ models. Both factors were found to have significant effects on both backscatter measurements, but their interaction was insignificant. In a post-hoc analysis of the effect of study basin on correlation, significant ($p < 0.05$) correlations with $S_{v(echo)}$ were found in each basin overall for all $S_{v(net)}$ models, and the linear models had negative slopes in every case except for Model 1 in Owen Basin.

Some interesting patterns emerged when both frequency band and basin were included as grouping variables. No matter which $S_{v(net)}$ model was used, correlations were significant in Owen Basin over all frequency bands ($p < 0.05$). Slopes for the Owen Basin linear models were positive in Models 1 and 3, and negative in Model 2, mirroring the trend when only frequency band was used as a grouping variable; R^2 values ranged from 0.15 to 0.48 (see Appendix D for full results). The results are more complicated for Grand Manan Basin. Using Model 1, there were no significant correlations ($p > 0.05$ for all frequency bands); using Model 2, there was a single significant correlation in the 130 to 200 kHz frequency band, with a negatively sloped linear model and R^2 of 0.13; and using Model 3, there were significant correlations in the 130 to 200 kHz and 455 to 769 kHz frequency bands, with positively sloped linear models. The R^2 value was 0.12 for the 130 to 200 kHz band correlation, and 0.29 for the 455 to 769 kHz band correlation.

Model correlation including community composition as a grouping variable (by itself and alongside frequency band) was also examined, for the same reason as described above. When Model 1 was used with community composition as the sole grouping variable, only *C. finmarchicus*-dominant communities had a significant correlation; the connected linear model had a negative slope and an R^2 value of 0.08 (see Appendix E for full results). Using Model 2, all communities had significant correlations with negative slopes, and R^2 values of between ~0.13 (for small copepod-dominant communities) and ~0.44 (for all other community types). All communities had significant correlations with negative slopes when Model 3 was used as well; R^2 values ranged from 0.40 (for *C. finmarchicus*-dominant communities) to 0.12 (for small copepod-dominant communities).

When both community composition and frequency band were used as grouping variables, most of the correlations were insignificant, with only a few exceptions. Using Model 1, low biomass communities had significant ($p < 0.05$) correlations in the high frequency bands (200 to 455 kHz and 455 to 769 kHz) with high (> 0.4) R^2 values; small copepod dominant nets also had a significant correlation in the 455 to 769 kHz frequency band, with an R^2 value of 0.13. With Model 2, only low biomass communities had significant correlations, in the 0 to 130 kHz and 200 to 455 kHz frequency bands ($R^2 > 0.4$ for both). Finally, the trend for Model 3 was the same as in Model 1, with low biomass communities having significant correlations in the 200 to 455 kHz and 455 to 769 kHz frequency bands, and $R^2 > 0.4$ for both models. Slope trends were the same as all other correlations; Models 1 and 3 generally had positive slopes, whereas Model 2 had negative slopes, with only a few exceptions.

3.5 Correlation between glider-echosounder backscatter and biomass

Because the ultimate goal of this thesis is to test the echosounder's ability to detect the abundance of large copepods, correlations between masked $S_{v(echo)}$ and the log10 of overall and subsets of biomass were performed (Figure 21). Correlations in all frequency bands between masked $S_{v(echo)}$ and the log10 of *C. finmarchicus* biomass within the nets had positive slopes and were significant (Table 10). R^2 values were moderately strong at all frequency bands (R^2 between 0.15 and 0.35). Correlations between masked $S_{v(echo)}$ and the total biomass were insignificant, had slopes close to 0, and had no R^2 values greater than 0.02 in any frequency band (Table 10). The same is true of correlations between masked $S_{v(echo)}$ and copepod biomass, although the correlation in the 455 to 769 kHz is only barely insignificant (Table 10). Correlations in all frequency bands between masked $S_{v(echo)}$ and the log10 of *C. finmarchicus* biomass within the nets had positive (albeit still close to 0) slopes and were significant (Table 10). R^2 values were still not particularly strong (all $R^2 < 0.4$), but were stronger than the other correlations' R^2 values.

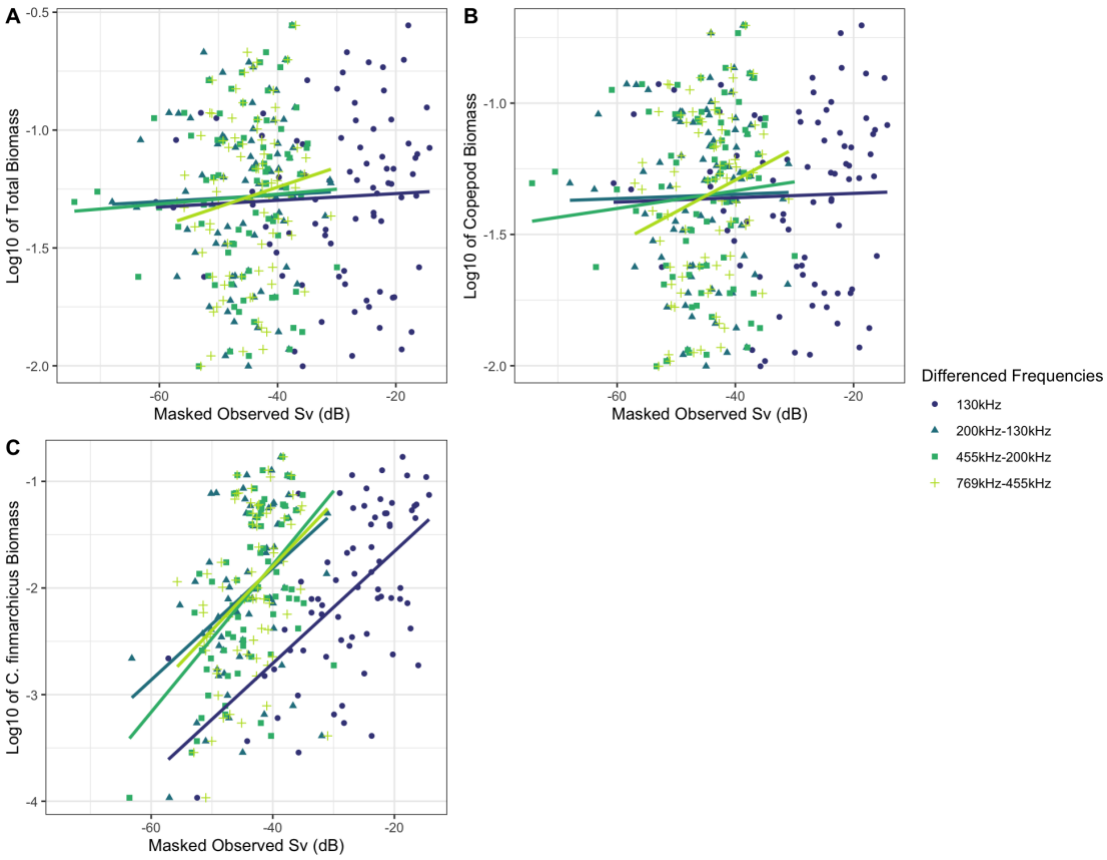

Figure 21. Correlations between masked $S_{v(echo)}$ and the log10 of total (A), copepod (B), and *C. finmarchicus* (C) biomass found within the MultiNet samples.

Table 10. Regression coefficients for correlations between masked $S_{v(echo)}$ and the log10 of biomasses. Only frequency band is included as a grouping variable.

Biomass Model	**Frequency Band (kHz)**	**Slope**	**Intercept**	**R^2**	**p-value**	**RMSE**
Total	0 to 130	0.0017 ± 0.0037	-1.23 ± 0.11	0.0028	0.6	0.34
Total	130 to 200	0.0016 ± 0.0055	-1.21 ± 0.25	0.0010	0.8	0.34
Total	200 to 455	0.0022 ± 0.0051	-1.18 ± 0.23	0.0025	0.7	0.34
Total	455 to 769	0.0084 ± 0.0071	-0.90 ± 0.32	0.018	0.2	0.35
Copepods Only	0 to 130	0.0011 ± 0.0035	-1.32 ± 0.11	0.0012	0.8	0.32
Copepods Only	130 to 200	0.00086 ± 0.0052	-1.31 ± 0.24	0.00034	0.9	0.32
Copepods Only	200 to 455	0.0035 ± 0.0048	-1.19 ± 0.22	0.0068	0.5	0.33
Copepods Only	455 to 769	0.012 ± 0.0066	-0.81 ± 0.30	0.041	0.07	0.34
C. finmarchicus Only	0 to 130	0.054 ± 0.0087	-0.57 ± 0.25	0.35	<0.0001	1.02
C. finmarchicus Only	130 to 200	0.058 ± 0.014	0.54 ± 0.62	0.20	<0.0001	0.82
C. finmarchicus Only	200 to 455	0.069 ± 0.014	1.00 ± 0.62	0.26	<0.0001	0.87
C. finmarchicus Only	455 to 769	0.060 ± 0.017	0.60 ± 0.77	0.15	0.0008	0.83

3.6 Influence of siphonophores on acoustic detection of plankton layers

While performing the correlations between expected and observed backscatter, it was noted that some MultiNet samples contained gelatinous siphonophore body parts but no pneumatophores. Therefore, to investigate a potential source of error, expected backscatter was recalculated with an assumed minimum number of pneumatophores. In this thought experiment, every net that had siphonophore parts but no pneumatophores was instead treated as if it had a single pneumatophore. It was found through a Wilcoxon signed rank test that this minimum estimate significantly ($p > 0.05$) changed the mean expected acoustic backscatter. However, when the correlation values were compared between the two types of expected backscatter (with the actual count of pneumatophores, and with a minimum estimate of pneumatophores), they were found to not be significantly different overall or when grouped by frequency or community composition ($p > 0.05$ in all cases).

Discussion

The acoustic scattering of multi-species zooplankton communities is difficult to examine, due to the many factors that can influence backscatter. It is even more challenging to draw conclusions about zooplankton biomass from acoustic observations. However, in communities which are *C. finmarchicus*-dominant and which lack scatterers that may obscure their backscatter (such as amphipods or similarly sized copepods), my analysis indicates it is possible to derive an estimate of *C. finmarchicus* biomass, with a measurable degree of certainty, using scattering from the 200 to 455 kHz frequency bands (Tables 8 and 9). Echosounder data can also be used to quantify the location of scattering layers in the water column at higher resolution and deeper depths than MultiNet systems, and in more spatial dimensions than an OPC.

4.1 Mesozooplankton layers and concentrations observed by echosounder and MultiNet

The zooplankton community of the outer Bay of Fundy has been studied in the past, and its typical composition is fairly well known. Historically, most of the zooplankton biomass in the bay is composed of copepods, with the majority of large copepods occurring at depths ≥100 m and the majority of small copepods occurring at depths ≤50 m during daylight hours. Euphausiids (primarily *M. norvegica*), chaetognaths, and amphipods are also present in significant numbers (Murison and Gaskin, 1989). *M. norvegica* is known to undergo diel vertical migration, staying below depths of approximately 70 m during the day and migrating to shallower depths

between sunset and sunrise to feed on their typical prey of smaller zooplankton (Kulka et al., 1982; Baumgartner et al., 2003a).

This daytime vertical distribution is similar to what was observed by the glider-mounted echosounder. The acoustic data showed a strong scattering layer in the mid-water column most prevalent at 130 kHz, and layers of weak scatterers near the surface and seafloor at higher frequencies (455 kHz and 769 kHz). These acoustic layers are higher resolution than those obtained by traditional sampling methods, with variability observable down to 0.5 m intervals. Acoustic observations are also continuous from the surface to 3 m above the seafloor, which is closer than vessel-based instruments can get to the seafloor. Given that the deep layer of weak scatterers is thin relative to the water column depth and located close to the bottom of the ocean, it is easily missed by the MultiNet or other vessel-based sampling devices. The fact that the glider-mounted echosounder was able to acoustically observe this deep layer of weak scatterers is an important finding, as it indicates that the MultiNet, as well as other conventional shipboard sampling systems used in past studies (Baumgartner et al., 2003a; Baumgartner et al., 2003b; Michaud and Taggart, 2011; Murison and Gaskin, 1989), likely missed a significant portion of the biomass present in the basin during the day, leading to an underestimation of the biomass present in the area. Vessel-based sampling usually takes place during daylight hours and is even more likely to miss significant portions of the biomass present in the water column, as vertically migrating zooplankton will be concentrated in deeper waters, potentially below the effective sampling depth of vessel-based sampling. During summer and fall, *C. finmarchicus* enters diapause and much of the population remains at deep depths during both day and

night (Baumgartner et al., 2003a). The biomass of this life stage present in the Bay of Fundy has likely been underestimated in all previous regional studies because none of them used an echosounder to measure biomass-distribution.

The zooplankton community of Owen Basin, which is more influenced by coastal waters due to its closer proximity to shore and shallower depth, has not been studied as well as Grand Manan Basin. There is one Atlantic Zonal Monitoring Program station position close to Owen Basin (Prince 5), but it is on the edge of the basin slope and conducts only depth-integrated zooplankton tows (Mitchell et al., 2002; Therriault et al., 1998). Therefore, as far as I am aware, my thesis represents the first depth-stratified catalogue of zooplankton found within Owen Basin and shows the marked differences between its zooplankton community and that of Grand Manan Basin. The most notable difference is the increased prevalence of small copepod species through the entire water column, as opposed to being concentrated only at the surface as was found in Grand Manan Basin. Over half of the total biomass of zooplankton samples in Owen Basin was *C. typicus*, in contrast to its contribution of just over 20% to Grand Manan Basin's total biomass. Euphausiids comprised a greater amount of absolute biomass in Owen Basin, but a smaller proportion of the total biomass. Large copepod species other than *C. finmarchicus* were also found more often in Owen Basin than in Grand Manan Basin. However, there was still a significant population of late-stage *C. finmarchicus* in that basin, including some near-seafloor patches in excess of 1000 individuals/m^3 measured by the OPC. There is a shallow shelf that separates Grand Manan and Owen Basin that likely acts as somewhat of a barrier to open-ocean water mass advection from the Gulf of Maine. Right whales may not use Owen Basin because

they need ultra-dense concentrations of *C. finmarchicus* to maximize their caloric intake. It may be that, although concentrations of C5 *C. finmarchicus* in Owen Basin are high, they are simply not quite high enough for the whales.

The presence of zooplankton community variability, at differing depths within each basin and between the two study basins, allowed the echosounder performance to be tested in a variety of different conditions as the glider moved both horizontally and vertically through these communities. The performance of the echosounder must be characterised in a variety of environments to get an overall picture of its efficacy compared to traditional sampling methods because the received backscatter from a ping is a complicated function of the frequency, community structure (including abundance, species composition, and size distribution), and abiotic factors (Benoit-Bird et al., 2015). Discussion of the echosounder's performance is found in the next section.

Late-stage *C. finmarchicus* concentrations were only slightly lower than average for the critical right whale habitat of Grand Manan Basin, though not catastrophically low. Prior to and around the 2010 regime shift, in the absence of feeding whales, C5 *C. finmarchicus* concentrations in the deep Grand Manan Basin have been close to 500-1000 individuals/m^3 when measured with depth-stratified net sampling and OPC deployments (Baumgartner et al., 2003a; Michaud and Taggart, 2011); I found a median of just under 300 stage-C5 individuals/m^3 in the same area and depth strata, with patches of over 2000 stage-C5 individuals/m^3 estimated in some areas with the OPC. The echosounder data also indicates that a significant portion of diapausing *C. finmarchicus* biomass is located close to the seafloor, where it has the potential to be missed by traditional sampling methods. Therefore, it is possible that Grand Manan

Basin could still be a suitable feeding ground for North Atlantic right whales given only a slight increase in *C. finmarchicus* influx to create patches of great enough density for feeding to become energetically efficient again.

Small copepods such as *C. typicus* are a suboptimal prey choice for right whales, in terms of both their energy content and the whales' filtering efficiency (Mayo et al., 2001). Migrating North Atlantic right whales may feed on *Centropages* and *Pseudocalanus* species in Cape Cod Bay out of necessity and convenience, but within the Bay of Fundy and Great South Channel regions, they are thought to switch to a diet almost exclusively composed of lipid-rich diapausing *C. finmarchicus* due to its historic abundance in the area (Costa et al., 2006). Right whales also appear to feed on euphausiids only incidentally due in part to the speed at which they must swim to catch swarms of euphausiids compared to copepods. A southern right whale was observed swimming at up to 9 knots in order to feed on surface swarms of euphausiids, over 5 knots faster than their usual swimming speed. North Atlantic right whales, with historical access to swarms of much slower copepods, appear to make the choice of exploiting only copepods and capturing euphausiids either accidentally or opportunistically (Murison and Gaskin, 1989).

A primary driver in this change of zooplankton community structure in the Bay of Fundy since 2010 is climate change. A movement northward of the Gulf Stream's mean path beginning in 2010 and a slowing of the Atlantic meridional overturning circulation have both resulted in more warm water entering and lingering in the Gulf of Maine, which sits just south of the Bay of Fundy. This increase in temperature coincided with a decrease in late-stage *C. finmarchicus* abundance and right whale

breeding success (Meyer-Gutbrod et al., 2021), and clearly the lack of prey availability is severe enough to drive North Atlantic right whales elsewhere—the year 2020 was the first year in four decades that zero observations of right whales were made in the Bay of Fundy during their traditional fall feeding season. North Atlantic right whales are among the most endangered baleen whales in existence, with less than 400 individuals remaining as of the most recent estimates of their population (Fisheries and Oceans Canada, 2014; Pettis et al., 2022). While in the Bay of Fundy, these animals feed near-exclusively on *Calanus* copepods, particularly *C. finmarchicus*, which used to be found in great numbers in Grand Manan Basin and other parts of the Bay of Fundy, providing an important food source for the whales' northern migration (Costa et al., 2006; Baumgartner et al., 2003a). Because a significant population of the whales' preferred prey resource still exists in the region, there must be alternate factors that explain the whales' abandonment of this feeding ground other than absolute abundance of *C. finmarchicus*.

4.2 Echosounder performance

Qualitatively, the echosounder performed well in this study, in that it captured similar relative biomass patterns as the shipboard samplers and was able to distinguish layers of meso- and macrozooplankton in the water column with finer detail than the MultiNet, and at deeper depths than the OPC. The glider-mounted echosounder's quantitative performance varied depending on the acoustic model used to calculate the expected backscatter from the MultiNet samples. With all models, expected S_v ($S_{v(net)}$, $S_{v(copepod)}$, and $S_{v(cfin)}$) tended to be lower than $S_{v(echo)}$, but this is expected behaviour.

Multiple studies have noted the underestimation of zooplankton by biological net sampling due to various reasons. Di Mauro et al. (2009) found that small copepods (including earlier life stages of calanoid copepods) can be underestimated by over 90% when using a net with mesh size ≥ 200 μm due to passing through the net mesh without being captured. Larger copepods and gelatinous zooplankton may also be extruded through the net mesh due to the pressure exerted by the water flowing in through the net opening, and all zooplankton in general may break apart or disintegrate when subjected to the preservation process, leading to an overall underestimation of abundance (Whitmore et al., 2019).

Large zooplankton such as euphausiids also exhibit avoidance behaviour during MultiNet sampling (Whitmore et al., 2019). One method of minimising this avoidance behaviour is the use of strobe lights mounted on the MultiNet to stun large zooplankton so they can be more effectively collected, and therefore their concentration in the nets would more accurately reflect their concentration *in situ* (Sameoto et al., 1993). Because the MultiNet used in this study did not have a strobe light, it is likely that the concentration of euphausiids in the net samples is significantly lower than the true concentration of euphausiids in the Bay of Fundy, with a size distribution that is skewed to be smaller than the true population distribution. As euphausiids are significant contributors to backscatter at all frequencies used in this thesis and tend to overshadow backscatter from copepods when present (Ruckdeschel, 2017), their avoidance of the nets is very likely to have contributed to the underestimation of expected S_v when compared to observed S_v.

Nevertheless, some general trends emerge when the correlations between $S_{v(echo)}$ and various expected S_v models are examined, and I found that an acoustic model that takes as many different taxa into account as possible gave the best results. Within this acoustic model, the frequency bands that gave the best correlation were 200 to 455 kHz, and 455 to 769 kHz. The correlation coefficients between $S_{v(echo)}$ and $S_{v(net)}$, and $S_{v(echo)}$ and $S_{v(cfin)}$, were nearly identical in these frequency bands, indicating that *C. finmarchicus* was likely the primary contributor to the observed backscatter in these frequency bands. However, there was considerable uncertainty in the relationships. The negative correlations between $S_{v(echo)}$ and $S_{v(copepod)}$, on the other hand, is an unexpected result, and may indicate that the echosounder is unable to detect small copepods even at high abundances and frequencies. As $S_{v(copepod)}$ (i.e. the theoretical contribution of all copepods to the backscatter) increases, there is proportionally less biomass from larger, (and possibly more easily sensed) taxa, resulting in a decrease in $S_{v(echo)}$.

The correlation between $S_{v(echo)}$ and the log10 of total and copepod-only biomass indicated less agreement than the correlation between $S_{v(echo)}$ and corresponding $S_{v(net)}$ models; however, the correlation between $S_{v(echo)}$ and the log10 of *C. finmarchicus*-only biomass had similar R^2 values to the correlation between $S_{v(echo)}$ and $S_{v(cfin)}$. Warren and Wiebe (2008) performed a similar analysis, with similar results, and concluded that physical processes in the water column (e.g., turbulent microstructures, internal waves, thermocline boundaries, etc.) were contributing a significant amount to the measured backscatter, making the correlation between it and biomass worse. This could also be the case in the Bay of Fundy, as it is an area of significant oceanographic activity due to the strong tidal currents. Turbulent microstructure can, in some cases, scatter sound

similarly to zooplankton, resulting in an overestimate of zooplankton biomass unless it is accounted for (Lavery et al., 2007).

Even in the absence of physical contributors to the backscatter, the correlation between biomass and measured backscatter can vary significantly. Wiebe et al. (1996), Fielding et al. (2004), and Jiang et al. (2007) found R^2 values between 0.09 and 0.32 for their correlations between collected zooplankton biomass and acoustic backscatter data collected in the same area using echosounders on a towed platform behind a vessel, on a vessel hull itself, and on a deep water moored platform, respectively. Since all three of these papers also correlated S_v with dry weight inferred from literature values, it can be concluded that this thesis' R^2 values are within the normal range. The very low R^2 values I found for correlations with total and copepod biomass may be explained by the overwhelming presence of small copepods, which are easily sampled by the MultiNet and contribute a good deal to the relative biomass of the samples, but which the echosounder may have difficulty sensing. In the common case of wanting to obtain a ballpark estimate of biomass from acoustic samples, I recommend using the 200 to 455 kHz linear model to predict *C. finmarchicus* biomass from S_v. The correlation will hold in all types of communities tested here, as community composition was not found to significantly affect the correlation.

Some sources of uncertainty remain with the data collection and correlation. Chief among these is the acoustic model used to obtain $S_{v(net)}$ and its subsets, as acoustic modelling is a complex procedure with a great deal of uncertainty (Benoit-Bird et al., 2015). This thesis included only siphonophore pneumatophores, euphausiids, and copepods in the acoustic model; amphipods, siphonophore gelatinous structures, and

other, rarer taxa were not modelled, and therefore may have contributed to the underestimation of $S_{v(net)}$ when compared with $S_{v(echo)}$. Another source of uncertainty within the acoustic model is the possibility of size bias when measuring the lengths of sampled animals in order to model their target strength (Ruckdeschel, 2017). As described above, larger animals exhibit more net avoidance, leading to a biased size distribution in the nets; because larger animals contribute more to acoustic backscatter, this can lead to a disagreement between the observed and expected backscatter.

Another potential source of uncertainty occurs due to the glider's position underwater. In past echosounder performance studies, the echosounder has been mounted either directly on a boat or mounted on a tow-body and towed behind a boat (Guihen et al. 2014; Lavery et. al 2007). In this configuration, its position is much more controlled than on a glider, and there is a high degree of certainty that the echosounder is sampling the same area as the validating instrument. There is less certainty of position of a glider, which can be more affected by strong tidal currents than a vessel, altering its position in the water column both horizontally and vertically. When the glider is underwater, it is unable to communicate its position via GPS in real-time and it only moves between waypoints by dead-reckoning using the GPS coordinates it received at its latest surfacing.

In this case, the Bay of Fundy's strong tidal currents worked in the study's favour. With careful planning and timing, the glider was launched at the peak of a tidal cycle in the direction the tide was about to flow, causing it to both conserve power as it worked with the tide and to sail in more or less a straight line. Because of this, it is nearly certain that the glider and the vessel were sampling the same water mass and

zooplankton community, with a reasonable margin of error. In areas with weaker or less predictable currents, it may be necessary to utilise the glider's propeller more or to increase the frequency with which the glider surfaces to transmit its position, in order to have a greater degree of certainty of its path.

4.3 Evolution and future directions

Gliders and glider-mounted instruments are still a relative novelty in the field of marine science and oceanography. Since the beginning of their production and use in the late 1980s to early 2000s, AUVs have undergone a tremendous amount of advancement (Jenkins et al., 2003; Benoit-Bird et al., 2018). In particular, the continual development of more compact sensors with lower power requirements has meant that AUVs can now carry a wide variety of measurement instruments without sacrificing the ability to sample over long periods of time that makes autonomous platforms so attractive. It is only recently that multifrequency echosounders have joined the group of sensors that are suitable for mounting on gliders (Benoit-Bird et al., 2018), but they have already been used in a multitude of studies examining zooplankton community characteristics (Benoit-Bird et al., 2018; Ohman et al., 2019; Benoit-Bird et al., 2021).

This is not the first study to experiment with new glider-mounted sensors, especially as technology has continued to evolve. Benoit-Bird et al. (2018) used a pair of echosounders, one pointing upwards and one pointing downwards, to sample the entire water column on each dive instead of a triangular slice and supplied important *in situ* data about theoretical drivers of diel vertical migration. The use of glider-mounted echosounders with lower frequency pings is also well documented as a measurement

tool for krill populations and factors affecting their distribution (Ruckdeschel et al., 2020; Reiss et al., 2021). Glider-mounted sensors have also been used to study features such as pH decreases from ocean acidification (Saba et al., 2019; Wright-Fairbanks et al., 2020), changes in dissolved O_2 (Kohut et al., 2013), fronts between water masses with different properties (Flexas et al., 2018), and many other studies (Rudnick, 2016). Gliders, and, more broadly, AUVs, are becoming increasingly common tools in oceanography, and this thesis contributes important findings to this growing body of work.

My thesis uses a four-frequency echosounder with a minimum frequency of 130 kHz and a maximum frequency of 769 kHz, which is higher than the maximum frequency used in most other studies (Benoit-Bird et al., 2018; Warren and Wiebe, 2008). In theory, this should allow for detection of even smaller organisms, especially when coupled with the movement of a glider through the water column removing the attenuation issue of such high frequencies; however, this thesis found that, in practice, small copepods remain difficult to measure via active acoustic techniques even when in highly concentrated swarms. Thankfully, however, small zooplankton are easy to sample with nets, OPCs, and video plankton recorders (VPRs); if the study of small zooplankton is the goal, one of these tools should be selected as opposed to an echosounder.

Now that the performance of the glider-mounted echosounder is known, it can be deployed for longer missions to collect acoustic data that can then be converted to *C. finmarchicus* biomass. It is already known that North Atlantic right whales have been making increasing use of the Gulf of St. Lawrence since sometime between 2010 to

2015, with recurrent tragic results (Crowe et al., 2021; Davies and Brillant, 2019). Identifying the availability of right whale prey in the Gulf of St. Lawrence would be beneficial for right whale conservation efforts, and may also help to predict future range shifts of this endangered species before mass mortality events due to ship strikes in less protected areas occur, as one did in 2017 in the Gulf of St. Lawrence (Davies and Brillant, 2019).

An even more recent development in the field of glider-mounted sensors is a plankton imaging system that adheres to the necessary low power requirements. In theory, a glider-mounted imaging device would be able to determine composition of plankton swarms present in the glider's path to an even greater degree of precision than by using an echosounder, possibly down to the family or genus level depending on the clarity of the images. Ohman et al. (2019) have shown that this composition determination is possible with their Zooglider setup, but further exploration of this technology is needed to determine its capabilities and limits. Another possible combination of tools is the concurrent use of passive and active acoustics (in other words, mounting both a hydrophone and an echosounder to a glider) to sense both whales and potential prey patches. Passive acoustic monitoring of large whales via gliders has already been established as viable (Baumgartner et al., 2013), and continued expansion of these efforts would be of great benefit to large whale conservation efforts. Next steps in this area would be to attempt to associate these whales with their surrounding prey field, and potentially predict where they may be found in the near future based on prey biomass and density calculations from active acoustic data in near real time.

4.4 Conclusions

In conclusion, with proper setup, a glider-mounted echosounder is a useful tool in detecting swarms of large copepods and other large zooplankton, especially in places that cannot be sampled by vessel-based equipment such as close to the seafloor. Given that gliders can collect data in all weather conditions and for months at a time, they are able to survey large areas with a fraction of the cost it would require to obtain an equivalent amount of data from vessel-based instrumentation. The use of glider-mounted echosounders to study large copepods such as *C. finmarchicus* holds a great deal of promise and should be investigated further to create more accurate models to relate backscatter to zooplankton concentrations and biomass by studying other species, performing bench experiments with known concentrations of zooplankton, and/or utilizing alternative validation techniques such as glider-mounted plankton imaging systems. Further research should apply the linear model given in this thesis to solve the inverse problem and obtain absolute estimates of *C. finmarchicus* concentration from the glider-echosounder acoustic backscatter.

Bibliography

Atkinson, A., P. Ward, and E.J. Murphy. 1996. “Diel Periodicity of Subantarctic Copepods: Relationships between Vertical Migration, Gut Fullness and Gut Evacuation Rate.” *Journal of Plankton Research* 18 (8): 1387–1405. https://doi.org/10.1093/plankt/18.8.1387.

Bailey, Helen, S.R. Benson, G.L. Shillinger, S.J. Bograd, P.H. Dutton, S.A. Eckert, S.J. Morreale, et al. 2012. “Identification of Distinct Movement Patterns in Pacific Leatherback Turtle Populations Influenced by Ocean Conditions.” *Ecological Applications* 22 (3): 735–47. https://doi.org/10.1890/11-0633.

Båmstedt, U., and A. Ervik. 1984. “Local Variations in Size and Activity among *Calanus finmarchicus* and *Metridia longa* (Copepoda, Calanoida) Overwintering on the West Coast of Norway.” *Journal of Plankton Research* 6 (5): 843–57. https://doi.org/10.1093/plankt/6.5.843.

Basedow, S.L., D. McKee, I. Lefering, A. Gislason, M. Daase, E. Trudnowska, E.S. Egeland, M. Choquet, and S. Falk-Petersen. 2019. “Remote Sensing of Zooplankton Swarms.” *Scientific Reports* 9 (1): 686. https://doi.org/10.1038/s41598-018-37129-x.

Baumgartner, Mark F. 2003. “Comparisons of *Calanus finmarchicus* Fifth Copepodite Abundance Estimates from Nets and an Optical Plankton Counter.” *Journal of Plankton Research* 25 (7): 855–68. https://doi.org/10.1093/plankt/25.7.855.

Baumgartner, Mark F., and B.R. Mate. 2003. “Summertime Foraging Ecology of North Atlantic Right Whales.” *Marine Ecology Progress Series* 264 (December): 123–35. https://doi.org/10.3354/meps264123.

Baumgartner, Mark F., T.V.N. Cole, R.G. Campbell, G.J. Teegarden, and E.G. Durbin. 2003. “Associations between North Atlantic Right Whales and Their Prey, *Calanus finmarchicus*, over Diel and Tidal Time Scales.” *Marine Ecology Progress Series* 264 (December): 155–66. https://doi.org/10.3354/meps264155.

Baumgartner, Mark F., T.V.N. Cole, P.J. Clapham, and B.R. Mate. 2003. “North Atlantic Right Whale Habitat in the Lower Bay of Fundy and on the SW Scotian Shelf during 1999-2001.” *Marine Ecology Progress Series* 264 (December): 137–54. https://doi.org/10.3354/meps264137.

Baumgartner, Mark F., D.M. Fratantoni, T.P. Hurst, M.W. Brown, T.V.N. Cole, S.M. Van Parijs, and M. Johnson. 2013. “Real-Time Reporting of Baleen Whale Passive Acoustic Detections from Ocean Gliders.” *The Journal of the Acoustical Society of America* 134 (3): 1814–23. https://doi.org/10.1121/1.4816406.

Becker, K.N., and J.D. Warren. 2014. “Material Properties of Northeast Pacific Zooplankton.” *ICES Journal of Marine Science* 71 (9): 2550–63. https://doi.org/10.1093/icesjms/fsu109.

Benoit-Bird, K.J. 2009. “Dynamic 3-Dimensional Structure of Thin Zooplankton Layers Is Impacted by Foraging Fish.” *Marine Ecology Progress Series* 396 (December): 61–76. https://doi.org/10.3354/meps08316.

Benoit-Bird, K.J., and G. Lawson. 2015. “Ecological Insights from Pelagic Habitats Acquired Using Active Acoustic Techniques.” *Annual Review of Marine Science* 8 (1). https://doi.org/10.1146/annurev-marine-122414-034001.

Benoit-Bird, K.J., T.P. Welch, C.M. Waluk, J.A. Barth, I. Wangen, P. McGill, C. Okuda, G.A. Hollinger, M. Sato, and S. McCammon. 2018. “Equipping an Underwater Glider with a New Echosounder to Explore Ocean Ecosystems.” *Limnology and Oceanography: Methods* 16 (11): 734–49. https://doi.org/10.1002/lom3.10278.

Benoit-Bird, Kelly J., and Mark A. Moline. 2021. “Vertical Migration Timing Illuminates the Importance of Visual and Nonvisual Predation Pressure in the Mesopelagic Zone.” *Limnology and Oceanography* 66 (8): 3010–19. https://doi.org/10.1002/lno.11855.

Chave, R., J. Buermans, D. Lemon, J.C. Taylor, C. Lembke, C. DeCollibus, G.K. Saba, and C.S. Reiss. 2018. “Adapting Multi-Frequency Echo-Sounders for Operation on Autonomous Vehicles.” In *OCEANS 2018 MTS/IEEE Charleston*, 1–6. https://doi.org/10.1109/OCEANS.2018.8604815.

Colbo, K., T. Ross, C. Brown, and T. Weber. 2014. “A Review of Oceanographic Applications of Water Column Data from Multibeam Echosounders.” *Estuarine, Coastal and Shelf Science* 145 (May): 41–56. https://doi.org/10.1016/j.ecss.2014.04.002.

Costa, A.D., E.G. Durbin, and C.A. Mayo. 2006. “Variability in the Nutritional Value of the Major Copepods in Cape Cod Bay (Massachusetts, USA) with Implications for Right Whales.” *Marine Ecology* 27 (2): 109–23. https://doi.org/10.1111/j.1439-0485.2006.00087.x.

Crowe, L.M., M.W. Brown, P.J. Corkeron, P.K. Hamilton, C. Ramp, S. Ratelle, A.S.M. Vanderlaan, and T.V.N. Cole. 2021. “In Plane Sight: A Mark-Recapture Analysis of North Atlantic Right Whales in the Gulf of St. Lawrence.” *Endangered Species Research* 46 (December): 227–51. https://doi.org/10.3354/esr01156.

Davies, K.T.A., and S.W. Brillant. 2019. “Mass Human-Caused Mortality Spurs Federal Action to Protect Endangered North Atlantic Right Whales in Canada.” *Marine Policy* 104 (June): 157–62. https://doi.org/10.1016/j.marpol.2019.02.019.

Davies, K.T.A., M.W. Brown, P.K. Hamilton, A.R. Knowlton, C.T. Taggart, and A.S.M. Vanderlaan. 2019. “Variation in North Atlantic Right Whale *Eubalaena glacialis* Occurrence in the Bay of Fundy, Canada, over Three Decades.” *Endangered Species Research* 39 (June): 159–71. https://doi.org/10.3354/esr00951.

Davis, C.S., F.T. Thwaites, S.M. Gallager, and Q. Hu. 2005. “A Three-Axis Fast-Tow Digital Video Plankton Recorder for Rapid Surveys of Plankton Taxa and Hydrography.” *Limnology and Oceanography: Methods* 3 (2): 59–74. https://doi.org/10.4319/lom.2005.3.59.

De Robertis, A., and I. Higginbottom. 2007. “A Post-Processing Technique to Estimate the Signal-to-Noise Ratio and Remove Echosounder Background Noise.” *ICES Journal of Marine Science* 64 (6): 1282–91. https://doi.org/10.1093/icesjms/fsm112.

Di Mauro, R., F. Capitanio, and M.D. Viñas. 2009. “Capture Efficiency for Small Dominant Mesozooplankters (Copepoda, Appendicularia) off Buenos Aires Province (34ºS-41ºS), Argentine Sea, Using Two Plankton Mesh Sizes.”

Brazilian Journal of Oceanography 57 (3): 205–14. https://doi.org/10.1590/S1679-87592009000300004.

Escribano, R., and I.A. McLaren. 1992. "Influence of Food and Temperature on Lengths and Weights of Marine Copepods." *Journal of Experimental Marine Biology and Ecology* 159 (1): 77–88. https://doi.org/10.1016/0022-0981(92)90259-D.

Fielding, S., G. Griffiths, and H.S.J. Roe. 2004. "The Biological Validation of ADCP Acoustic Backscatter through Direct Comparison with Net Samples and Model Predictions Based on Acoustic-Scattering Models." *ICES Journal of Marine Science* 61 (2): 184–200. https://doi.org/10.1016/j.icesjms.2003.10.011.

Fisheries and Oceans Canada. 2014. "Recovery Strategy for the North Atlantic Right Whale (*Eubalaena glacialis*) in Atlantic Canadian Waters [Final]." Species at Risk Act Recovery Strategy Series.

Flexas, M.M., M.I. Troesch, S. Chien, A.F. Thompson, S. Chu, A. Branch, J.D. Farrara, and Y. Chao. 2018. "Autonomous Sampling of Ocean Submesoscale Fronts with Ocean Gliders and Numerical Model Forecasting." *Journal of Atmospheric and Oceanic Technology* 35 (3): 503–21. https://doi.org/10.1175/JTECH-D-17-0037.1.

Folt, C.L., and C.W. Burns. 1999. "Biological Drivers of Zooplankton Patchiness." *Trends in Ecology & Evolution* 14 (8): 300–305. https://doi.org/10.1016/S0169-5347(99)01616-X.

Gaardsted, F., K.S. Tande, and S.L. Basedow. 2010. "Measuring Copepod Abundance in Deep-Water Winter Habitats in the NE Norwegian Sea: Intercomparison of Results from Laser Optical Plankton Counter and Multinet." *Fisheries Oceanography* 19 (6): 480–92. https://doi.org/10.1111/j.1365-2419.2010.00558.x.

Gastauer, S., D. Chu, and M.J. Cox. 2019. "ZooScatR—An R package for modelling the scattering properties of weak scattering targets using the distorted wave Born approximation." *The Journal of the Acoustical Society of America* 145:1, EL102-EL108. https://doi.org/10.1121/1.5085655.

Gaube, P., D.B. Chelton, P.G. Strutton, and M.J. Behrenfeld. 2013. "Satellite Observations of Chlorophyll, Phytoplankton Biomass, and Ekman Pumping in Nonlinear Mesoscale Eddies." *Journal of Geophysical Research: Oceans* 118 (12): 6349–70. https://doi.org/10.1002/2013JC009027.

Van Guelpen, L., D.F. Markle, and D.J. Duggan. 1982. "An Evaluation of Accuracy, Precision, and Speed of Several Zooplankton Subsampling Techniques." *ICES Journal of Marine Science* 40 (3): 226–36. https://doi.org/10.1093/icesjms/40.3.226.

Guihen, D. 2018. "High-Resolution Acoustic Surveys with Diving Gliders Come at a Cost of Aliasing Moving Targets." Edited by Judi Hewitt. *PLOS ONE* 13 (8): e0201816. https://doi.org/10.1371/journal.pone.0201816.

Guihen, D., S.F., E.J. Murphy, K.J. Heywood, and G. Griffiths. 2014. "An Assessment of the Use of Ocean Gliders to Undertake Acoustic Measurements of Zooplankton: The Distribution and Density of Antarctic Krill (*Euphausia superba*) in the Weddell Sea.: Measurement of Zooplankton from a Glider."

Limnology and Oceanography: Methods 12 (6): 373–89. https://doi.org/10.4319/lom.2014.12.373.

Hazen, E.L., R.M. Suryan, J.A. Santora, S.J. Bograd, Y. Watanuki, and R.P. Wilson. 2013. "Scales and Mechanisms of Marine Hotspot Formation." *Marine Ecology Progress Series* 487 (July): 177–83. https://doi.org/10.3354/meps10477.

Herman, A.W. 1988. "Simultaneous Measurement of Zooplankton and Light Attenuance with a New Optical Plankton Counter." *Continental Shelf Research* 8 (2): 205–21. https://doi.org/10.1016/0278-4343(88)90054-4.

Herman, A.W. 1992. "Design and Calibration of a New Optical Plankton Counter Capable of Sizing Small Zooplankton." *Deep Sea Research Part A. Oceanographic Research Papers* 39 (3): 395–415. https://doi.org/10.1016/0198-0149(92)90080-D.

Hunter, J., and G. Thomas. 1974. "Effect of Prey Distribution and Density on the Searching and Feeding Behaviour of Larval Anchovy *Engraulis mordax* Girard." In: Blaxter, J.H.S. (eds) The Early Life History of Fish. Springer, Berlin, Heidelberg. https://doi.org/10.1007/978-3-642-65852-5_45. https://doi.org/10.1007/978-3-642-65852-5_45.

Jenkins, S.A., D.E. Humphreys, J. Sherman, J. Osse, C. Jones, N. Leonard, J. Graver, et al. 2003. "Underwater Glider System Study," May. https://escholarship.org/uc/item/1c28t6bb.

Jiang, S., T.D. Dickey, D.K. Steinberg, and L.P. Madin. 2007. "Temporal Variability of Zooplankton Biomass from ADCP Backscatter Time Series Data at the Bermuda Testbed Mooring Site." *Deep Sea Research Part I: Oceanographic Research Papers* 54 (4): 608–36. https://doi.org/10.1016/j.dsr.2006.12.011.

Johnson, H.D. 2021. "opcr: process and plot data from an optical plankton counter, v1.0.0." *Zenodo*. https://doi.org/10.5281/zenodo.5760977.

Kohut, J., C. Haldeman, J. Kerfoot, D. Adams, M. Borst, B. Friedman, and R. Schuster. 2013. "Monitoring Dissolved Oxygen in New Jersey Coastal Waters Using Autonomous Gliders: Multi-Year Trends and Event Response." In *2013 OCEANS - San Diego*, 1–9. https://doi.org/10.23919/OCEANS.2013.6741239.

Kosobokova, K.N., and R.R. Hopcroft. 2010. "Diversity and Vertical Distribution of Mesozooplankton in the Arctic's Canada Basin." *Deep Sea Research Part II: Topical Studies in Oceanography* 57 (1–2): 96–110. https://doi.org/10.1016/j.dsr2.2009.08.009.

Kulka, D.W., S. Corey, and T.D. Iles. 1982. "Community Structure and Biomass of Euphausiids in the Bay of Fundy." *Canadian Journal of Fisheries and Aquatic Sciences* 39 (2): 326–34. https://doi.org/10.1139/f82-045.

Landry, M.R., M.D. Ohman, R. Goericke, M.R. Stukel, and K. Tsyrklevich. 2009. "Lagrangian Studies of Phytoplankton Growth and Grazing Relationships in a Coastal Upwelling Ecosystem off Southern California." *Progress in Oceanography*, Eastern Boundary Upwelling Ecosystems: Integrative and Comparative Approaches, 83 (1): 208–16. https://doi.org/10.1016/j.pocean.2009.07.026.

Lavery, A.C., P.H. Wiebe, T.K. Stanton, G.L. Lawson, M.C. Benfield, and N. Copley. 2007. "Determining Dominant Scatterers of Sound in Mixed Zooplankton

Populations." *The Journal of the Acoustical Society of America* 122 (6): 3304–26. https://doi.org/10.1121/1.2793613.
Lavery, A.C., D. Chu, and J.N. Moum. 2010. "Measurements of Acoustic Scattering from Zooplankton and Oceanic Microstructure Using a Broadband Echosounder." *ICES Journal of Marine Science* 67 (2): 379–94. https://doi.org/10.1093/icesjms/fsp242.
Makabe, R., A. Tanimura, and M. Fukuchi. 2012. "Comparison of Mesh Size Effects on Mesozooplankton Collection Efficiency in the Southern Ocean." *Journal of Plankton Research* 34 (5): 432–36. https://doi.org/10.1093/plankt/fbs014.
Mayo, C.A., B.H. Letcher, and S. Scott. 2020. "Zooplankton Filtering Efficiency of the Baleen of a North Atlantic Right Whale, *Eubalaena glacialis*." *J. Cetacean Res. Manage.*, 225–29. https://doi.org/10.47536/jcrm.vi.286.
McClatchie, S. 1985. "Feeding Behaviour in *Meganyctiphanes norvegica* (M. Sars) (Crustacea: Euphausiacea)." *Journal of Experimental Marine Biology and Ecology* 86 (3): 271–84. https://doi.org/10.1016/0022-0981(85)90108-X.
Meyer-Gutbrod, E.L., C.H. Greene, and K.T.A. Davies. 2018. "Marine Species Range Shifts Necessitate Advanced Policy Planning: The Case of the North Atlantic Right Whale." *Oceanography* 31 (2): 19–23.
Meyer-Gutbrod, E.L., C.H. Greene, K.T.A. Davies, and D.G. Johns. 2021. "Ocean Regime Shift Is Driving Collapse of the North Atlantic Right Whale Population." *Oceanography* 34 (3): 22–31.
Michaud, J., and C.T. Taggart. 2011. "Spatial Variation in Right Whale Food, *Calanus finmarchicus*, in the Bay of Fundy." *Endangered Species Research* 15 (3): 179–94. https://doi.org/10.3354/esr00370.
Miller, C.B., and M.J. Clemons. 1988. "Revised Life History Analysis for Large Grazing Copepods in the Subarctic Pacific Ocean." *Progress in Oceanography* 20 (4): 293–313. https://doi.org/10.1016/0079-6611(88)90044-4.
Mitchell, M.R., G. Harrison, K. Pauley, A. Gagné, G. Maillet, and P. Strain. 2002. "Atlantic Zonal Monitoring Program Sampling Protocol." Canadian Technical Report of Hydrography and Ocean Sciences 223: iv + 23.
Murison, L.D., and D.E. Gaskin. 1989. "The Distribution of Right Whales and Zooplankton in the Bay of Fundy, Canada." *Canadian Journal of Zoology* 67 (6): 1411–20. https://doi.org/10.1139/z89-200.
Ohman, M.D., R.E. Davis, J.T. Sherman, K.R. Grindley, B.M. Whitmore, C.F. Nickels, and J.S. Ellen. 2019. "*Zooglider:* An Autonomous Vehicle for Optical and Acoustic Sensing of Zooplankton." *Limnology and Oceanography: Methods* 17 (1): 69–86. https://doi.org/10.1002/lom3.10301.
Pershing, A.J., K.E. Mills, N.R. Record, K. Stamieszkin, K.V. Wurtzell, C.J. Byron, D. Fitzpatrick, W.J. Golet, and E. Koob. 2015. "Evaluating Trophic Cascades as Drivers of Regime Shifts in Different Ocean Ecosystems." *Philosophical Transactions of the Royal Society B: Biological Sciences* 370 (1659): 20130265. https://doi.org/10.1098/rstb.2013.0265.
Pettis, H.M., R.M. Pace III, and P.K. Hamilton. 2022. "North Atlantic Right Whale Consortium 2021 Annual Report Card." North Atlantic Right Whale Consortium.

Pinel-Alloul, P. 1995. “Spatial Heterogeneity as a Multiscale Characteristic of Zooplankton Community.” *Hydrobiologia* 300 (1): 17–42. https://doi.org/10.1007/BF00024445.

Record, N.R., J.A. Runge, D.E. Pendleton, W.M. Balch, K.T.A. Davies, A.J. Pershing, C.L. Johnson, et al. 2019. “Rapid Climate-Driven Circulation Changes Threaten Conservation of Endangered North Atlantic Right Whales.” *Oceanography* 32 (2): 162–69.

Reiss, C.S., A.M. Cossio, J. Walsh, G.R. Cutter, and G.M. Watters. 2021. “Glider-Based Estimates of Meso-Zooplankton Biomass Density: A Fisheries Case Study on Antarctic Krill (*Euphausia superba*) Around the Northern Antarctic Peninsula.” *Frontiers in Marine Science* 8. https://www.frontiersin.org/article/10.3389/fmars.2021.604043.

Ruckdeschel, G.S. 2017. “Euphausiid Ecology And Water Mass Associations In Roseway Basin Measured From An Ocean Glider.” Halifax: Dalhousie University.

Ruckdeschel, G.S., K.T.A. Davies, and T. Ross. 2020. “Biophysical Drivers of Zooplankton Variability on the Scotian Shelf Observed Using Profiling Electric Gliders.” *Frontiers in Marine Science* 7 (July): 627. https://doi.org/10.3389/fmars.2020.00627.

Rudnick, D. L. 2016. “Ocean Research Enabled by Underwater Gliders.” *Annual Review of Marine Science* 8 (1): 519–41. https://doi.org/10.1146/annurev-marine-122414-033913.

Rudnick, D.L., R.E. Davis, C.C. Eriksen, D.M. Fratantoni, and M.J. Perry. 2004. “Underwater Gliders for Ocean Research.” *Marine Technology Society Journal* 38 (2): 73.

Saba, G.K., E. Wright-Fairbanks, B. Chen, W. Cai, A.H. Barnard, C.P. Jones, C.W. Branham, K. Wang, and T. Miles. 2019. “The Development and Validation of a Profiling Glider Deep ISFET-Based PH Sensor for High Resolution Observations of Coastal and Ocean Acidification.” *Frontiers in Marine Science* 6. https://www.frontiersin.org/article/10.3389/fmars.2019.00664.

Sameoto, D., N. Cochrane, and A. Herman. 1993. “Convergence of Acoustic, Optical, and Net-Catch Estimates of Euphausiid Abundance: Use of Artificial Light to Reduce Net.” *Canadian Journal of Fisheries and Aquatic Sciences* 50 (2): 334–46. https://doi.org/10.1139/f93-039.

Schofield, O., J. Kohut, D.A., L. Creed, J. Graver, C. Haldeman, J. Kerfoot, et al. 2007. “Slocum Gliders: Robust and Ready.” *Journal of Field Robotics* 24 (6): 473–85. https://doi.org/10.1002/rob.20200.

Simmonds, J., and D. MacLennan, eds. 2005. *Fisheries Acoustics*. Oxford, UK: Blackwell Publishing Ltd. https://doi.org/10.1002/9780470995303.

Skjoldal, H. R., P.H. Wiebe, L. Postel, T. Knutsen, S. Kaartvedt, and D.D. Sameoto. 2013. “Intercomparison of Zooplankton (Net) Sampling Systems: Results from the ICES/GLOBEC Sea-Going Workshop.” *Progress in Oceanography* 108 (January): 1–42. https://doi.org/10.1016/j.pocean.2012.10.006.

Smith, S.L., and P.V.Z. Lane. 1988. “Grazing of the Spring Diatom Bloom in the New York Bight by the Calanoid Copepods *Calanus finmarchicus, Metridia lucens*

and *Centropages typicus*." *Continental Shelf Research* 8 (5–7): 485–509. https://doi.org/10.1016/0278-4343(88)90065-9.
Sorochan, K.A, S. Plourde, R. Morse, P. Pepin, J. Runge, C. Thompson, and C.L. Johnson. 2019. "North Atlantic Right Whale (*Eubalaena glacialis*) and Its Food: (II) Interannual Variations in Biomass of Calanus Spp. on Western North Atlantic Shelves." *Journal of Plankton Research* 41 (5): 687–708. https://doi.org/10.1093/plankt/fbz044.
Steinberg, D.K., and M.R. Landry. 2017. "Zooplankton and the Ocean Carbon Cycle." *Annual Review of Marine Science* 9 (1): 413–44. https://doi.org/10.1146/annurev-marine-010814-015924.
Therriault, J.-C., P.P. Pepin, J. Gagnon, G.J. Helbig, A. Herman, D. Lefaivre, M. Mitchell, B. Pelchat, J. Runge, and D. Sameoto. 1998. "Proposal for a Northwest Atlantic Zonal Monitoring Program." Canadian Technical Report of Hydrography and Ocean Sciences 194: vii + 57.
Tsuda, A., H. Saito, and H. Kasai. 1999. "Life Histories of *Neocalanus flemingeri* and *Neocalanus plumchrus* (Calanoida: Copepoda) in the Western Subarctic Pacific." *Marine Biology* 135 (3): 533–44. https://doi.org/10.1007/s002270050654
Uye, S. 1982. "Length-Weight Relationships of Important Zooplankton from the Inland Sea of Japan." *Journal of the Oceanographical Society of Japan* 38 (3): 149–58. https://doi.org/10.1007/BF02110286.
Warren, J. 2001. "In Situ Measurements of Acoustic Target Strengths of Gas-Bearing Siphonophores." *ICES Journal of Marine Science* 58 (4): 740–49. https://doi.org/10.1006/jmsc.2001.1047.
Weydmann, A., J. Carstensen, I. Goszczko, K. Dmoch, A. Olszewska, and S. Kwasniewski. 2014. "Shift towards the Dominance of Boreal Species in the Arctic: Inter-Annual and Spatial Zooplankton Variability in the West Spitsbergen Current." *Marine Ecology Progress Series* 501 (March): 41–52. https://doi.org/10.3354/meps10694.
Whitmore, B.M., C.F. Nickels, and M.D. Ohman. 2019. "A Comparison between Zooglider and Shipboard Net and Acoustic Mesozooplankton Sensing Systems." *Journal of Plankton Research* 41 (4): 521–33. https://doi.org/10.1093/plankt/fbz033.
Wiebe, P.H., K.H. Burt, S.H. Boyd, and A.W. Morton. 1976. "A Multiple Opening/Closing Net And Environmental Sensing System For Sampling Zooplankton." *Journal of Marine Research* 34 (3–2): 313–26.
Wiebe, P.H., D.G. Mountain, T.K. Stanton, C.H. Greene, G. Lough, S. Kaartvedt, J. Dawson, and N. Copley. 1996. "Acoustical Study of the Spatial Distribution of Plankton on Georges Bank and the Relationship between Volume Backscattering Strength and the Taxonomic Composition of the Plankton." *Deep Sea Research Part II: Topical Studies in Oceanography* 43 (7): 1971–2001. https://doi.org/10.1016/S0967-0645(96)00039-2.
Woodley, T.H., and D.E. Gaskin. 1996. "Environmental Characteristics of North Atlantic Right and Fin Whale Habitat in the Lower Bay of Fundy, Canada." *Canadian Journal of Zoology* 74 (1): 75–84. https://doi.org/10.1139/z96-010.

Wright-Fairbanks, Elizabeth K., Travis N. Miles, Wei-Jun Cai, Baoshan Chen, and Grace K. Saba. 2020. “Autonomous Observation of Seasonal Carbonate Chemistry Dynamics in the Mid-Atlantic Bight.” *Journal of Geophysical Research: Oceans* 125 (11): e2020JC016505. https://doi.org/10.1029/2020JC016505.

Appendix A. Table summary of zooplankton taxa found in September 2020 MultiNet samples. Each taxon is classified as a copepod, a euphausiid, a siphonophore, or other (none of the above).

Taxa	Classification
Acartia hudsonica	Copepod
Acartia longiremis	Copepod
Acartia sp.	Copepod
Acartia tonsa	Copepod
Bivalvia (larva)	Other
Bryozoa (larva)	Other
Calanus finmarchicus	Copepod
Calanus glacialis	Copepod
Calanus hyperboreus	Copepod
Calanus sp.	Copepod
Caligidae	Copepod
Centropages hamatus	Copepod
Centropages typicus	Copepod
Chaetognatha	Other
Cirripedia (larva)	Other
Cirripedia (nauplius)	Other
Clausocalanus spp.	Copepod
Copepoda (nauplius)	Copepod
Crustacea	Other
Crustacea (larva)	Other
Ctenophora	Other
Diastylis sp.	Other
Diplostraca (formerly Cladocera)	Other
Egg	Other
Euphausiidae (larva)	Euphausiid
Eurytemora herdmani	Copepod
Evadne nordmanni	Other
Gastropoda (larva)	Other
Hydrozoa	Other
Hyperia galba	Other
Hyperiidae (juv)	Other

Meganyctiphanes norvegica	Euphausiid
Mesoplankton larva	Other
Metridia longa	Copepod
Metridia lucens	Copepod
Metridia sp.	Copepod
Microcalanus spp.	Copepod
Microsetella norvegica	Copepod
Oithona atlantica	Copepod
Oithona similis	Copepod
Ostracoda	Other
Paracalanus spp.	Copepod
Paraeuchaeta norvegica	Copepod
Paraeuchaeta sp.	Copepod
Parasagitta elegans	Other
Pasiphaea multidentata	Other
Physonectae (nectophore)	Siphonophore
Pleopis polyphemoides	Other
Pleuromamma robusta	Copepod
Podon sp.	Other
Polychaeta	Other
Polychaeta (larva)	Other
Pseudocalanus spp.	Copepod
Siphonophora	Siphonphore
Siphonophora (bract)	Siphonphore
Siphonophora (colony)	Siphonphore
Siphonophora (nectophore)	Siphonphore
Siphonophora (pneumatophore)	Siphonphore
Temora longicornis	Copepod
Thysanoessa inermi	Euphausiid
Thysanoessa longicaudata	Euphausiid
Thysanoessa sp.	Euphausiid
Tomopteris spp.	Other
Trachymedusae	Other

Appendix B. MultiNet depth figures from each tow.

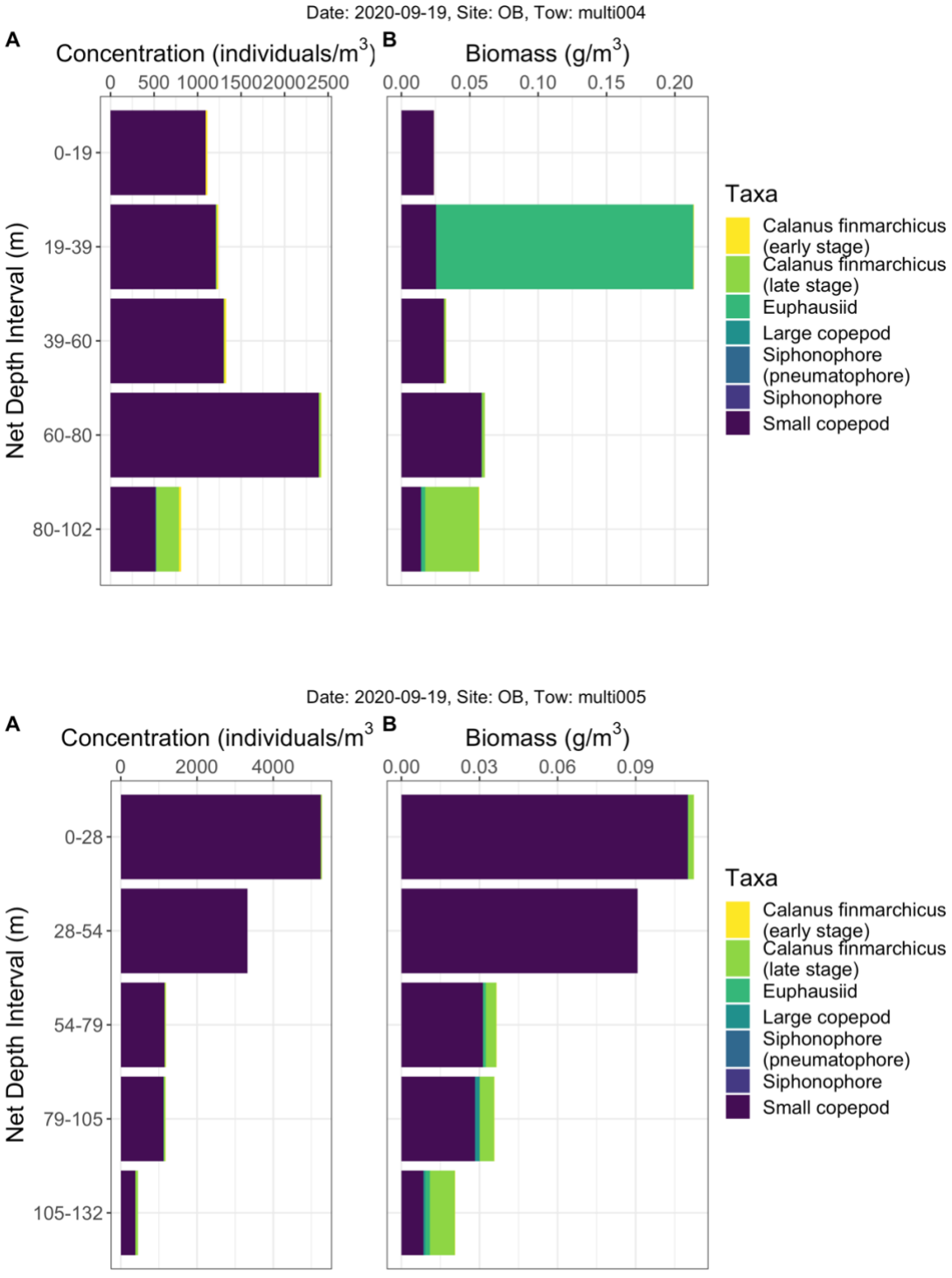

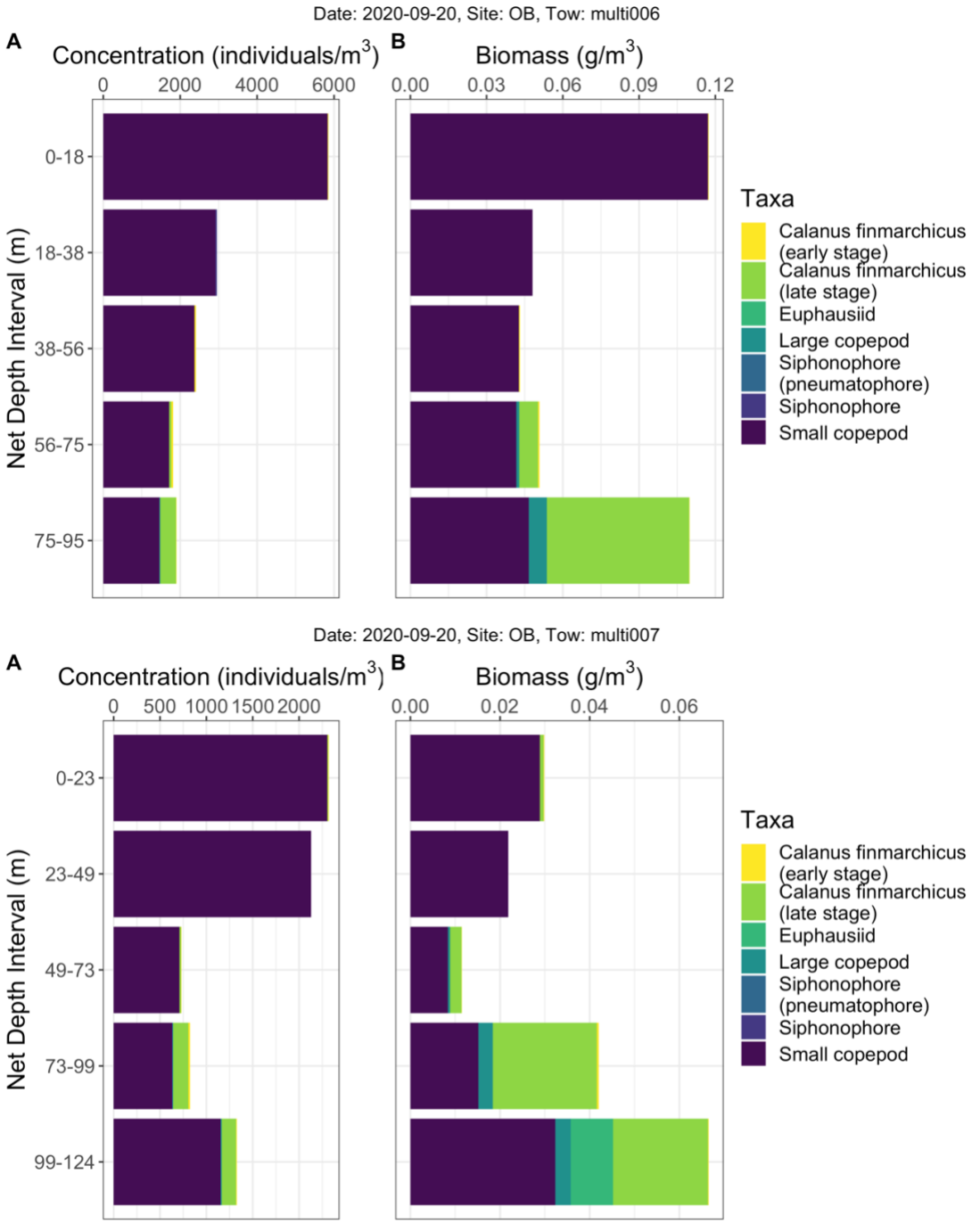
Date: 2020-09-20, Site: OB, Tow: multi006
A
Concentration (individuals/m3)
0
2000
4000
6000
B
Biomass (g/m3)
0.00
0.03
0.06
0.09
0.12
Net Depth Interval (m)
0-18
18-38
38-56
56-75
75-95
Taxa
Calanus finmarchicus (early stage)
Calanus finmarchicus (late stage)
Euphausiid
Large copepod
Siphonophore (pneumatophore)
Siphonophore
Small copepod
Date: 2020-09-20, Site: OB, Tow: multi007
A
Concentration (individuals/m3)
0
500
1000
1500
2000
B
Biomass (g/m3)
0.00
0.02
0.04
0.06
Net Depth Interval (m)
0-23
23-49
49-73
73-99
99-124
Taxa
Calanus finmarchicus (early stage)
Calanus finmarchicus (late stage)
Euphausiid
Large copepod
Siphonophore (pneumatophore)
Siphonophore
Small copepod

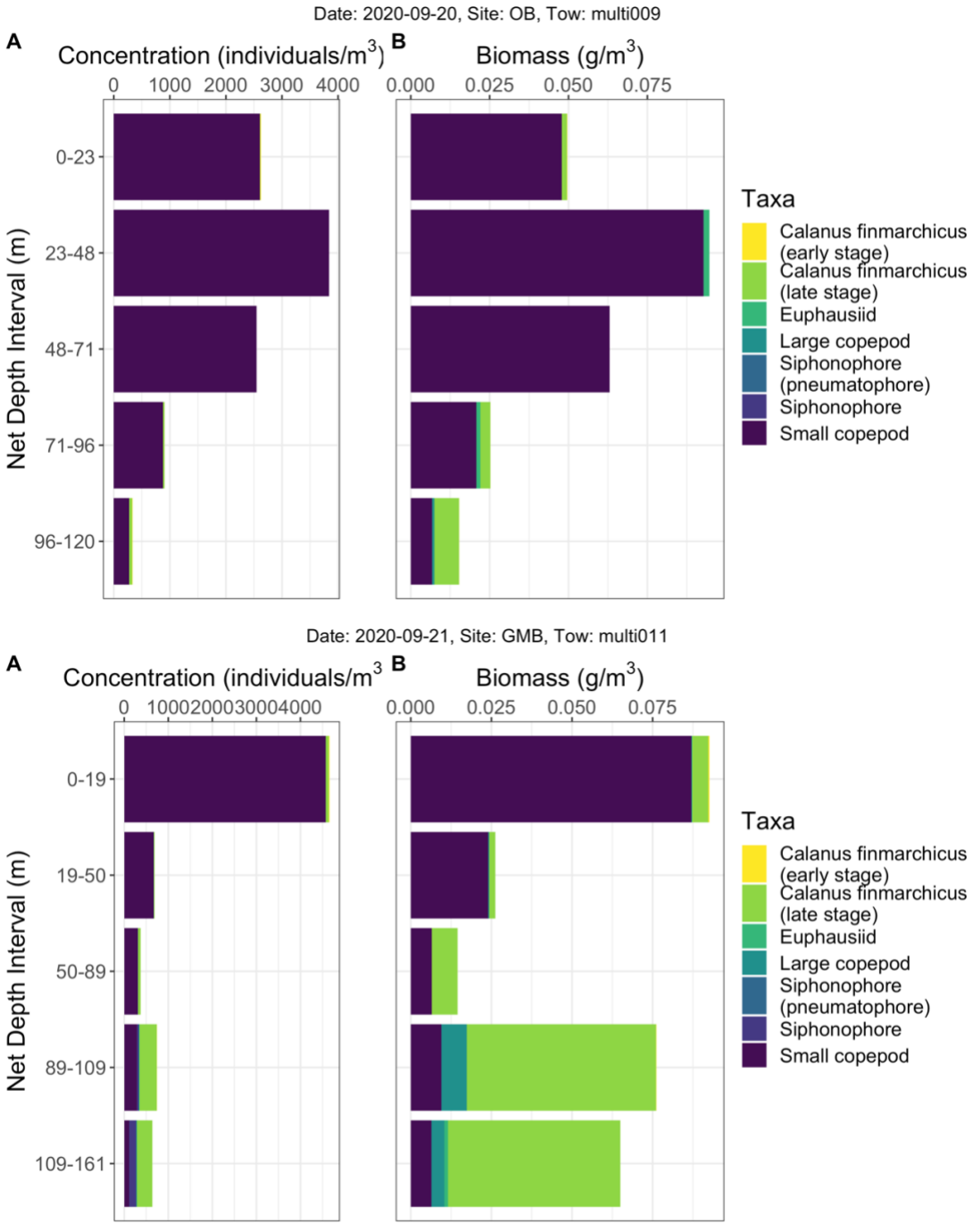
Date: 2020-09-20, Site: OB, Tow: multi009
A
Concentration (individuals/m3)
0
1000
2000
3000
4000
B
Biomass (g/m3)
0.000
0.025
0.050
0.075
Net Depth Interval (m)
0-23
23-48
48-71
71-96
96-120
Taxa
Calanus finmarchicus (early stage)
Calanus finmarchicus (late stage)
Euphausiid
Large copepod
Siphonophore (pneumatophore)
Siphonophore
Small copepod
Date: 2020-09-21, Site: GMB, Tow: multi011
A
Concentration (individuals/m3
0
1000
2000
3000
4000
B
Biomass (g/m3)
0.000
0.025
0.050
0.075
Net Depth Interval (m)
0-19
19-50
50-89
89-109
109-161
Taxa
Calanus finmarchicus (early stage)
Calanus finmarchicus (late stage)
Euphausiid
Large copepod
Siphonophore (pneumatophore)
Siphonophore
Small copepod

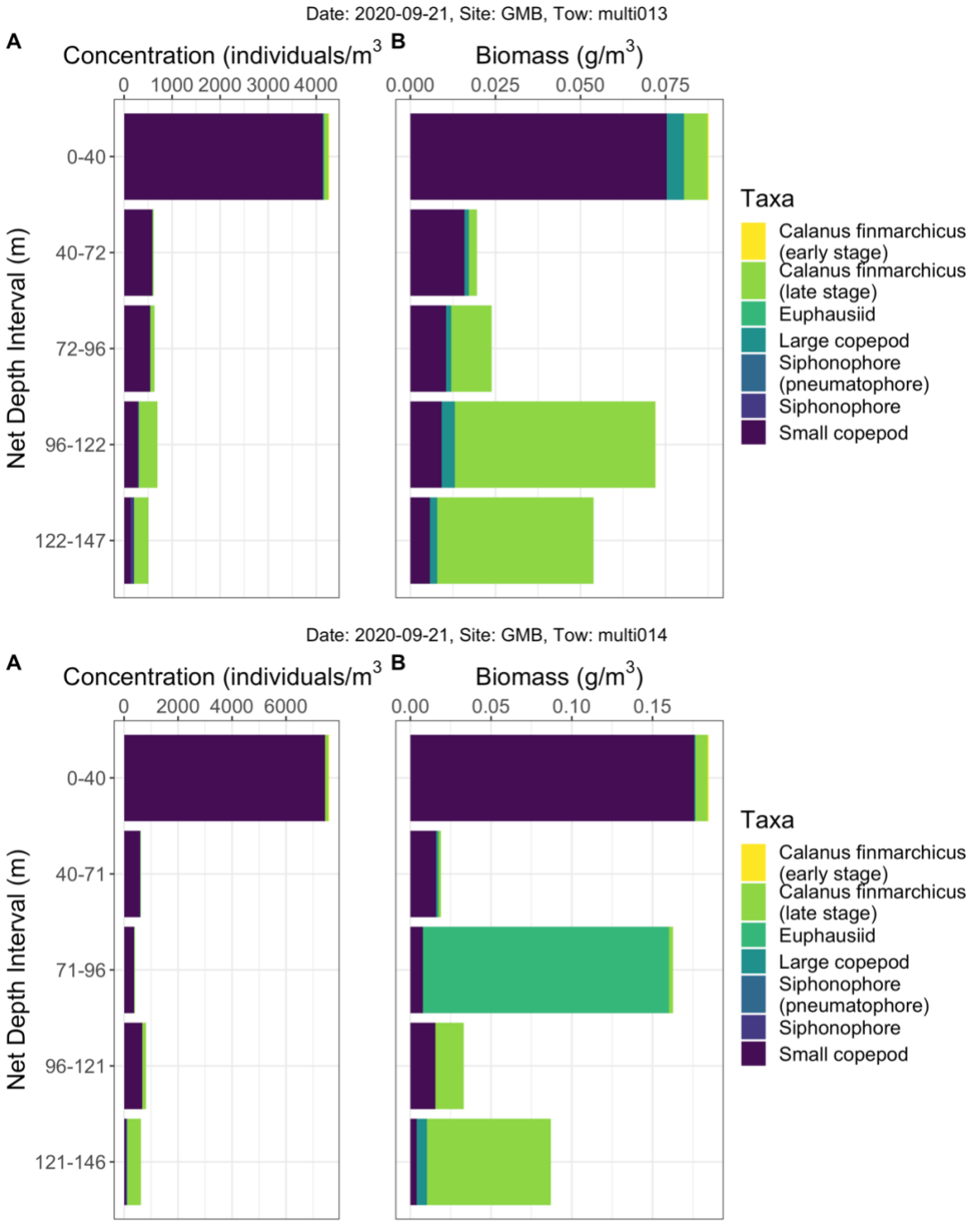
Date: 2020-09-21, Site: GMB, Tow: multi013
A
Concentration (individuals/m3
0 1000 2000 3000 4000
B
Biomass (g/m3)
0.000 0.025 0.050 0.075
Net Depth Interval (m)
0-40
40-72
72-96
96-122
122-147
Taxa
Calanus finmarchicus (early stage)
Calanus finmarchicus (late stage)
Euphausiid
Large copepod
Siphonophore (pneumatophore)
Siphonophore
Small copepod
Date: 2020-09-21, Site: GMB, Tow: multi014
A
Concentration (individuals/m3
0 2000 4000 6000
B
Biomass (g/m3)
0.00 0.05 0.10 0.15
Net Depth Interval (m)
0-40
40-71
71-96
96-121
121-146
Taxa
Calanus finmarchicus (early stage)
Calanus finmarchicus (late stage)
Euphausiid
Large copepod
Siphonophore (pneumatophore)
Siphonophore
Small copepod

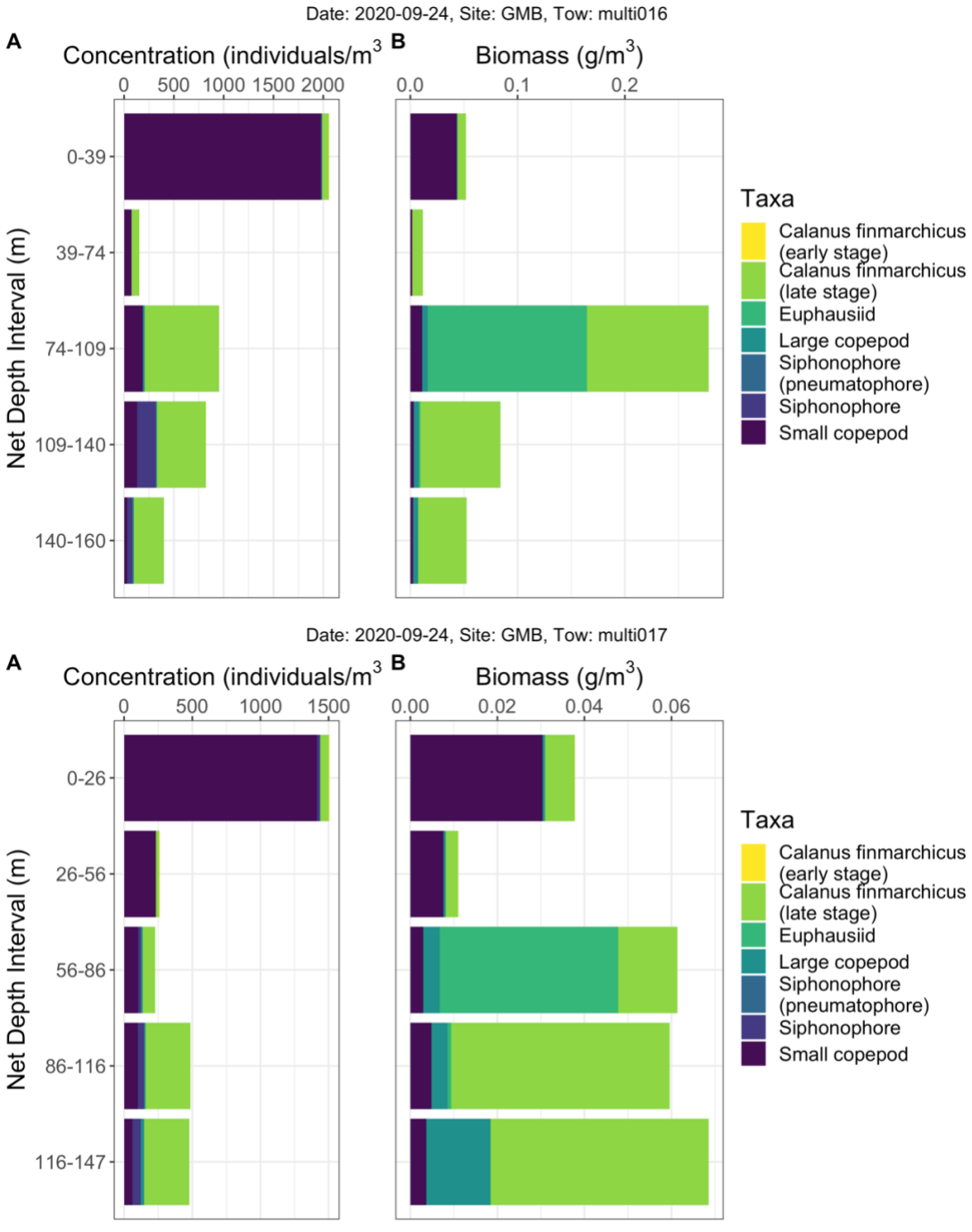
Date: 2020-09-24, Site: GMB, Tow: multi016
A
Concentration (individuals/m3
0
500
1000
1500
2000
B
Biomass (g/m3)
0.0
0.1
0.2
Net Depth Interval (m)
0-39
39-74
74-109
109-140
140-160
Taxa
Calanus finmarchicus (early stage)
Calanus finmarchicus (late stage)
Euphausiid
Large copepod
Siphonophore (pneumatophore)
Siphonophore
Small copepod
Date: 2020-09-24, Site: GMB, Tow: multi017
A
Concentration (individuals/m3
0
500
1000
1500
B
Biomass (g/m3)
0.00
0.02
0.04
0.06
Net Depth Interval (m)
0-26
26-56
56-86
86-116
116-147
Taxa
Calanus finmarchicus (early stage)
Calanus finmarchicus (late stage)
Euphausiid
Large copepod
Siphonophore (pneumatophore)
Siphonophore
Small copepod

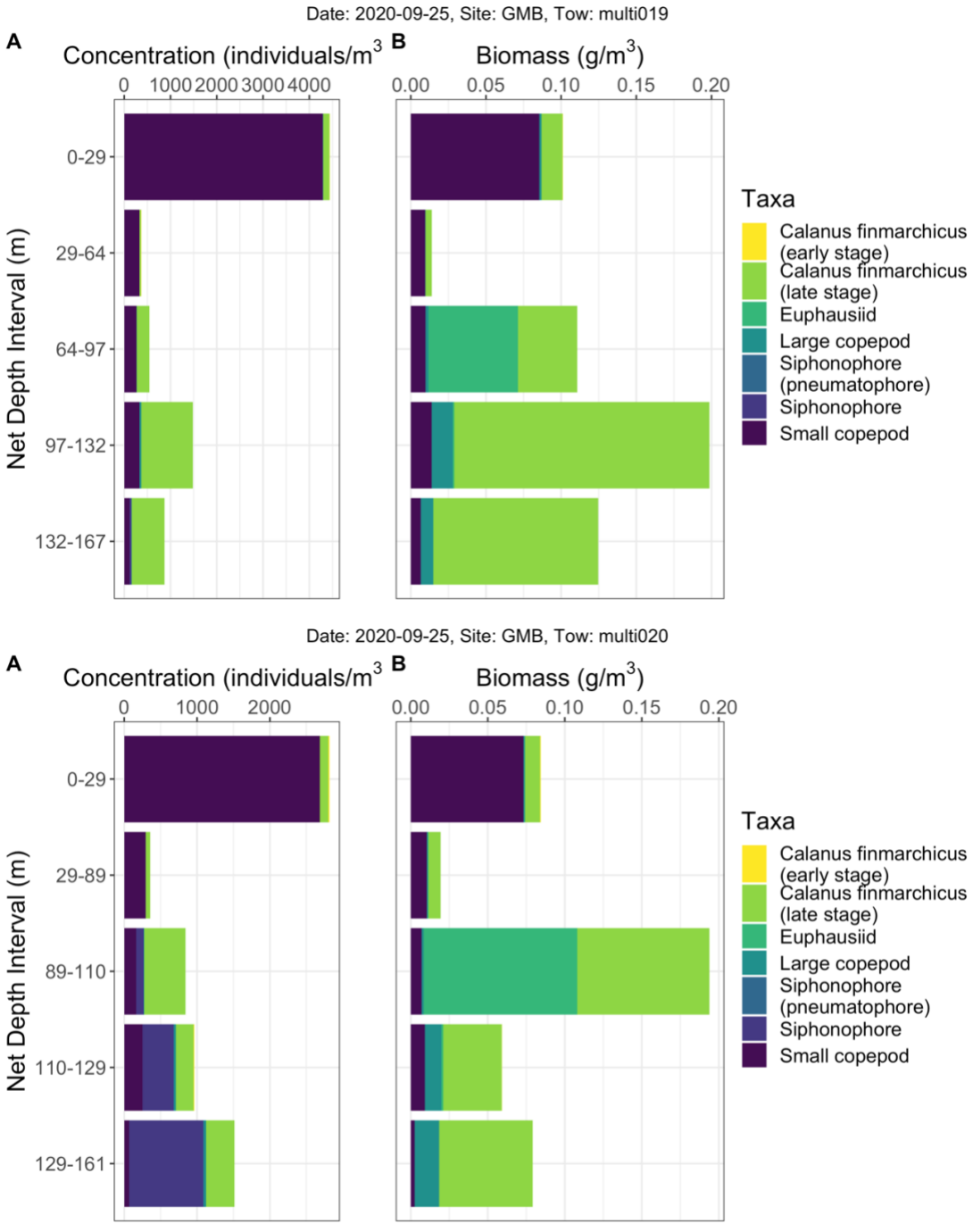
Date: 2020-09-25, Site: GMB, Tow: multi019
A
Concentration (individuals/m3
0
1000
2000
3000
4000
B
Biomass (g/m3)
0.00
0.05
0.10
0.15
0.20
Net Depth Interval (m)
0-29
29-64
64-97
97-132
132-167
Taxa
Calanus finmarchicus (early stage)
Calanus finmarchicus (late stage)
Euphausiid
Large copepod
Siphonophore (pneumatophore)
Siphonophore
Small copepod
Date: 2020-09-25, Site: GMB, Tow: multi020
A
Concentration (individuals/m3
0
1000
2000
B
Biomass (g/m3)
0.00
0.05
0.10
0.15
0.20
Net Depth Interval (m)
0-29
29-89
89-110
110-129
129-161
Taxa
Calanus finmarchicus (early stage)
Calanus finmarchicus (late stage)
Euphausiid
Large copepod
Siphonophore (pneumatophore)
Siphonophore
Small copepod

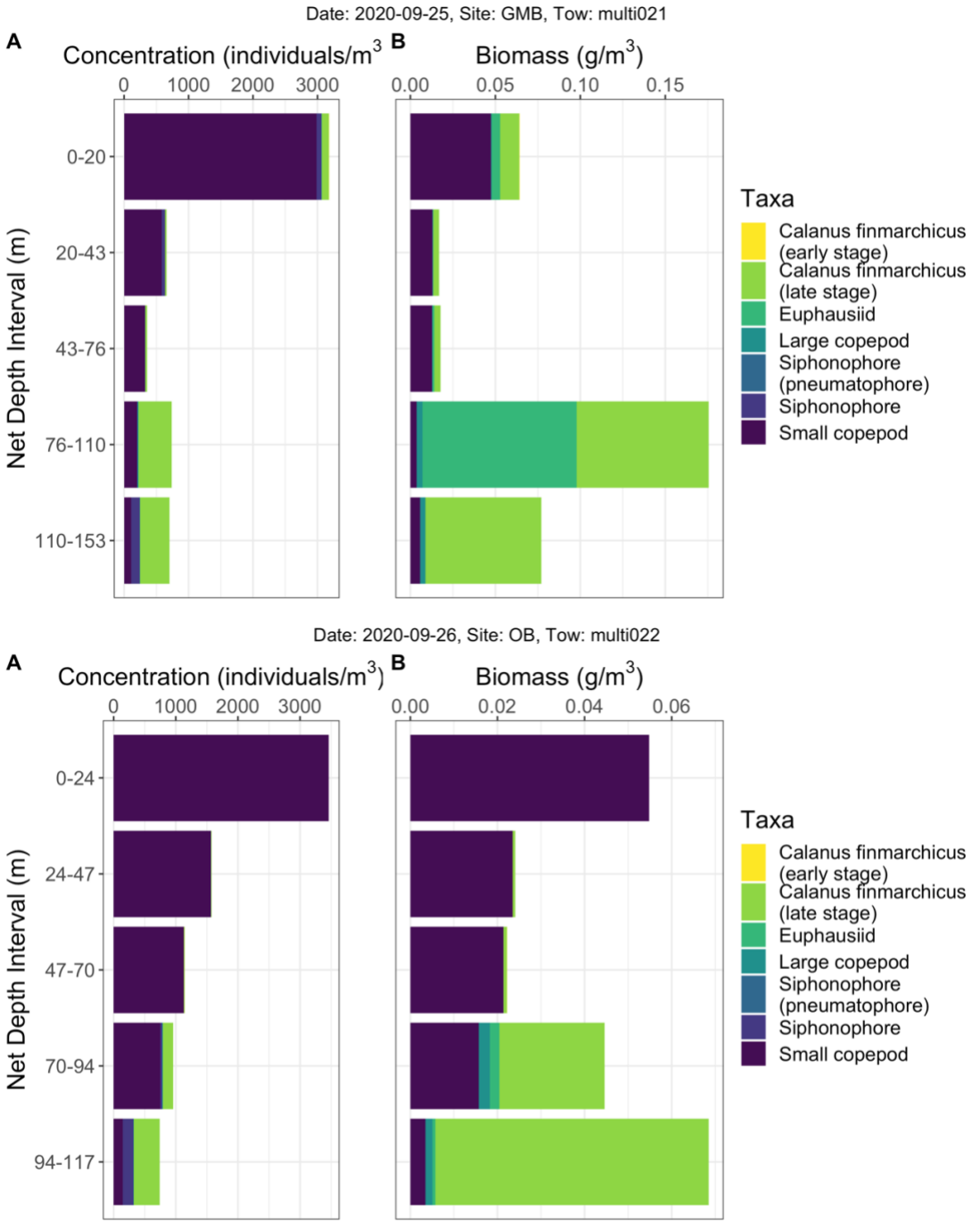
Date: 2020-09-25, Site: GMB, Tow: multi021
A
Concentration (individuals/m3)
0
1000
2000
3000
B
Biomass (g/m3)
0.00
0.05
0.10
0.15
Net Depth Interval (m)
0-20
20-43
43-76
76-110
110-153
Taxa
Calanus finmarchicus (early stage)
Calanus finmarchicus (late stage)
Euphausiid
Large copepod
Siphonophore (pneumatophore)
Siphonophore
Small copepod
Date: 2020-09-26, Site: OB, Tow: multi022
A
Concentration (individuals/m3)
0
1000
2000
3000
B
Biomass (g/m3)
0.00
0.02
0.04
0.06
Net Depth Interval (m)
0-24
24-47
47-70
70-94
94-117
Taxa
Calanus finmarchicus (early stage)
Calanus finmarchicus (late stage)
Euphausiid
Large copepod
Siphonophore (pneumatophore)
Siphonophore
Small copepod

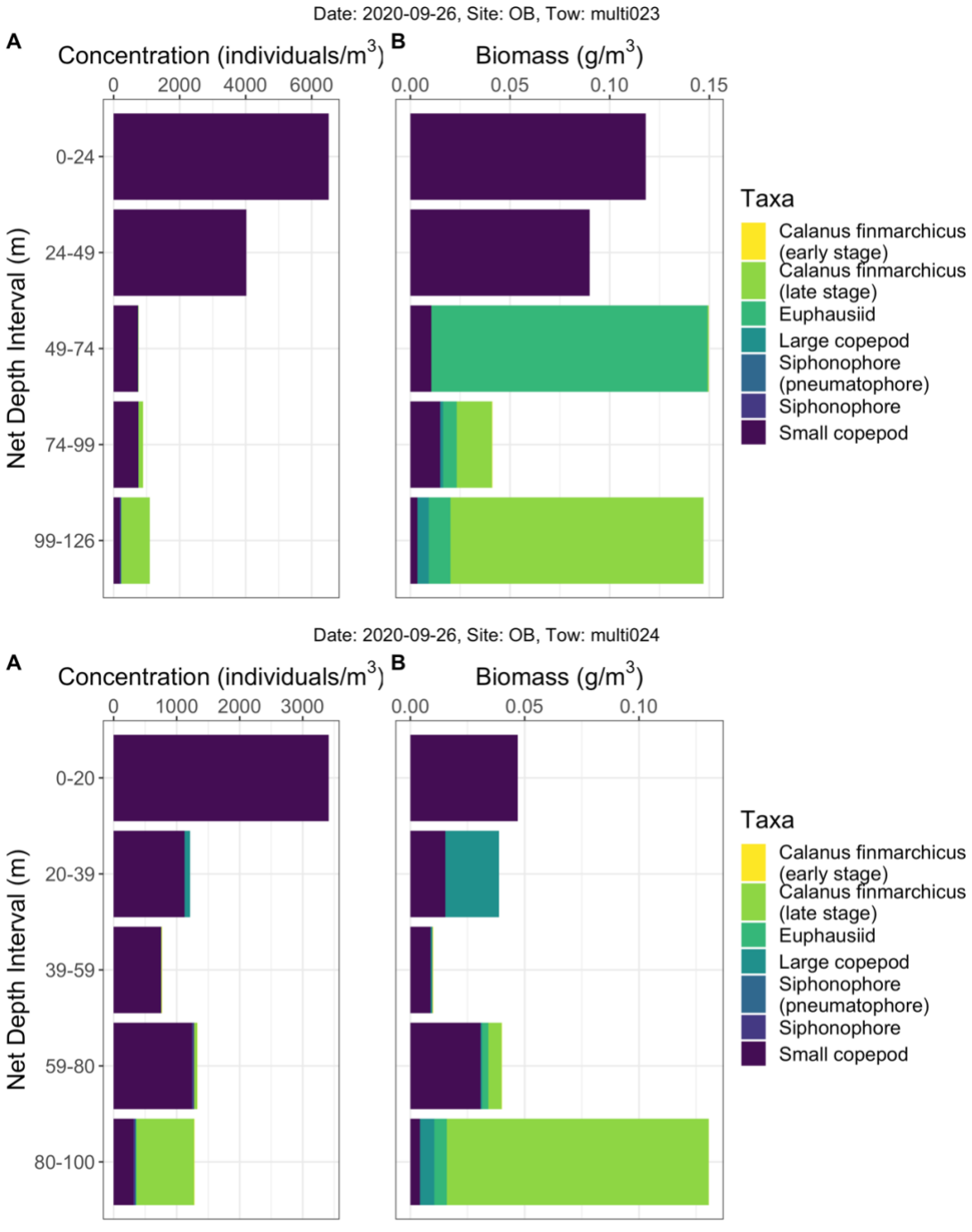
Date: 2020-09-26, Site: OB, Tow: multi023
A
Concentration (individuals/m3)
0
2000
4000
6000
B
Biomass (g/m3)
0.00
0.05
0.10
0.15
Net Depth Interval (m)
0-24
24-49
49-74
74-99
99-126
Taxa
Calanus finmarchicus (early stage)
Calanus finmarchicus (late stage)
Euphausiid
Large copepod
Siphonophore (pneumatophore)
Siphonophore
Small copepod
Date: 2020-09-26, Site: OB, Tow: multi024
A
Concentration (individuals/m3)
0
1000
2000
3000
B
Biomass (g/m3)
0.00
0.05
0.10
Net Depth Interval (m)
0-20
20-39
39-59
59-80
80-100
Taxa
Calanus finmarchicus (early stage)
Calanus finmarchicus (late stage)
Euphausiid
Large copepod
Siphonophore (pneumatophore)
Siphonophore
Small copepod

Appendix C. Corresponding MultiNet tows, OPC casts, and glider dive numbers. Bolded OPC casts provided adequate data for analysis; non-bolded casts suffered from high attenuance or depth spikes.

Date	Multinet Tow	OPC Casts	Dive Numbers
19 Sept 2020	multi004	OPC003/004	1-6
19 Sept 2020	multi005	**OPC005**/006	6-9
20 Sept 2020	multi006	**OPC007/008**	1-4
20 Sept 2020	multi007	OPC009/010	5-6
20 Sept 2020	multi009	OPC011/012	7
21 Sept 2020	multi011	**OPC013/014**	2-4
21 Sept 2020	multi013	**OPC015 (slow)/016 (slow)**	5-7
21 Sept 2020	multi014	**OPC017**/018	7
24 Sept 2020	multi016	**OPC021/022**	4-8
24 Sept 2020	multi017	**OPC023**/024	9
25 Sept 2020	multi019	**OPC027/028**	1-4
25 Sept 2020	multi020	**OPC029/030**	5-6
25 Sept 2020	multi021	**OPC031/032**	7
26 Sept 2020	multi022	**OPC033**/034	2-4
26 Sept 2020	multi023	**OPC035/036**	5-6
26 Sept 2020	multi024	OPC037/038	7

Appendix D. Linear model regression coefficients (± 1 STE) for all nets (n = 80) for the correlation between Sv(echo) and various Sv(net) models. Regression included basin and frequency band as grouping variables.

$S_{v(net)}$ Model	Frequency Band (kHz)	Basin	Slope	Intercept	R2	p-value	RMSE
Model 1 - $S_{v(net)}$	-	OB	0.39 ± 0.13	-75.66 ± 5.78	0.06	0.002	16.22
Model 1 - $S_{v(net)}$	-	GMB	-0.42 ± 0.11	-102.12 ± 4.35	0.08	0.0002	17.20
Model 2 - $S_{v(copepod)}$	-	OB	-0.58 ± 0.09	-136.96 ± 4.16	0.21	<0.00001	10.72
Model 2 - $S_{v(copepod)}$	-	GMB	-0.79 ± 0.08	-145.40 ± 3.08	0.39	<0.00001	10.71
Model 3 - $S_{v(cfin)}$	-	OB	-0.34 ± 0.14	-111.71 ± 5.85	0.048	0.02	12.62
Model 3 - $S_{v(cfin)}$	-	GMB	-0.64 ± 0.09	-117.80 ± 3.37	0.26	<0.00001	12.57
Model 1 - $S_{v(net)}$	0 to 130	OB	1.12 ± 0.24	-62.09 ± 8.88	0.37	0.00003	26.88
Model 1 - $S_{v(net)}$	130 to 200	OB	0.92 ± 0.30	-54.05 ± 14.59	0.20	0.004	18.21
Model 1 - $S_{v(net)}$	200 to 455	OB	0.60 ± 0.16	-60.24 ± 7.79	0.28	0.0005	17.31
Model 1 - $S_{v(net)}$	455 to 769	OB	0.56 ± 0.19	-56.78 ± 8.72	0.19	0.005	19.14
Model 1 - $S_{v(net)}$	0 to 130	GMB	-0.08 ± 0.51	-97.31 ± 12.02	0.00071	0.87	16.35
Model 1 - $S_{v(net)}$	130 to 200	GMB	0.57 ± 0.43	-65.37 ± 18.63	0.045	0.19	16.58
Model 1 - $S_{v(net)}$	200 to 455	GMB	-0.34 ± 0.26	-97.55 ± 11.13	0.042	0.20	17.49

Model 1 - $S_{v(net)}$	455 to 769	GMB	0.35 ± 0.21	-60.72 ± 9.33	0.070	0.099	21.47
Model 2 - $S_{v(copepod)}$	0 to 130	OB	-0.24 ± 0.04	-134.58 ± 1.51	0.48	<0.00001	16.38
Model 2 - $S_{v(copepod)}$	130 to 200	OB	-0.27 ± 0.06	-131.25 ± 3.07	0.32	0.0001	13.49
Model 2 - $S_{v(copepod)}$	200 to 455	OB	-0.24 ± 0.06	-116.13 ± 2.97	0.30	0.0002	13.61
Model 2 - $S_{v(copepod)}$	455 to 769	OB	-0.29 ± 0.09	-108.18 ± 4.04	0.22	0.002	20.31
Model 2 - $S_{v(copepod)}$	0 to 130	GMB	-0.18 ± 0.13	-134.46 ± 3.03	0.050	0.16	18.31
Model 2 - $S_{v(copepod)}$	130 to 200	GMB	-0.29 ± 0.12	-135.19 ± 5.34	0.13	0.02	15.38
Model 2 - $S_{v(copepod)}$	200 to 455	GMB	-0.01 ± 0.15	-109.18 ± 6.43	0.00019	0.93	13.57
Model 2 - $S_{v(copepod)}$	455 to 769	GMB	-0.24 ± 0.15	-110.03 ± 6.82	0.059	0.13	17.38
Model 3 - $S_{v(cfin)}$	0 to 130	OB	0.38 ± 0.10	-100.27 ± 3.52	0.31	0.001	24.66
Model 3 - $S_{v(cfin)}$	130 to 200	OB	0.36 ± 0.17	-88.66 ± 7.60	0.14	0.04	16.51
Model 3 - $S_{v(cfin)}$	200 to 455	OB	0.57 ± 0.17	-64.77 ± 7.69	0.30	0.002	17.71
Model 3 - $S_{v(cfin)}$	455 to 769	OB	0.45 ± 0.20	-63.29 ± 8.79	0.15	0.04	20.86
Model 3 - $S_{v(cfin)}$	0 to 130	GMB	0.22 ± 0.14	-103.12 ± 3.33	0.061	0.13	21.55
Model 3 - $S_{v(cfin)}$	130 to 200	GMB	0.31 ± 0.14	-87.41 ± 5.89	0.12	0.03	14.98
Model 3 - $S_{v(cfin)}$	200 to 455	GMB	0.19 ± 0.17	-78.72 ± 6.95	0.035	0.25	16.44
Model 3 - $S_{v(cfin)}$	455 to 769	GMB	0.57 ± 0.15	-53.03 ± 6.49	0.29	0.0003	25.19

Appendix E. Linear model regression coefficients (± 1 STE) for all nets (n = 80) for the correlation between Sv(echo) and various Sv(net) models. Regression included community composition and frequency band as grouping variables.

$S_{v(net)}$ Model	Frequency Band (kHz)	Community Composition	Slope	Intercept	R^2	p-value	RMSE
Model 1 - $S_{v(net)}$	-	*C. finmarchicus* dominant	-0.32 ± 0.11	-94.11 ± 4.12	0.09	0.004	18.52
Model 1 - $S_{v(net)}$	-	Euphausiid dominant	0.058 ± 0.045	-63.09 ± 1.87	0.05	0.21	28.85
Model 1 - $S_{v(net)}$	-	Low biomass	-0.32 ± 0.18	-109.50 ± 7.61	0.06	0.09	17.57
Model 1 - $S_{v(net)}$	-	Small copepod dominant	-0.10 ± 0.11	-101.76 ± 5.12	0.006	0.37	17.70
Model 2 - $S_{v(copepod)}$	-	*C. finmarchicus* dominant	-0.88 ± 0.11	-148.61 ± 3.98	0.43	<0.00001	10.87
Model 2 - $S_{v(copepod)}$	-	Euphausiid dominant	-0.84 ± 0.17	-150.52 ± 7.22	0.44	<0.00001	11.07
Model 2 - $S_{v(copepod)}$	-	Low biomass	-0.87 ± 0.13	-151.79 ± 5.67	0.45	0.00003	11.18
Model 2 - $S_{v(copepod)}$	-	Small copepod dominant	-0.44 ± 0.09	-128.80 ± 4.28	0.14	<0.00001	11.27
Model 3 - $S_{v(cfin)}$	-	*C. finmarchicus* dominant	-0.82 ± 0.11	-119.17 ± 3.97	0.40	<0.00001	15.29
Model 3 - $S_{v(cfin)}$	-	Euphausiid dominant	-0.60 ± 0.24	-118.55 ± 9.77	0.17	0.017	12.22
Model 3 - $S_{v(cfin)}$	-	Low biomass	-0.67 ± 0.16	-126.05 ± 6.42	0.29	0.00008	12.95
Model 3 - $S_{v(cfin)}$	-	Small copepod dominant	-0.45 ± 0.12	-118.03 ± 5.13	0.12	0.00024	13.06
Model 1 - $S_{v(net)}$	0 to 130	*C. finmarchicus* dominant	0.75 ± 0.47	-73.34 ± 10.74	0.11	0.13	22.67

Model 1 - $S_{v(net)}$	130 to 200	*C. finmarchicus* dominant	0.68 ± 0.50	-57.81 ± 20.33	0.08	0.19	17.40
Model 1 - $S_{v(net)}$	200 to 455	*C. finmarchicus* dominant	0.38 ± 0.19	-65.18 ± 7.95	0.15	0.06	18.35
Model 1 - $S_{v(net)}$	455 to 769	*C. finmarchicus* dominant	0.095 ± 0.14	-69.71 ± 5.92	0.02	0.51	22.47
Model 1 - $S_{v(net)}$	0 to 130	Euphausiid dominant	-0.11 ± 0.16	-67.34 ± 4.32	0.08	0.51	31.28
Model 1 - $S_{v(net)}$	130 to 200	Euphausiid dominant	-0.092 ± 0.12	-68.30 ± 5.37	0.09	0.48	29.74
Model 1 - $S_{v(net)}$	200 to 455	Euphausiid dominant	0.15 ± 0.16	-60.75 ± 7.40	0.13	0.39	27.63
Model 1 - $S_{v(net)}$	455 to 769	Euphausiid dominant	0.17 ± 0.17	-57.72 ± 7.78	0.14	0.36	29.5
Model 1 - $S_{v(net)}$	0 to 130	Low biomass	0.96 ± 0.47	-81.52 ± 13.40	0.27	0.07	36.19
Model 1 - $S_{v(net)}$	130 to 200	Low biomass	0.39 ± 0.74	-84.77 ± 33.72	0.02	0.61	19.53
Model 1 - $S_{v(net)}$	200 to 455	Low biomass	0.52 ± 0.16	-68.68 ± 7.07	0.50	0.007	16.41
Model 1 - $S_{v(net)}$	455 to 769	Low biomass	0.53 ± 0.14	-59.44 ± 6.67	0.56	0.003	18.41
Model 1 - $S_{v(net)}$	0 to 130	Small copepod dominant	0.26 ± 0.20	-99.84 ± 7.64	0.05	0.21	26.25
Model 1 - $S_{v(net)}$	130 to 200	Small copepod dominant	0.38 ± 0.25	-84.72 ± 12.32	0.06	0.14	19.18
Model 1 - $S_{v(net)}$	200 to 455	Small copepod dominant	0.24 ± 0.11	-80.67 ± 5.24	0.13	0.03	15.84
Model 1 - $S_{v(net)}$	455 to 769	Small copepod dominant	0.20 ± 0.15	-75.34 ± 6.86	0.05	0.18	16.94
Model 2 - $S_{v(copepod)}$	0 to 130	*C. finmarchicus* dominant	-0.17 ± 0.10	-135.46 ± 2.38	0.11	0.11	19.31
Model 2 - $S_{v(copepod)}$	130 to 200	*C. finmarchicus* dominant	-0.10 ± 0.13	-128.2 ± 5.47	0.03	0.47	16.51

Model 2 - $S_{v(copepod)}$	200 to 455	*C. finmarchicus* dominant	-0.18 ± 0.17	-117.36 ± 7.19	0.05	0.31	12.35
Model 2 - $S_{v(copepod)}$	455 to 769	*C. finmarchicus* dominant	0.05 ± 0.17	-99.08 ± 6.87	0.0035	0.79	17.93
Model 2 - $S_{v(copepod)}$	0 to 130	Euphausiid dominant	-0.16 ± 0.19	135.66 ± 5.04	0.10	0.44	20.12
Model 2 - $S_{v(copepod)}$	130 to 200	Euphausiid dominant	-0.18 ± 0.12	-132.01 ± 5.34	0.27	0.18	16.43
Model 2 - $S_{v(copepod)}$	200 to 455	Euphausiid dominant	0.09 ± 0.21	-105.59 ± 9.69	0.032	0.67	13.94
Model 2 - $S_{v(copepod)}$	455 to 769	Euphausiid dominant	-0.01 ± 0.24	-101.15 ± 10.91	0.00016	0.98	17.77
Model 2 - $S_{v(copepod)}$	0 to 130	Low biomass	-0.34 ± 0.09	-140.78 ± 2.46	0.59	0.0022	17.57
Model 2 - $S_{v(copepod)}$	130 to 200	Low biomass	-0.44 ± 0.21	-143.59 ± 9.46	0.29	0.06	16.63
Model 2 - $S_{v(copepod)}$	200 to 455	Low biomass	-0.39 ± 0.11	-126.77 ± 4.73	0.55	0.0037	11.37
Model 2 - $S_{v(copepod)}$	455 to 769	Low biomass	-0.31 ± 0.16	-115.08 ± 7.59	0.25	0.08	15.83
Model 2 - $S_{v(copepod)}$	0 to 130	Small copepod dominant	-0.08 ± 0.04	-126.78 ± 1.50	0.10	0.057	16.19
Model 2 - $S_{v(copepod)}$	130 to 200	Small copepod dominant	-0.12 ± 0.06	-122.28 ± 3.00	0.1	0.058	12.93
Model 2 - $S_{v(copepod)}$	200 to 455	Small copepod dominant	-0.08 ± 0.05	-106.06 ± 2.54	0.063	0.14	16.16
Model 2 - $S_{v(copepod)}$	455 to 769	Small copepod dominant	-0.14 ± 0.08	99.59 ± 3.90	0.075	0.11	22.74
Model 3 - $S_{v(cfin)}$	0 to 130	*C. finmarchicus* dominant	0.11 ± 0.10	-101.62 ± 2.27	0.054	0.29	17.11
Model 3 - $S_{v(cfin)}$	130 to 200	*C. finmarchicus* dominant	0.07 ± 0.12	-93.82 ± 5.03	0.015	0.58	13.31
Model 3 - $S_{v(cfin)}$	200 to 455	*C. finmarchicus* dominant	0.18 ± 0.16	-75.39 ± 6.55	0.055	0.28	18.86

Model 3 - $S_{v(cfin)}$	455 to 769	*C. finmarchicus* dominant	0.04 ± 0.15	-72.51 ± 6.22	0.0037	0.78	24.92
Model 3 - $S_{v(cfin)}$	0 to 130	Euphausiid dominant	0.98 ± 0.41	-83.14 ± 11.18	0.48	0.055	32.61
Model 3 - $S_{v(cfin)}$	130 to 200	Euphausiid dominant	0.24 ± 0.40	-91.22 ± 17.71	0.058	0.57	15.08
Model 3 - $S_{v(cfin)}$	200 to 455	Euphausiid dominant	0.81 ± 0.53	-51.06 ± 24.37	0.28	0.18	21.27
Model 3 - $S_{v(cfin)}$	455 to 769	Euphausiid dominant	1.05 ± 0.54	-31.59 ± 24.53	0.39	0.098	29.21
Model 3 - $S_{v(cfin)}$	0 to 130	Low biomass	0.19 ± 0.10	-108.64 ± 2.84	0.25	0.10	24.97
Model 3 - $S_{v(cfin)}$	130 to 200	Low biomass	0.27 ± 0.16	-94.24 ± 7.47	0.21	0.14	16.99
Model 3 - $S_{v(cfin)}$	200 to 455	Low biomass	0.30 ± 0.11	-79.18 ± 4.61	0.45	0.017	14.91
Model 3 - $S_{v(cfin)}$	455 to 769	Low biomass	0.34 ± 0.11	-68.15 ± 5.02	0.50	0.01	19.87
Model 3 - $S_{v(cfin)}$	0 to 130	Small copepod dominant	0.13 ± 0.08	-109.59 ± 2.49	0.10	0.10	23.58
Model 3 - $S_{v(cfin)}$	130 to 200	Small copepod dominant	0.03 ± 0.12	-104.70 ± 5.76	0.0029	0.79	16.93
Model 3 - $S_{v(cfin)}$	200 to 455	Small copepod dominant	0.21 ± 0.11	-82.66 ± 4.95	0.13	0.061	14.51
Model 3 - $S_{v(cfin)}$	455 to 769	Small copepod dominant	0.02 ± 0.15	-82.87 ± 6.70	0.00086	0.88	17.49

Curriculum Vitae

Candidate's Full Name: Delphine Spickler Mossman

Universities Attended:

Stony Brook University (2016-2020)
Bachelor of Science
Applied Math and Statistics
Marine Vertebrate Biology
Honours

University of New Brunswick (2020-present)
Master of Science
Biology

Presentations:

Ocean Sciences Meeting, 2022. "Performance of a glider-mounted multi-frequency echosounder for detecting dense mesozooplankton layers."

Publications:

2021. "Validating the ability of a glider-mounted fisheries echosounder to measure mesozooplankton concentration throughout the water column." CMOS Bulletin.

2020. "Reprise for Salmon: A Look at Pacific Salmon Populations Twenty Years After *Song for the Blue Ocean*." Stony Brook University.